Not reviewed, for internal circulation only

ATLAS Note

ATL-COM-MUON-2017-008

Draft version 0.1

Small-Diameter Monitored Drift Tube (sMDT) BMG Chamber Construction and Testing

O. Kortner[a], H. Kroha[a], K. Schmidt-Sommerfeld[a], E. Takasugi[a]

[a]*Max-Planck-Institut für Physik*

5th May 2017

The construction and testing of new small-diameter Monitored Drift Tube (sMDT) BMG chambers is presented.

© 2017 CERN for the benefit of the ATLAS Collaboration.
Reproduction of this article or parts of it is allowed as specified in the CC-BY-4.0 license.

Not reviewed, for internal circulation only

Contents

Not reviewed, for internal circulation only

1 Introduction

The Monitored Drift Tube (MDT) chambers are one of four systems in the ATLAS Muon Spectrometer (see Fig. 1). The other systems are the Cathode Strip Chambers (CSCs), Thin Gap Chambers (TGCs), and Resistive Plate Chambers (RPCs). The MDT chambers have demonstrated that they provide very precise and robust tracking over large areas of the Muon Spectrometer. The Muon Spectrometer is designed to detect charged particles at pseudo-rapidities of $|\eta| \leq 2.7$ and accurately measure their momenta. More information about the Muon Spectrometer can be found in the ATLAS Muon TDR [1].

New chambers were constructed and tested to improve the rate capability of the MDT system, especially when the LHC luminosity is increased. These new chambers will also increase the precision of the muon momentum measurements and triggering. The small diameter Monitored Drift Tube (sMDT) chambers are one type of these new chambers designed for the higher-luminosity of future LHC operations. These new sMDT chambers consist of eight layers of pressurized drift tubes. These eight layers are split into two multilayers, positioned on either side of a spacer frame. These chambers have been constructed and were installed in January 2017 (during the 2016–2017 Winter Shutdown).

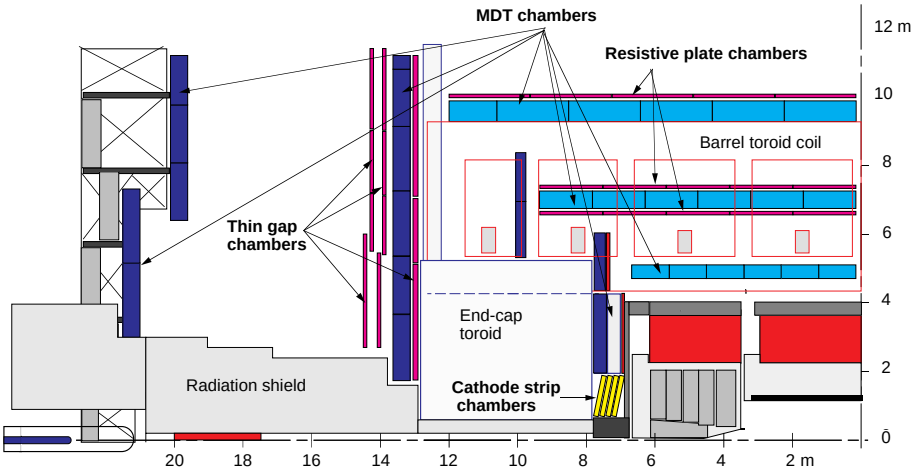

Figure 1: Quadrant view of the ATLAS Muon Spectrometer. The MDT chambers in the barrel (light blue) and in the endcap (dark blue) are in three layers. Figure from the ATLAS Muon TDR [1].

2 Monitored Drift Tube (MDT) Chambers

The MDT chambers are the main system for the ATLAS Muon Spectrometer's precision tracking system. They are precisely constructed and constantly monitored to quantify any deformations or changes in position during operation. The MDT chambers provide the primary momentum measurement in the Muon Spectrometer. They use pressurized drift tubes which are 30 mm in diameter and filled with Ar/CO_2 gas (with a 93:7 ratio), pressurized to 3 bar.

The MDT chambers are arranged into three layers in the barrel and three layers in both of the endcaps. The three layers in the barrel form coaxial cylinders around the beam axis, and the endcaps form circular disks all centered on the beam axis. The chambers in the innermost layer (both in the endcap and in the barrel) consist of eight layers of tubes, split into two equal multilayers, whereas the remaining chambers consist

Not reviewed, for internal circulation only

Table 1: MDT chamber parameters

Parameter	Design value
Tube diameter	30 mm
Wire diameter	50 μm
Gas mixture	Ar/CO_2 (93:7 ratio)
Gas pressure	3 bar (absolute)
Gas gain	2×10^4
Wire potential	3080 V
Average drift velocity	$\sim$ 20.7 μm/ns

of six layers of tubes, also split into two equal multilayers. The chambers themselves are rectangular in the barrel region, but trapezoidal in the endcaps to create circular disks of MDT chambers. A table of the general MDT chamber parameters can be seen in Tab. 1.

A cross-section of one drift tube can be seen in Fig. 2. As a charged particle passes through the tube, the Ar/CO_2 gas is ionized. The electrons from the ionization clusters drift toward the anode wire. These drift velocities depend strongly on the radius, ranging from 10 μm/ns close to the tube wall, 26 μm/ns halfway between the wall and the wire, and 52 μm/ns close to the wire. These electrons create a sequence of pulses which are read out by the electronics seen in Fig. 3. More details about the MDT chamber electronics can be found in [2].

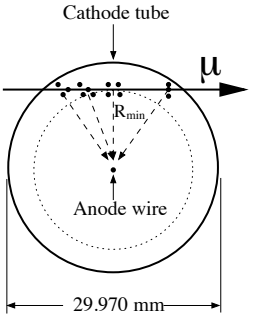

Figure 2: Cross section of a tube from an MDT chamber [2].

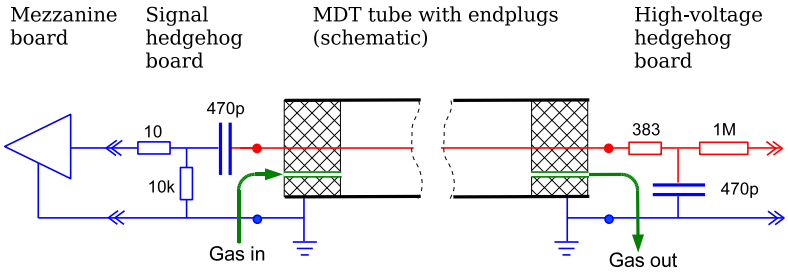

Figure 3: Schematic of a tube from an MDT chamber [2].

Not reviewed, for internal circulation only

3 Small-Diameter Monitored Drift Tube (sMDT) Chambers

Small-diameter Monitored Drift Tube (sMDT) chambers utilize the same technology as the existing MDT chambers. However they differ in one major way: the tube diameter used is reduced by a factor of two in the sMDT chambers as opposed to the MDT chambers. This leads to a maximum drift time in the sMDT chambers which is almost one-fourth the time in a standard MDT chamber (see Fig. 4). This allows for an increase in rate capability of these new tubes of approximately one order of magnitude. Furthermore, the sMDT chambers themselves are geometrically smaller allowing them to be fitted into locations where standard MDT chambers are too large.

Table 2: MDT versus sMDT chamber parameters. The difference in HV ensures that the electric field inside the tubes, and therefore the gas gain, is identical in both types of chambers.

Parameter	MDT	sMDT
Diameter	30 mm	15 mm
Maximum drift time	700 ns	185 ns
Wire potential	3080 V	2730 V
Wire diameter	50 μm	
Gas mixture	Ar/CO_2 (93:7 ratio)	
Gas pressure	3 bar (absolute)	
Gas gain	2×10^4	
Chamber resolution	$\sim$ 40 μm	

The current production of sMDT chambers are designed to fit into the barrel region of the ATLAS detector (see Fig. 5). There will be 12 such chambers. Gaps are required in each chamber to allow for the ATLAS calibration system (A cutaway of the chamber can be seen in Fig. 6). Over 4,000 tubes are required for the construction of the sMDT chambers. Each chamber takes approximately one month to complete, after which their seals and electronics are tested.

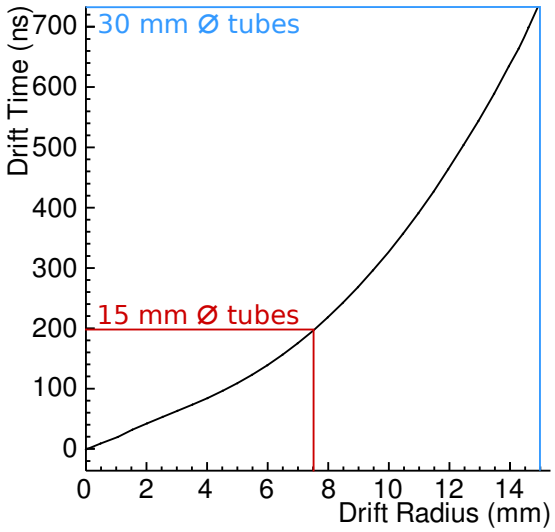

Figure 4: Maximum drift time versus tube radius. The old 30 mm tube drift time is noted in blue, whereas the new 15 mm tube drift time is noted in red.

Not reviewed, for internal circulation only

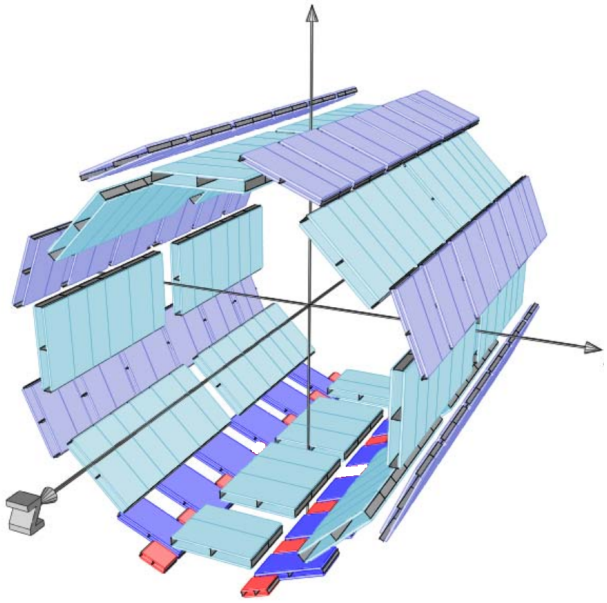

Figure 5: Location of the new sMDT chambers (shown in red).

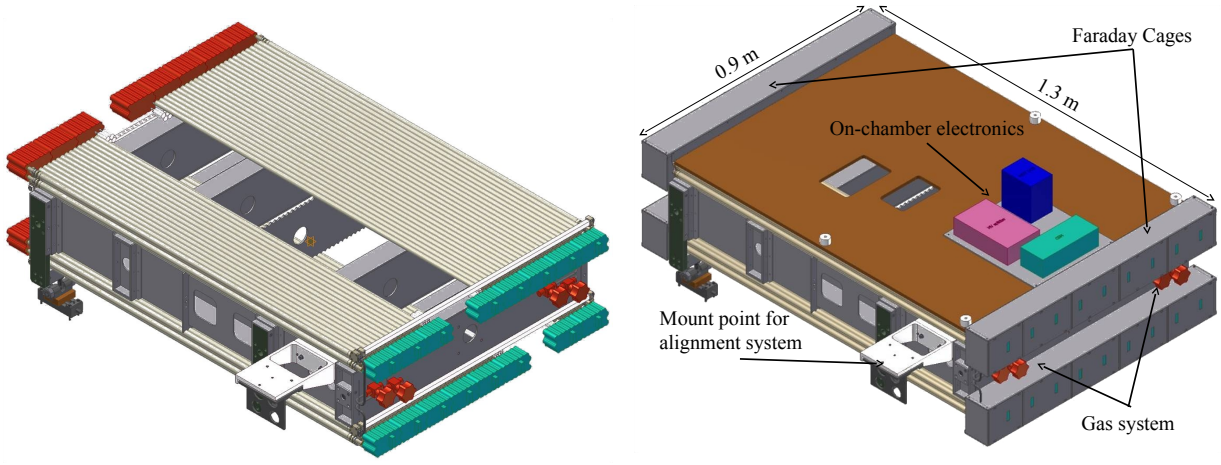

Figure 6: sMDT chamber cutaway without (left) and with (right) electronics and gas system installed.

4 sMDT BMG Chamber Construction

The sMDT BMG chamber construction takes place inside a clean room at MPI Munich. Each individual tube used in the sMDT chambers is 1129 mm in length with a 15 mm diameter. Endplugs on either end cap the tube. Each tube is recorded in an MySQL database[3] along with the results from every test conducted on the tubes[1].

The new sMDT chambers are designed to have as many similar components as possible to simplify the design and assembly. The 12 new chambers are of eight different types, but use the same type of spacer structures, Faraday cages, electronics for both High Voltage (HV) and Read Out (RO). The location of the chambers in the ATLAS Muon Spectrometer also means that they need to have gaps to allow for the ATLAS alignment system to pass through them (see Fig. 8). These so-called "cutouts" are the only major difference in the chambers. Due to the symmetry of the system, eight different types of chambers are required (the specific tube layout can be found in the figure noted after the chamber number):

Not reviewed, for internal circulation only

[1] The database can be found at: http://134.107.29.19/ for sMDT tube production (BME, BMG, and BIS productions), and http://134.107.29.19/BMG_tube_overview.php for BMG specific tubes. These pages are only accessible from within the MPI network.

Not reviewed, for internal circulation only

1. BMG-3A-12 (Fig. 29)
2. BMG-3A-14 (Fig. 30)
3. BMG-2A-12/BMG-2C-14 (Fig. 31)
4. BMG-1A-12/BMG-1C-14 (Fig. 32)
5. BMG-1C-12/BMG-1A-14 (Fig. 33)
6. BMG-2C-12/BMG-2A-14 (Fig. 34)
7. BMG-3C-12 (Fig. 35)
8. BMG-3C-14 (Fig. 36)

The placement of the different sMDT chambers with the paired chambers can be seen in Fig. 7.

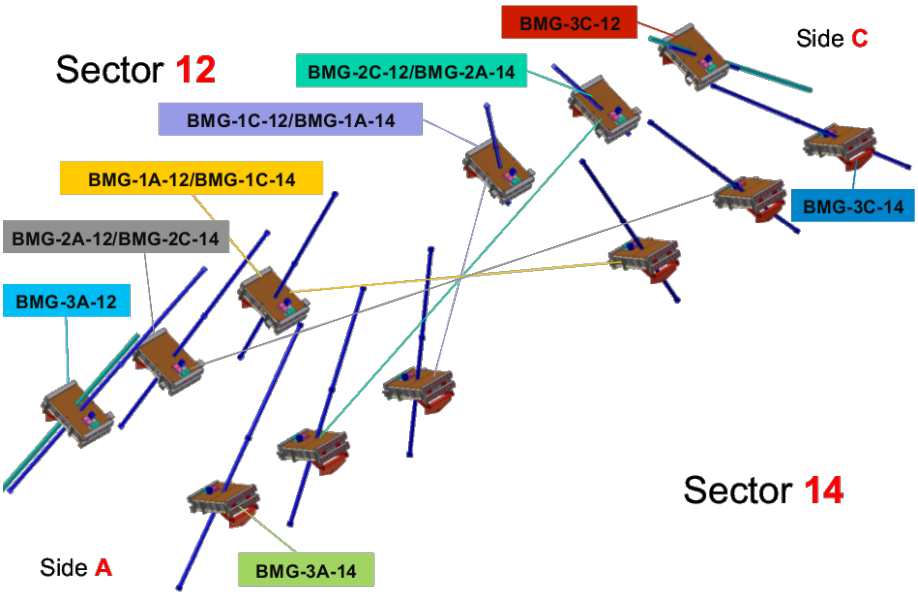

Figure 7: Positions of the new sMDT chambers in free space. Individual chamber production numbers are given. The dark blue lines passing through each chamber indicate the alignment structure of the ATLAS detector. The symmetric chambers, i.e., those with the same cutouts, are indicated by the thin lines. Figure courtesy Sergey Podkladkin.

Each new sMDT chamber consists of two multilayers of tubes. Every multilayer has four layers, each with 54 tubes minus those corresponding to the cutouts. In between each multilayer is some spacer structure. Surrounding the tube layers is the gas system, HV and RO electronics, a Faraday cage, alignment elements (axial and praxial), and protective covers, similar to the MDT chambers (see Fig. 3). Furthermore, on-chamber electronics boxes are installed. On the exterior, kinematical supports as well as survey target supports are installed. A protective cover is installed over any remaining exposed surfaces. It must be noted that these chambers do not have in-plane alignment. In total, the 12 new sMDT chambers will require a minimum of 4,328 tubes.

Not reviewed, for internal circulation only

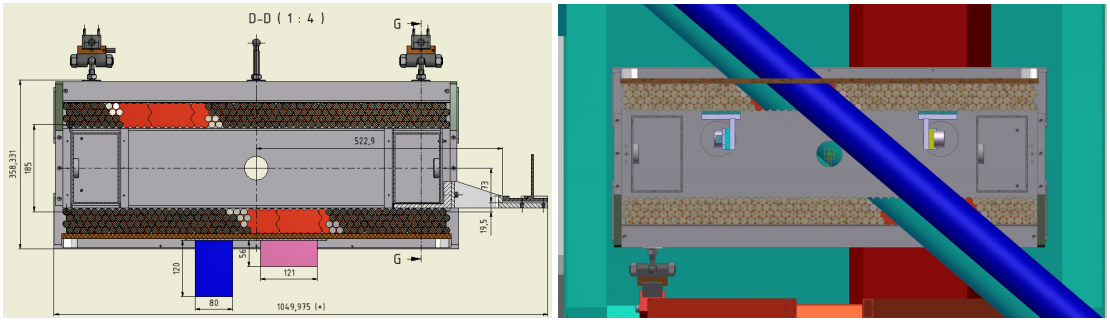

Figure 8: Cross-section of a chamber with the cutout in red (left), and the same cross-section of a chamber with the ATLAS alignment system overlaid (right). Figure courtesy Sergey Podkladkin.

5 sMDT Tube Construction and Testing

The tube construction starts with the crimping of one endplug into the tube. The Tungsten-Rhenium (W-Re) wire with 0.05 mm diameter is then semi-automatically threaded into the tube using air pressure (see Fig. 11). The wire is then fastened to the first endplug with a copper tubelet, fixing the wire in place on one end. The second endplug is crimped, but the wire is not fixed on this end of the tube. These endplugs not only hold the wire at the correct position (± 5 μm) and tension, but also provide an airtight seal for the tube and enable HV supply and signal readout. A cross section of a tube can be seen in Fig. 9, and an exploded view and cutaway of an endplug can be seen in Fig. 10 with the gas system and grounding system.

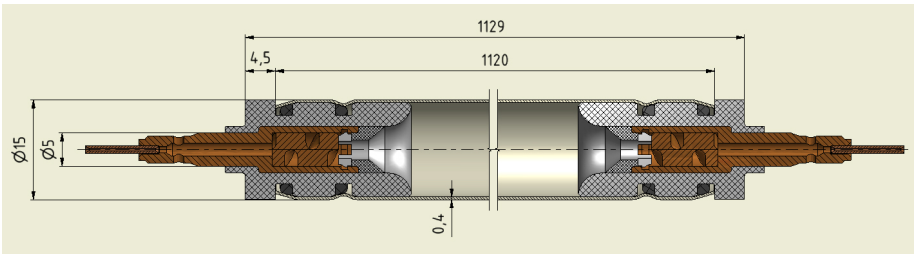

Figure 9: Cross section of one sMDT tube with dimensions of various portions noted.

The wire is then tensioned to 400 g for 10 seconds. This tension is removed, and the wire is re-tensioned to 350 ± 15 g. This tension is fixed with another copper tubelet on the other end, which is crimped into place.

The wire tension is checked by applying a magnetic field to the wire, and passing an alternating current across the wire, which vibrates it. By noting the vibrational amplitude of the wire, the fundamental frequency of the wire can be found, which is directly related to the tension of the wire:

$$T = \frac{\pi L^2 d^2 f^2 \rho}{g} \tag{1}$$

where T is the tension in grams, f is the frequency, d is the diameter of the wire, L is the length of the wire, and ρ is the density of the wire. Tab. 3 show the values used in the calculation. Furthermore, this measurement can be done without breaking the airtight seal on the tube endplugs and can be repeated

Not reviewed, for internal circulation only

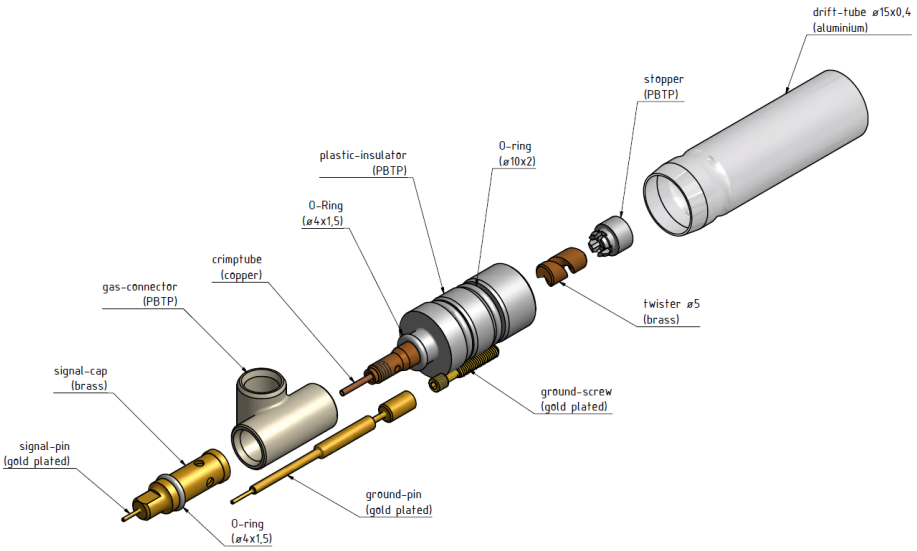

Figure 10: Exploded view of the tube endplug. Included in the lower left is the gas connection as well as signal readout as well as the grounding pin and screw for the tube.

multiple times (see Fig. 12). Multiple measurements are necessary as the wire relaxes in the tube over time, which leads to a decrease in the tension.

The wire tension is therefore re-measured at least one week after the first test to measure the tension loss, after the gas leak and HV dark current tests are performed. Tubes which have a tension loss of more than 18 g are rejected. The change in tension is shown in Fig. 13. The majority of tubes are within the 5–10 g tension loss range, but there are some which have lost as much as 25–30 g of their tension. Not shown on the plots are those which have lost over 300 g of tension, i.e., those whose wire have broken inside the tube due to either mishandling of the tube or a defect in the wire.

This second test also ensures that the final tension of the tubes is still above 335 g, as in the previous construction period, for the BME sMDT chamber construction, a loss in tension was seen [4]. These results are stored in the online MySQL database so they can be checked in real time.

Table 3: Wire parameters used in the calculation of the wire frequency using Eq. 1.

Constant	Value
L [mm]	1100
d [mm]	5×10^{-5}
ρ [g·cm^{-3}]	19.3
g [m/s^2]	9.81

The results of the tension test are shown in Fig. 14. The tension limits (350 ± 15 g) are shown in dotted red lines. All passing tubes are colored green, while the failing tubes are colored red. The vast majority of the tubes pass, with most of the tubes being clustered around 350 g.

Not reviewed, for internal circulation only

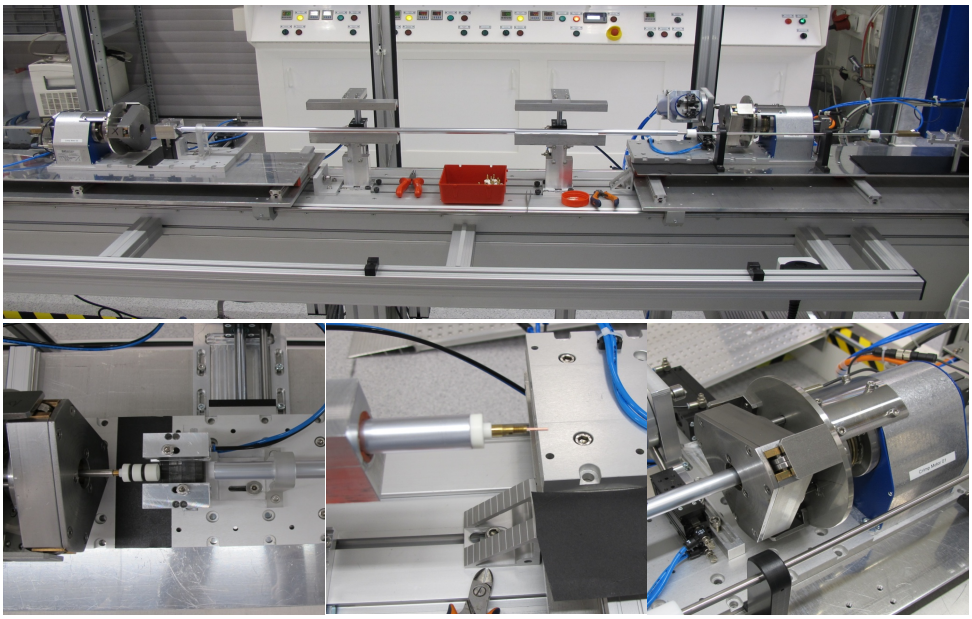

Figure 11: Wiring machine (top) with closeup of the endplug before insertion into the tube (bottom left), after insertion (bottom center), and component which affixes the endplug into the tube (bottom right).

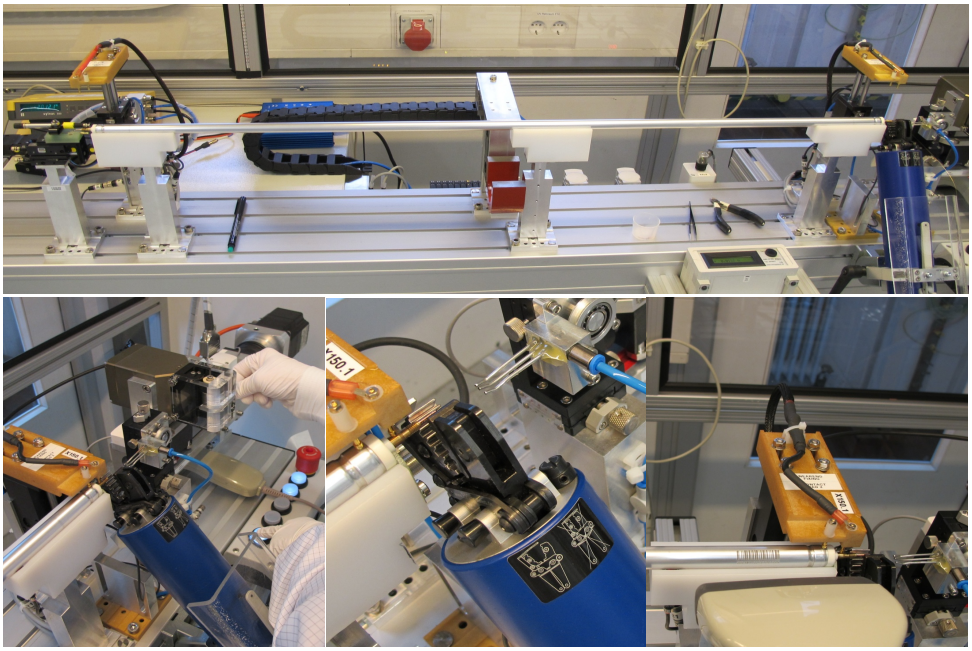

Figure 12: Wire tensioning machine (top), with a closeup of the tensioning device (bottom left), tube crimping (bottom center). The final step of entering the fundamental wire frequency and resistance into the database using the barcode associated with the tube (bottom right). The red component in the center of the top image is the magnet which, coupled with an alternating current, allows for a measurement of the wire tension without opening the tube.

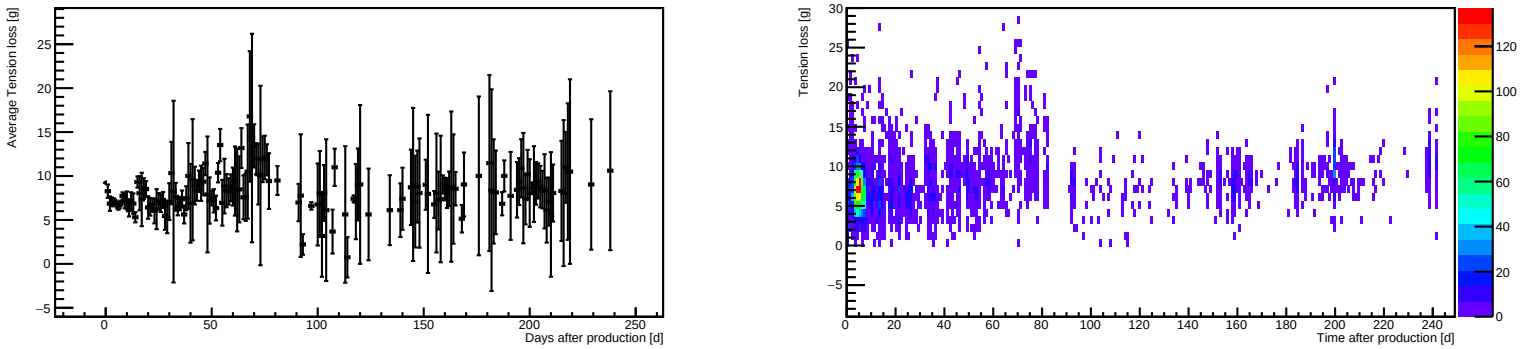

Figure 13: Average loss in tension (left) and the tension loss per tube (right) is shown as a function of time. On average, the tension decreases by approximately 5–10 g.

Not reviewe

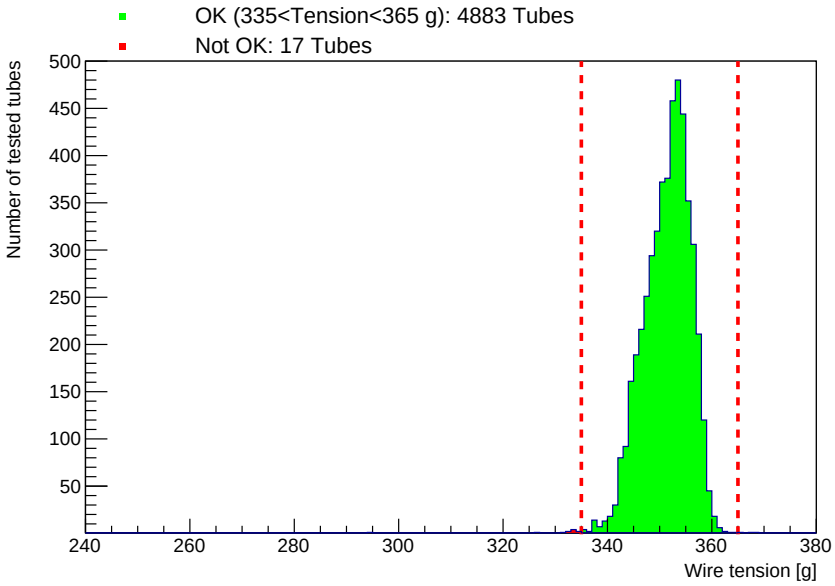

Figure 14: Tension measurements for all tested tubes. The required tension limits are shown in dotted red. The tubes which pass are in green, while the tubes which fail are in red.

Not reviewed, for internal circulation only

Once the wire has been tensioned and measured, the gas seals are tested on the tube. The tubes are placed in an evacuated testing cylinder, which is also known as a "Torpedo". The sMDT tube is then filled with a mixture of 95% Ar, 5% He and pressurized to 2 bar to imitate the 2 bar overpressure found under nominal working conditions. A leak detector, installed on the Torpedo, measures the amount of gas which escapes into the Torpedo from the tube. The measurement is then corrected for the difference between the gas mixture used and an all-argon gas. This leakage is required to be less than 10^{-5} mbar·l/s of argon. The leak rates are also recorded on the online MySQL database.

Figure 15: Gas leak testing. The central cylinder is the testing cylinder ("Torpedo"), which contains the tube. The lower left is the gas connection to the sMDT tube. The upper right leakage detector measures any gas which has leaked from the sMDT tube to the Torpedo.

The results of the gas leak test can be seen in Fig. 16. As before, the red dotted line shows the acceptable leak rate limit of 10^{-5} mbar·l/s. The leak detection unit has a minimum detection sensitivity of 3×10^{-8} mbar·l/s, which is indicated by the dotted blue line. A large fraction of the tubes not only pass, but have a leak rate below the sensitivity of the detection unit, indicating that the construction and crimping process on the tubes is not only sound but reliably results in tubes which are in essence completely gas tight.

After the gas seals have been tested, the sMDT tube is taken to HV testing. The tubes are filled with the nominal working gas (93% Ar, 7% CO_2) at 3 bar. The voltage is then slowly raised to 3,015 V, which is above the working voltage of 2,730 V. The dark current from the tube is continuously measured, and recorded after it stabilizes, which takes approximately 10 minutes. The measurement device can test up to 15 tubes at a time, each with a separate HV source and current measurement device (see Fig. 17). The maximum allowed dark current is 2 nA per tube. Again, all results from the current test are recorded online in the MySQL database.

The results of the HV test can be seen in Fig. 18. The limit of 2 nA is denoted by a dotted red line. The measurement device has a minimum sensitivity of 0.5 nA, which is shown by the dotted blue line. While most of the tubes are under the limit, there is a larger distribution of tubes which are above the allowed dark current. Not shown in the plots are those whose dark current is effectively infinite, i.e., the wire broke during transportation causing a short between the tube wall and the wire.

During the course of the tube construction, other factors can disqualify a tube, including defects in the

Not reviewed, for internal circulation only

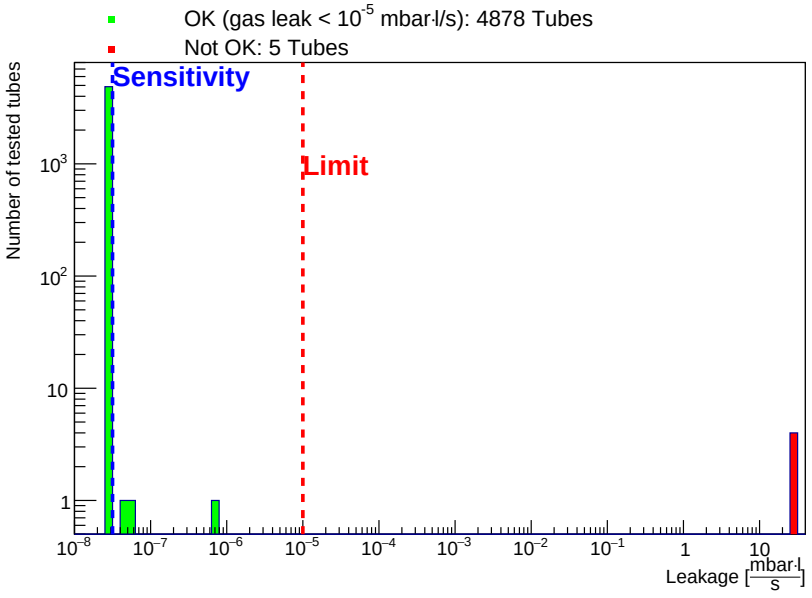

Figure 16: Measured gas leak rates for tubes. The limit (10^{-5} mbar·l/s) is shown in red, while the sensitivity of the leak detector (3×10^{-8} mbar·l/s) is shown in blue. The tubes which pass are in green, while the tubes which fail are in red.

Figure 17: HV testing apparatus. This setup can test up to 15 tubes simultaneously. On the bottom right is the HV source connected to each chamber with individual current measurements for each tube.

Not reviewed, for internal circulation only

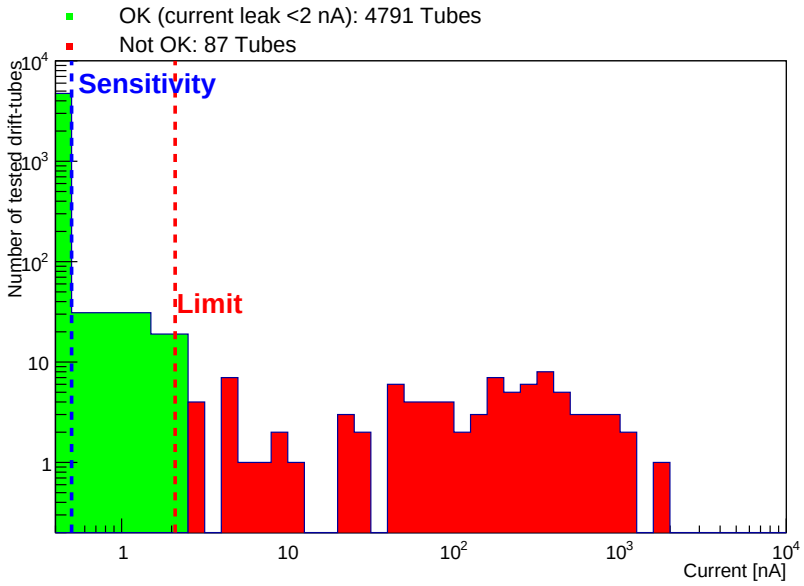

Figure 18: Measured dark current for tubes. The limit (2 nA) is shown in red, while the sensitivity of the dark current detector (0.5 nA) is shown in blue. The tubes which pass are in green, while the tubes which fail are in red.

tube itself upon arrival, the breaking of the wire during handling, or a failure in the tubelets or endplugs. A chart showing the production losses can be seen in Fig. 19. The relative losses are enumerated in Tab. 4 and shown in Fig. 20. These tube statuses (if not directly related to the tests conducted on the tube) are also recorded in the MySQL database as a "Tube Status". Their codes and meanings are listed in Tab. 5.

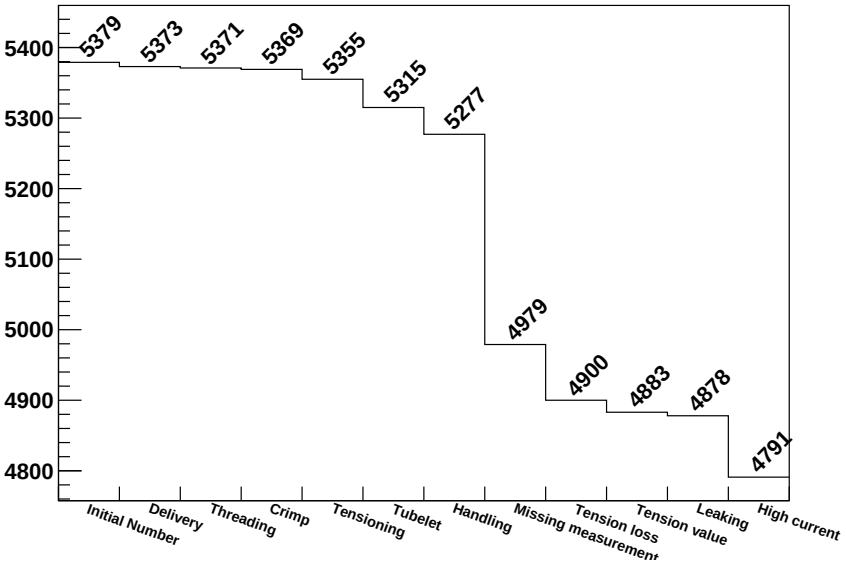

Figure 19: Tube production losses

The largest loss (5.5%) can be seen in the so-called "Missing Measurement" error. This happens when a measurement for a tube (e.g., dark current, gas leak, or tension) is missing from the MySQL database. As a precautionary measure, the tube is listed as rejected. This "Missing Measurement" tends to be the second

Not reviewed, for internal circulation only

Table 4: Tube production loss percentages

5, 379 Tubes	Total number
89.0686%	OK
1.6174%	High current
0.0929541%	Leaking
0.316044%	Tension value
1.46867%	Tension loss
5.54006%	Missing measurement
0.706451%	Handling
0.743633%	Tubelet
0.260271%	Tensioning
0.0371816%	Crimp
0.0371816%	Threading
0.111545%	Delivery

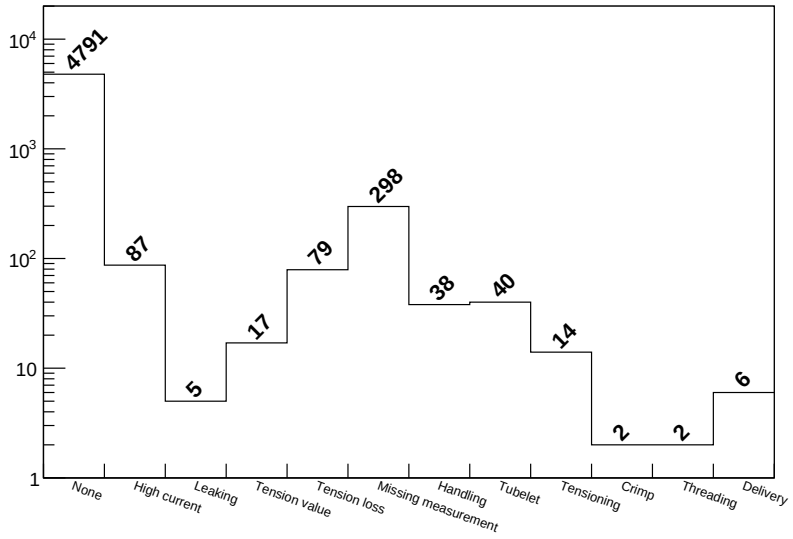

Figure 20: Tube production loss by category

Table 5: Tube status and their meanings.

Status Code	Meaning
0	OK
1	Dead On Arrival
10	Threading Error
11	Endplug Crimp Error
12	Tear During Tensioning
13	Crimp Tube Error
20	Tear During Handling

Not reviewed, for internal circulation only

tension test, as production and testing was halted after the required tubes (plus at least 10% spare) were produced. Thus, there are almost 300 tubes which could also be used as spare if the missing tests were to be conducted. Tension loss and high current are the main losses during testing at a rate of approximately 1.5% each. These could be seen in the individual test result plots (Figs. 13 and 18 compared to, e.g., Fig. 14). The remaining categories have a less than 1% loss rate. The overall pass rate of the constructed tubes is almost 90%, with 4,791 tubes ready for use in chamber construction. As a minimum of 4,328 tubes are needed, this leaves 463 tubes (10.6% of total tubes needed) as spare.

6 Chamber Construction

Once enough tubes for a chamber are produced, they are used to construct an sMDT chamber. Alignment combs (see Fig. 21) are used to ensure that the tubes, and more importantly the wires inside the tubes, are positioned in the proper place. This is crucial because the wires give the position readout of hits when a charged particle, e.g., a muon, passes through the tubes in a chamber. This is done by fixing the endplugs as closely as possible to a predetermined grid pattern. For each layer in the comb, there is a bottom half and top half which come together to encase and hold the tube endplugs in place. Because of the concentricity of the wire-and-endplug assembly, precise location of the endplug leads to precise positioning of the wires within the tube. A schematic of the whole jig system can be seen in Fig. 22, while the combs in particular can be seen in Fig. 23.

First, a layer of tubes is placed into the appropriate slots in the combs. As each tube is installed, their number, the chamber they are installed in, and their position inside that chamber is recorded in the MySQL database. Grounding pins are also inserted into the combs. After the first layer is in place, epoxy is laid down to prepare for the next layer of tubes (see Fig. 26). A weight (with grooves for the tubes, see item 3 in Fig. 22) is used to keep the tubes from shifting as the epoxy is left to set. This weight can also be raised to accomodate the (eight) different layers of tubes. This process is repeated until the first multilayer (four layers' worth of tubes) is installed. An alignment frame and spacer are inserted, as well as mount points for the praxial (outside the chamber) and axial (inside the chamber) alignment elements (see Fig. 25). After this, the second multilayer is started. A schematic of the spacer and alignment frame can be seen in Fig. 24. After the second multilayer (again, with four layers' worth of tubes) is completed, the epoxy is left to set. Once the epoxy has set, the combs are removed from the chamber (see Fig. 27). A schematic for an entire chamber (in this case, BMG-2A-14) can be seen in Fig. 28. The positions of tubes for each chamber can be seen in Figs. 29–36. Also noted in the figures is where "placeholder" tube ends were installed, marked with the darker cicles. These dummy endplugs can be seen in the bottom of Fig. 21.

Not reviewed, for internal circulation only

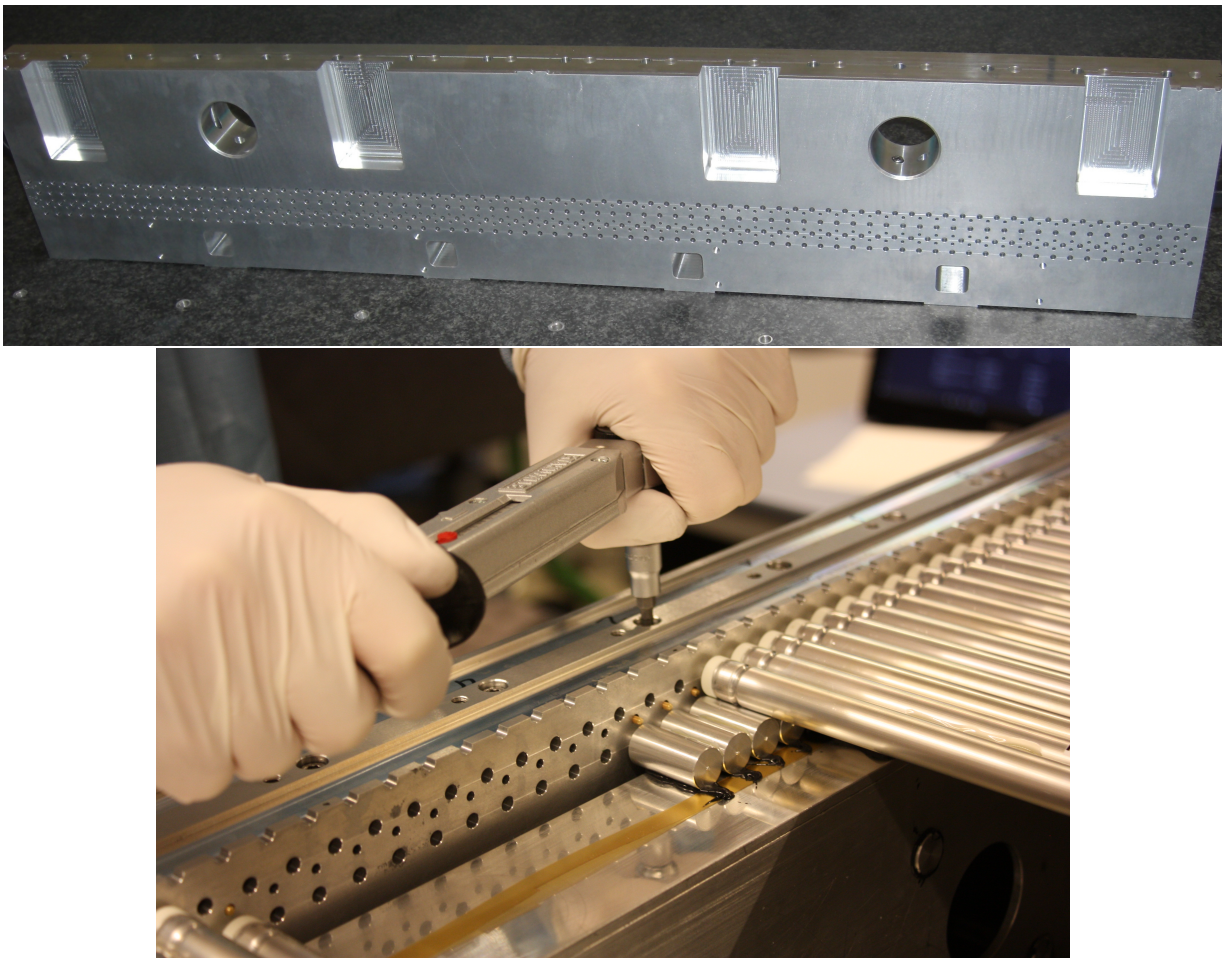

Figure 21: Alignment comb (top) used to align the tubes in each layer. The larger holes align the tubes, while the smaller holes guide the grounding contacts. Alignment comb in use with tubes installed (bottom).

Not reviewed, for internal circulation only

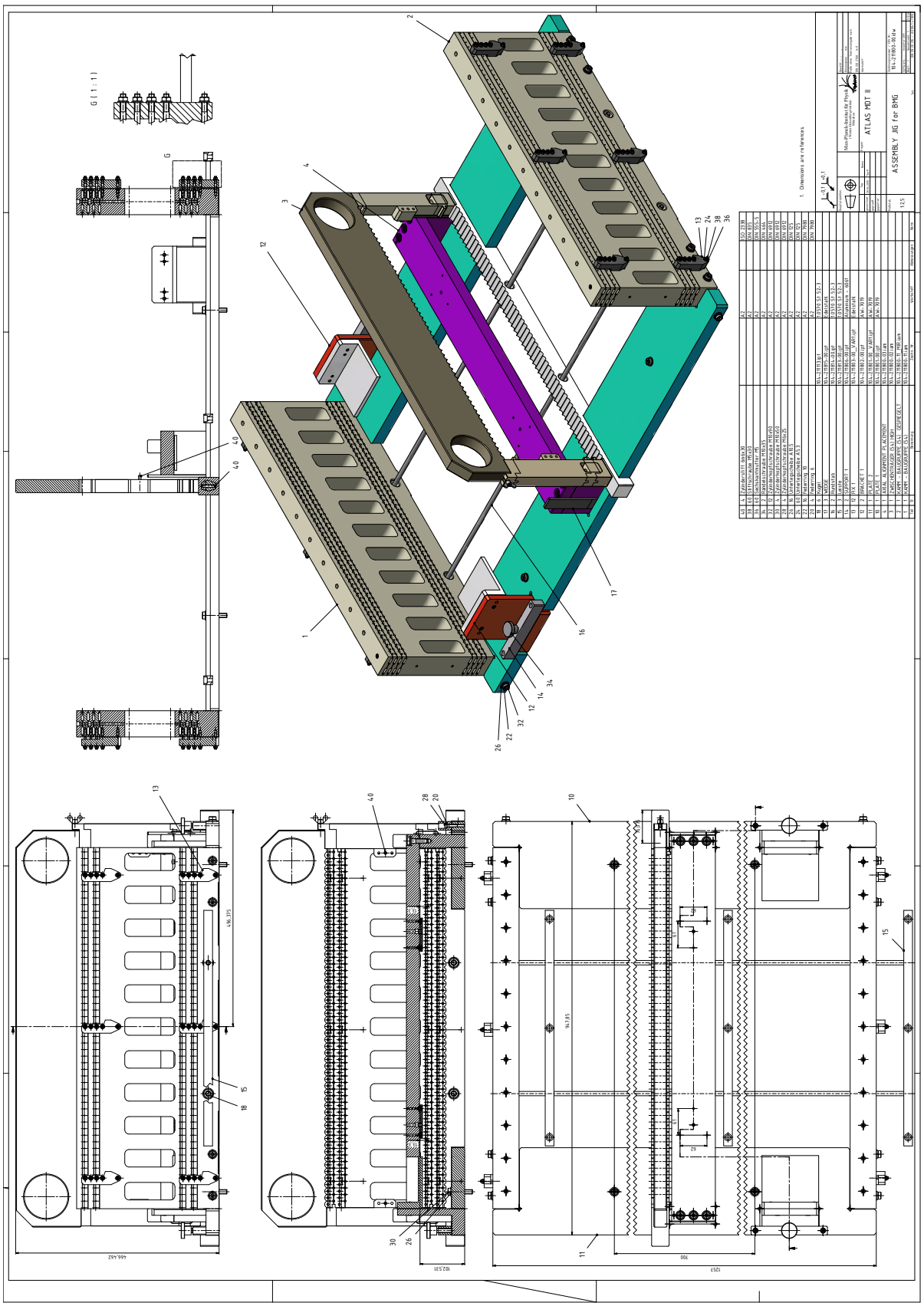

Figure 22: Schematic of the complete alignment jig setup. This includes the comb for holding the tubes in place, the template for placing the alignment platforms, and the weight used to keep the tubes in place as the epoxy sets.

Not reviewed, for internal circulation only

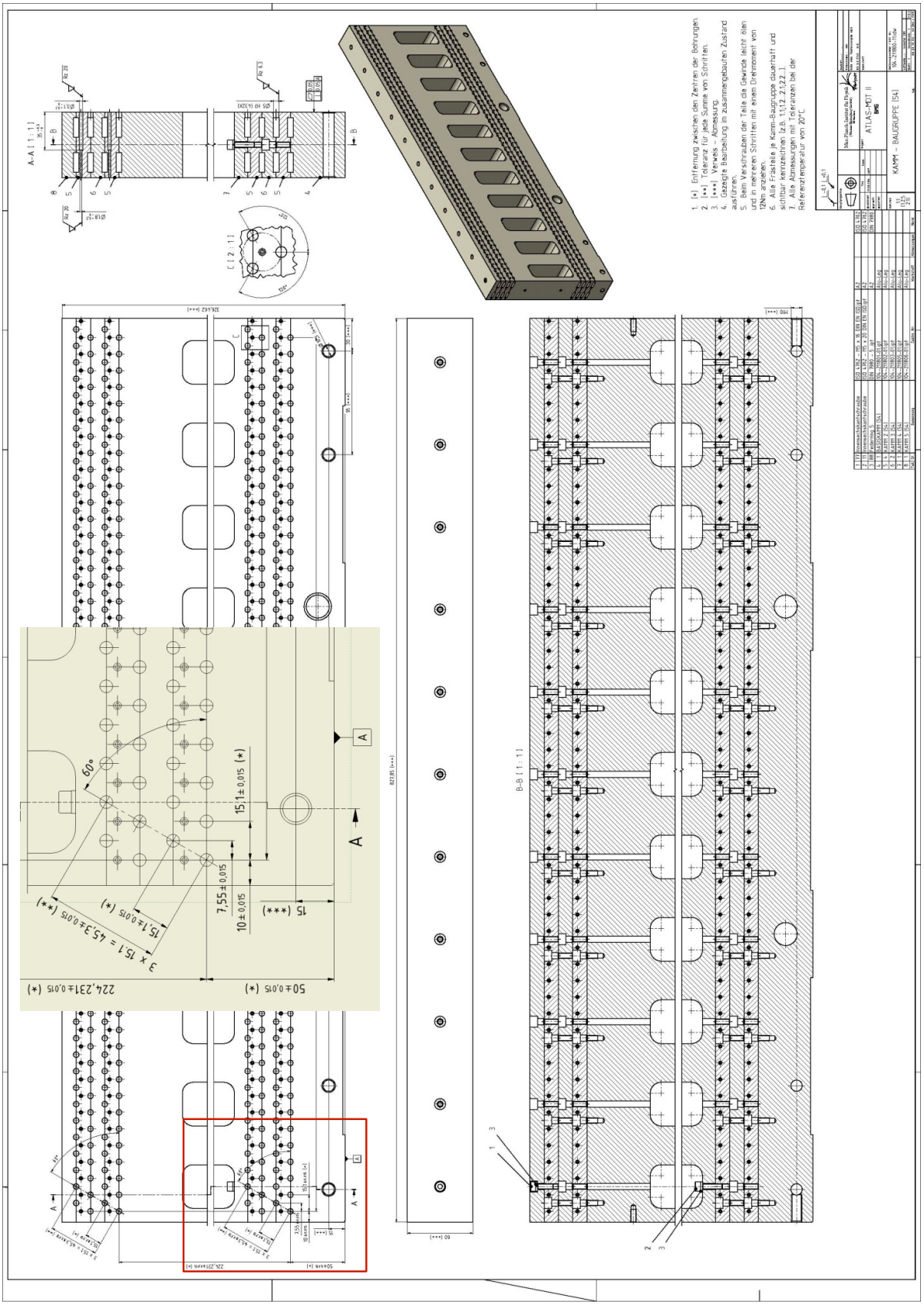

Figure 23: Schematic of the alignment combs. Inset is a closeup of the boxed area, showing the orientation of the tube placement grooves and ground pin holes.

Not reviewed, for internal circulation only

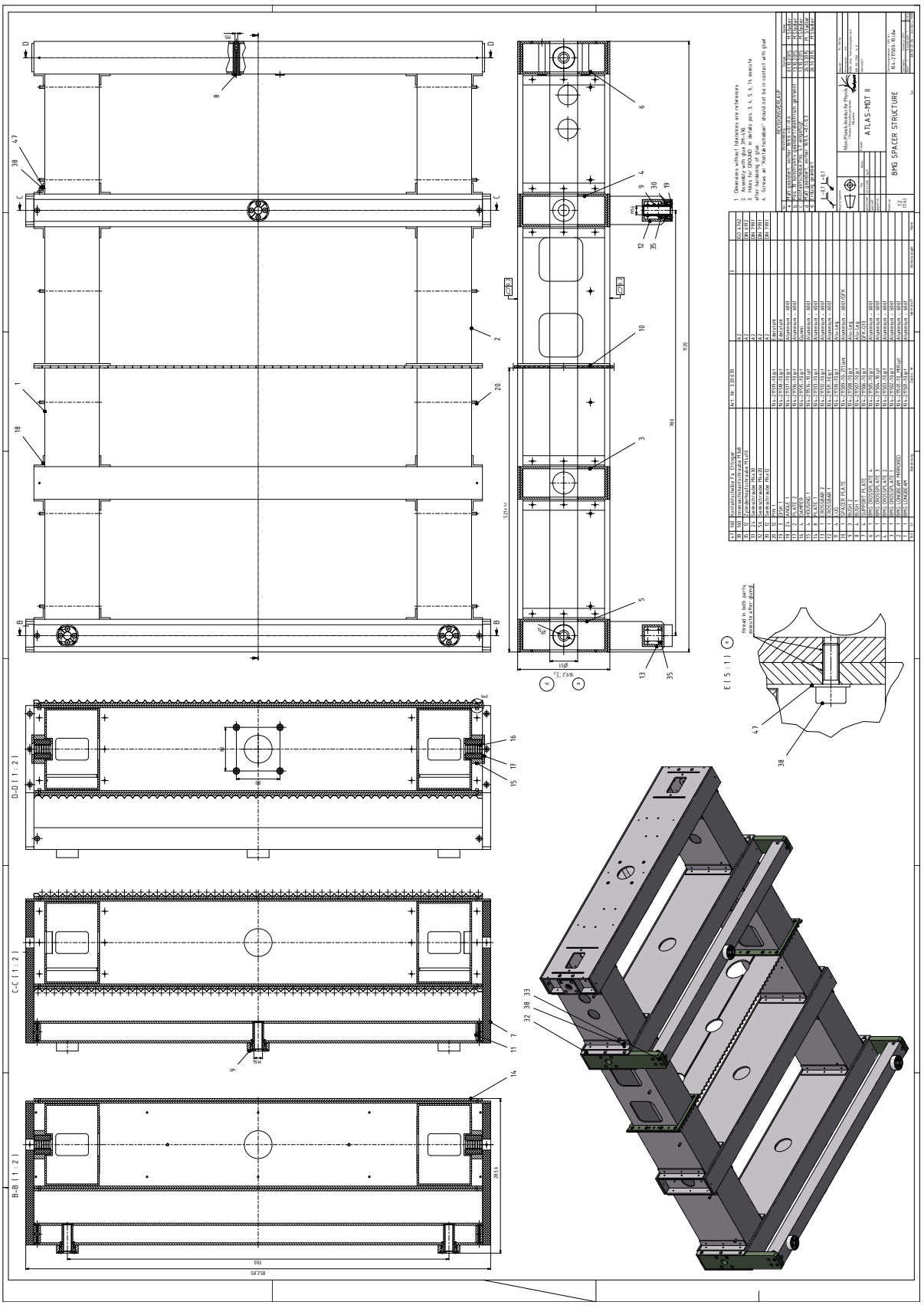

Figure 24: Schematic of the spacer and alignment frame.

Not reviewed, for internal circulation only

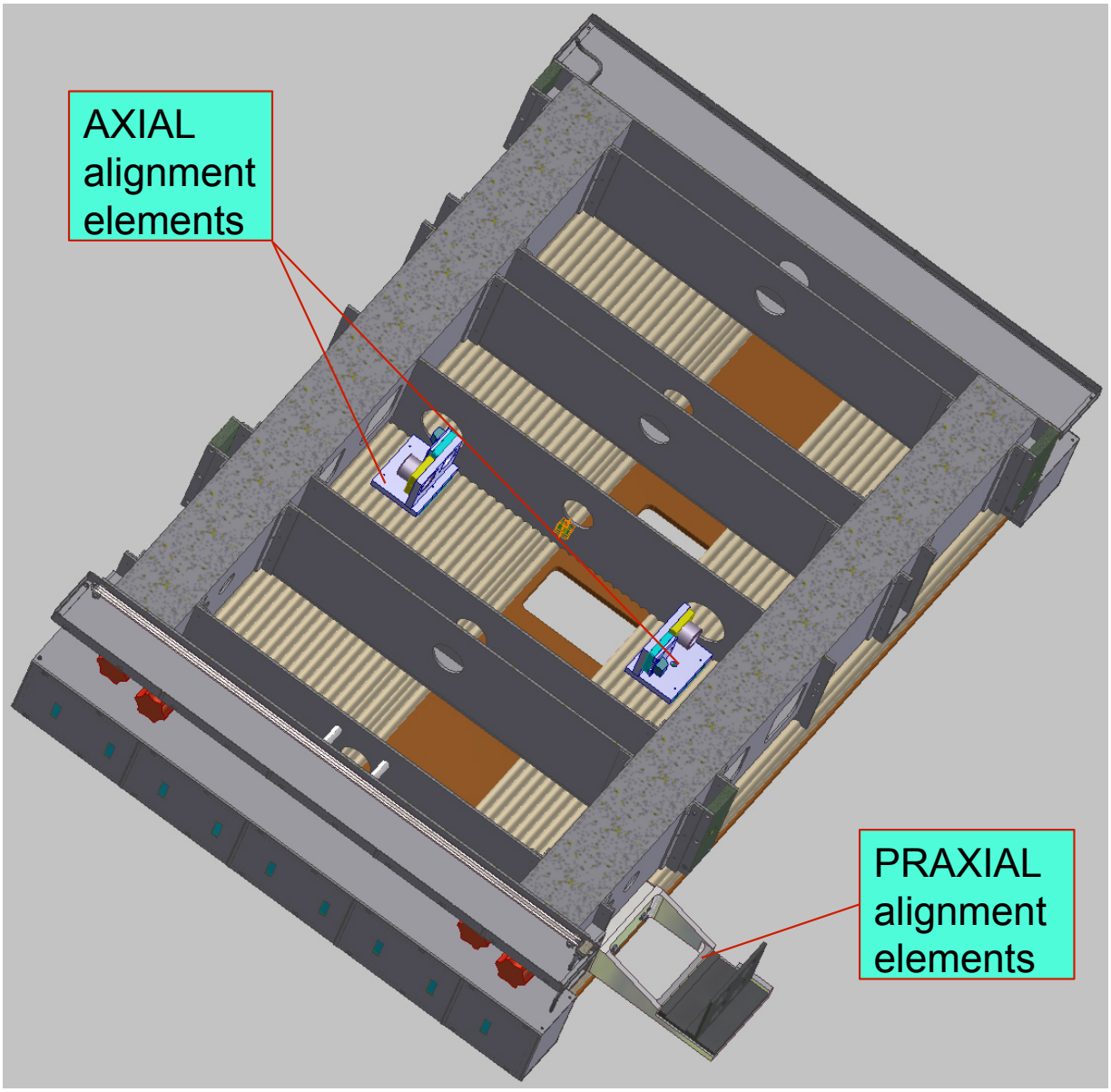

Figure 25: Chamber with the location of the axial (interior to the chamber) and praxial (exterior to the chamber) alignment elements highlighted.

Figure 26: The first layer of tubes is set down using tube alignment combs (top left) and completed (top right). Epoxy is laid down to prepare for the second layer of tubes (bottom left) and the second layer is started (bottom right). The small laptop is used to record the tube numbers as they are installed in the chamber.

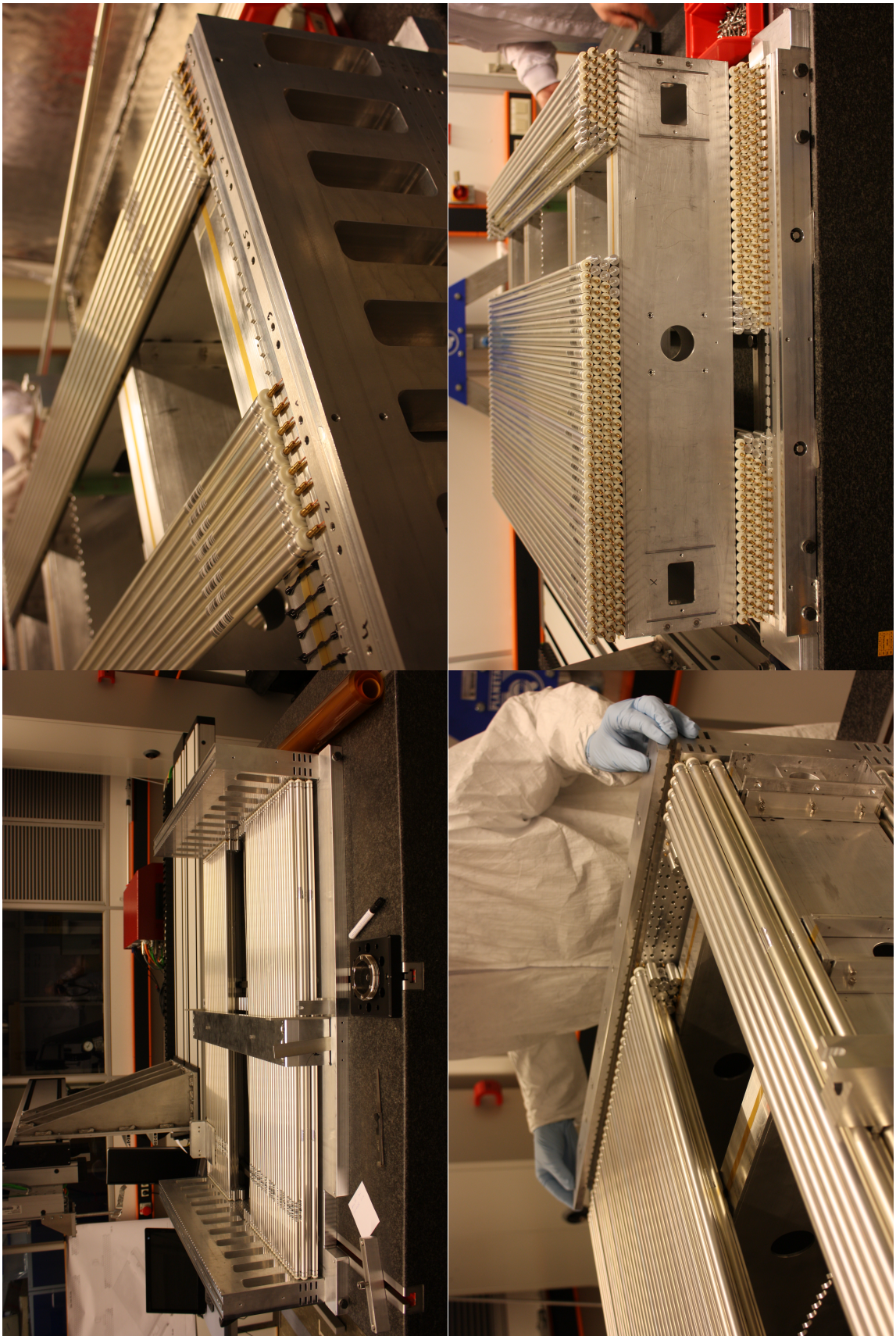

Figure 27: The alignment frame between the two multilayers is put in pace (top left) and the second multilayer is started (top right). The second multilayer is completed (bottom left). Once the epoxy has set, the combs are removed to show the completed chamber (bottom right).

Not reviewed, for internal circulation only

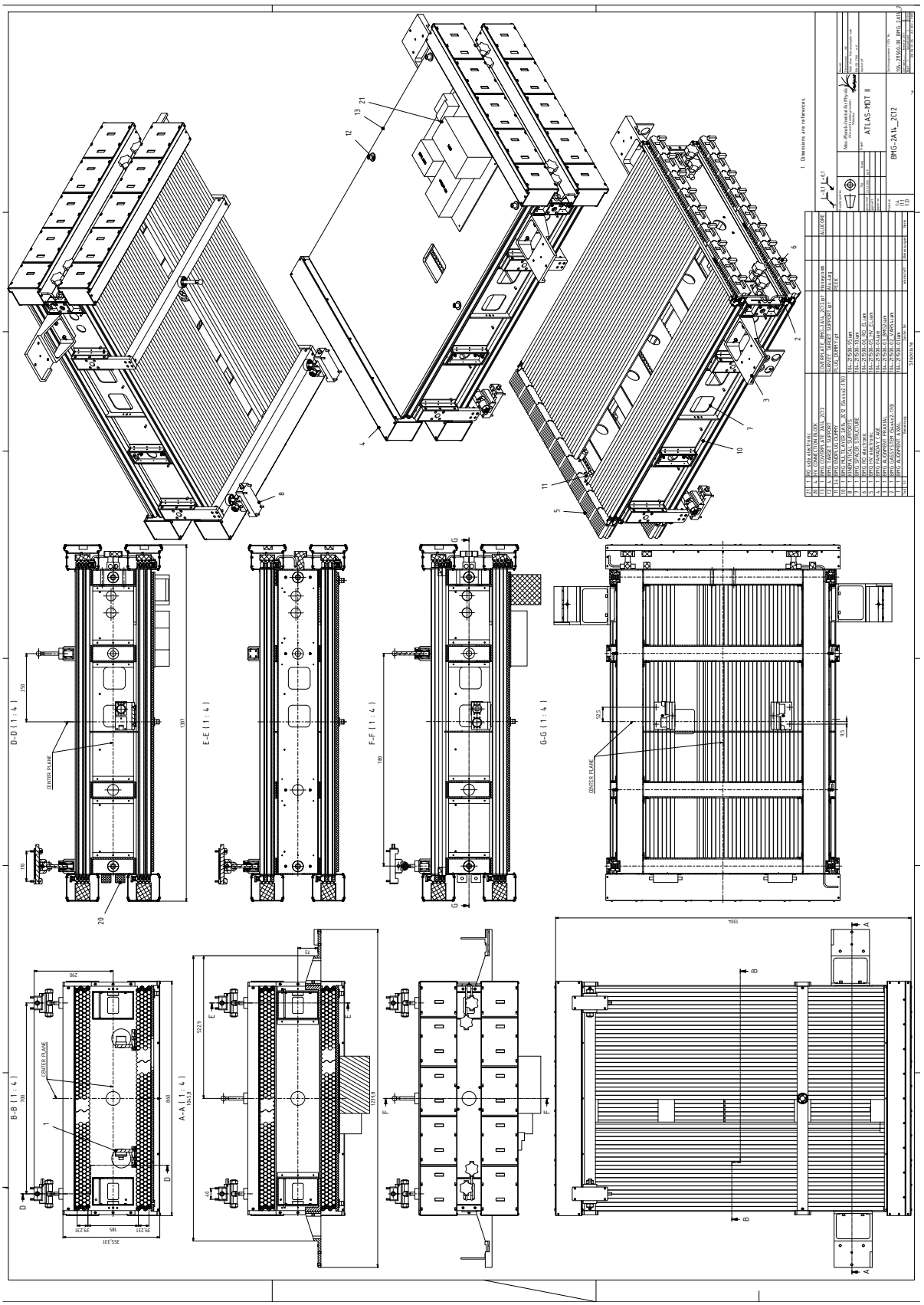

Figure 28: Complete schematic of the BMG-2A-14 chamber.

Not reviewed, for internal circulation only

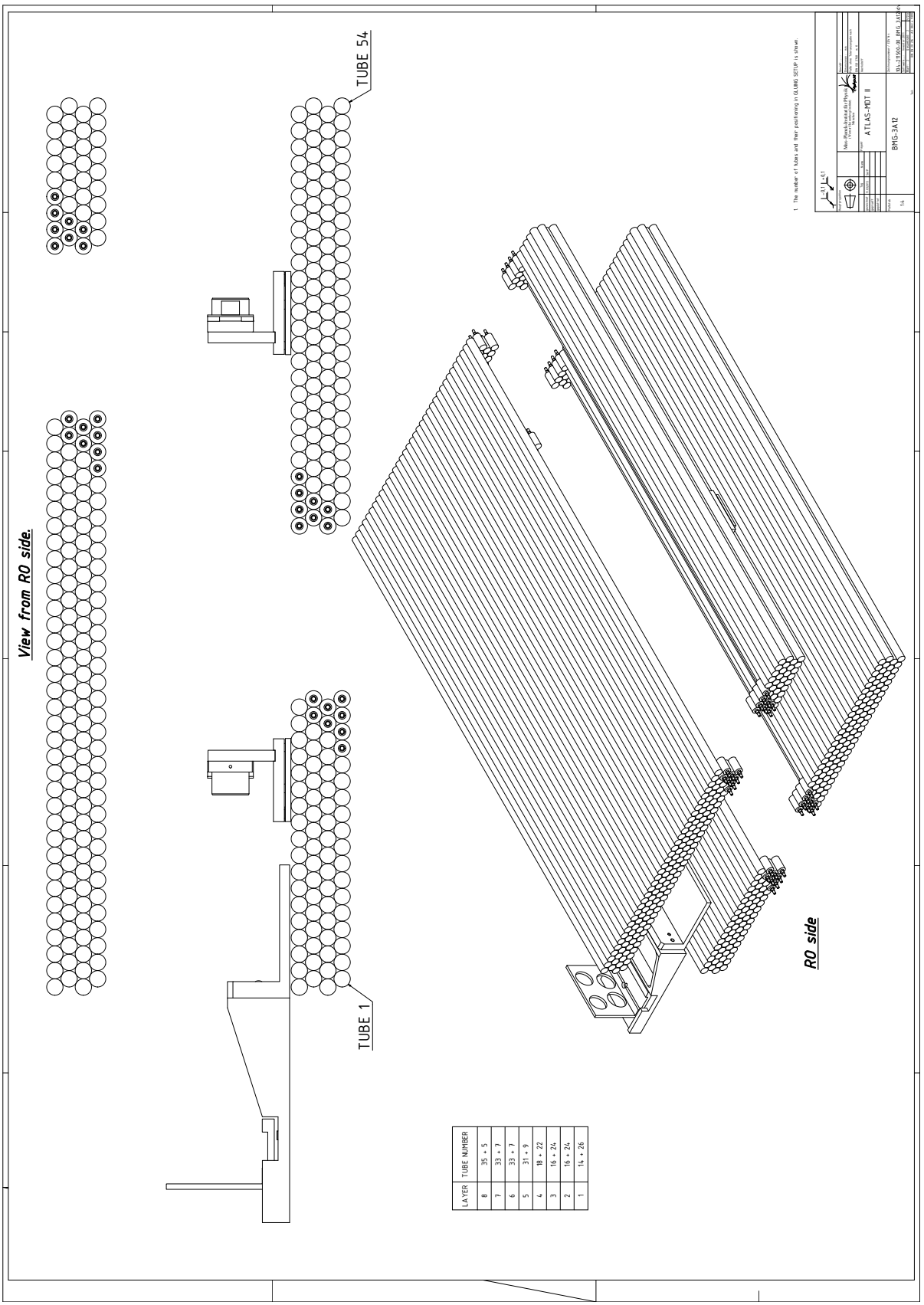

Figure 29: Schematic of the tube locations for BMG-3A-12.

Not reviewed, for internal circulation only

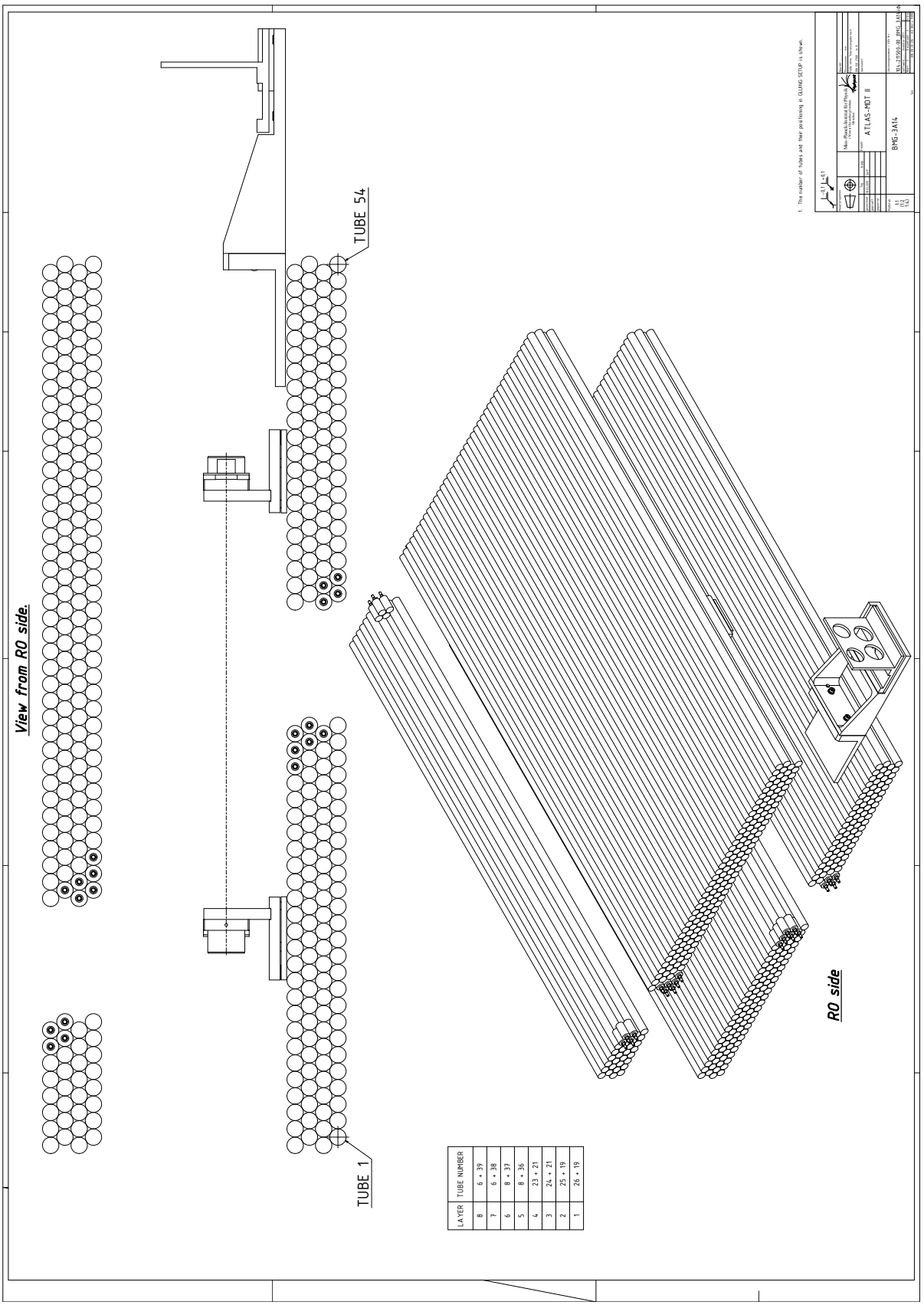

Figure 30: Schematic of the tube locations for BMG-3A-14.

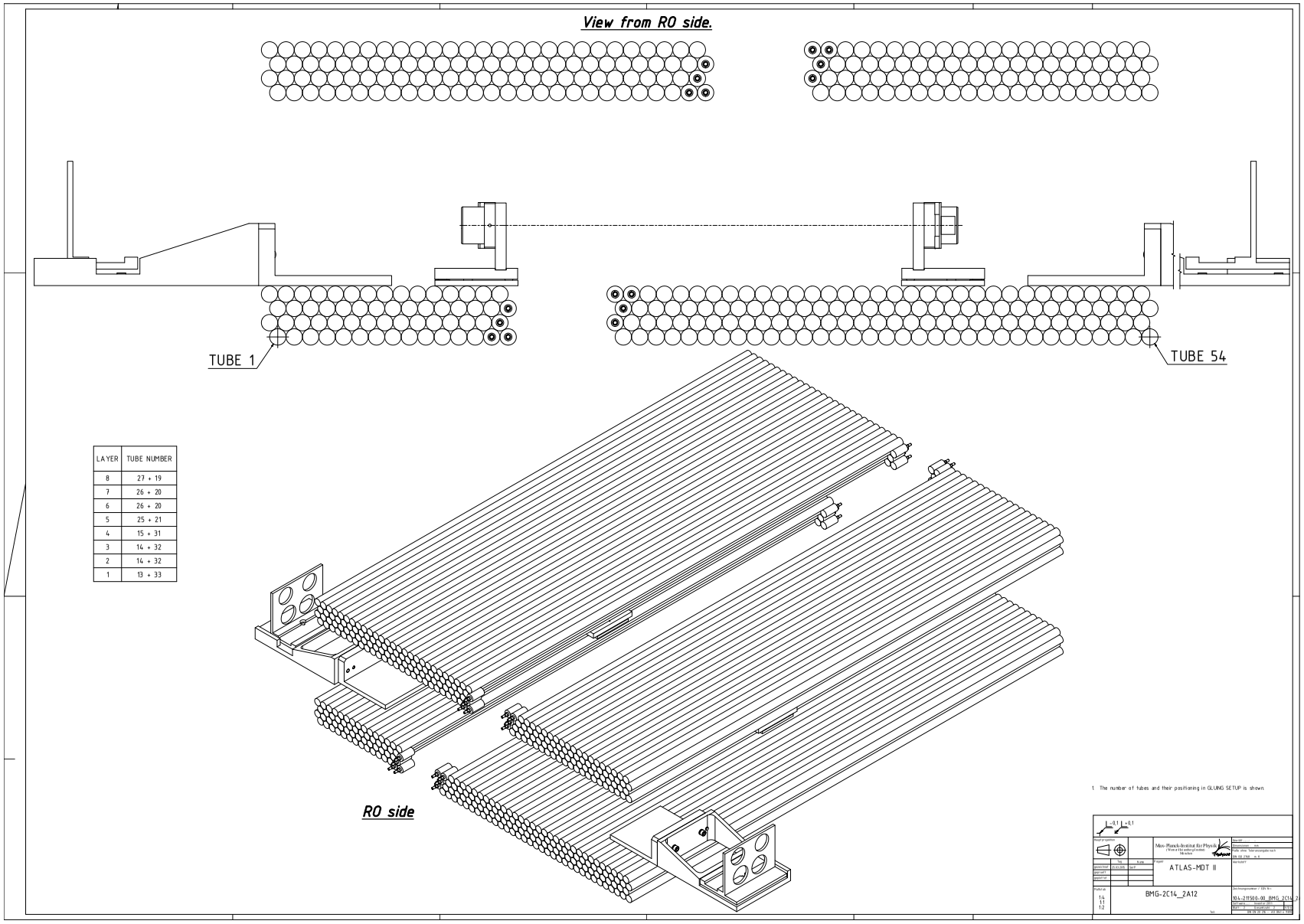

Figure 31: Schematic of the tube locations for BMG-2A-12 and BMG-2C-14.

Not reviewed, for internal circulation only

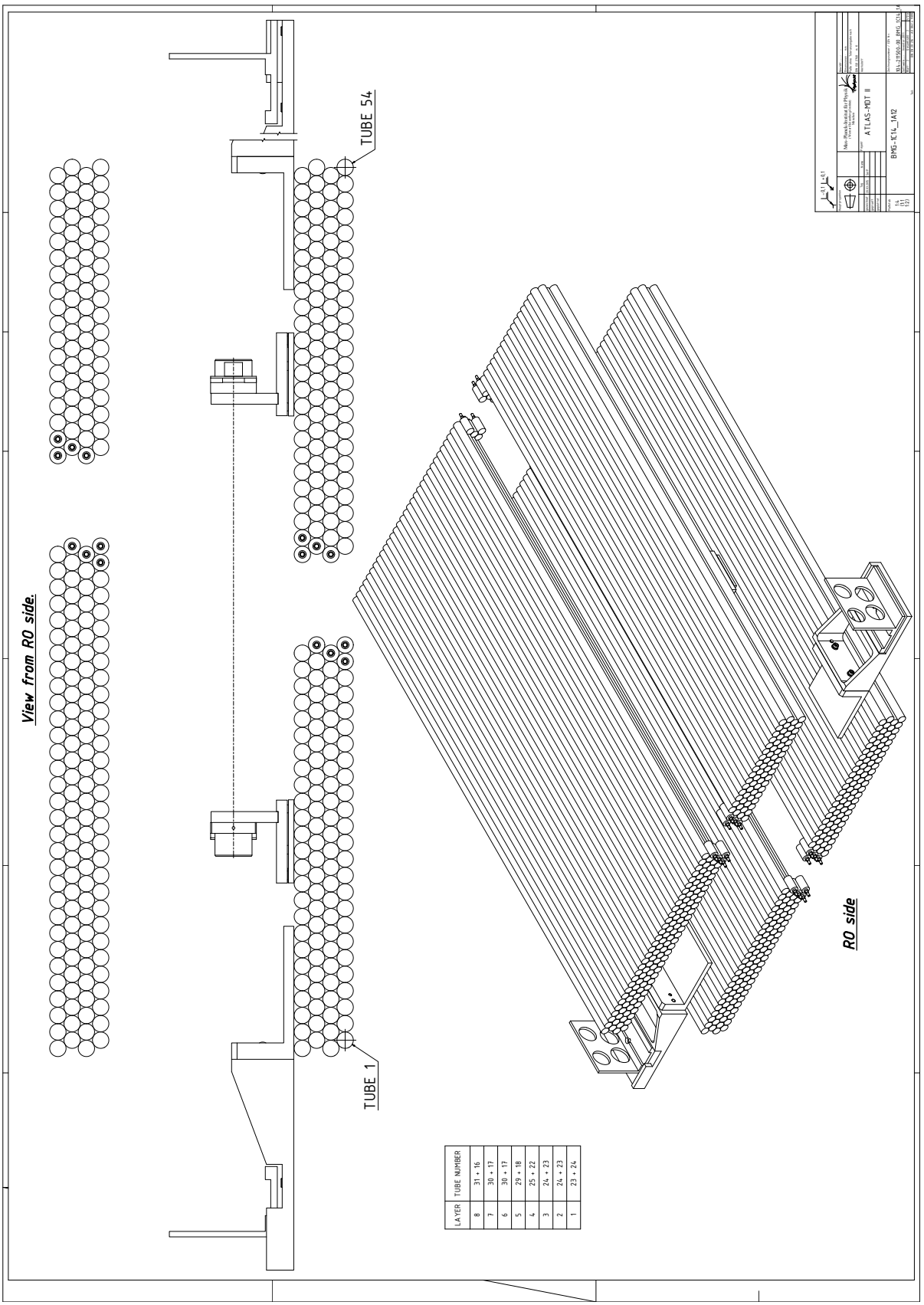

Figure 32: Schematic of the tube locations for BMG-1A-12 and BMG-1C-14.

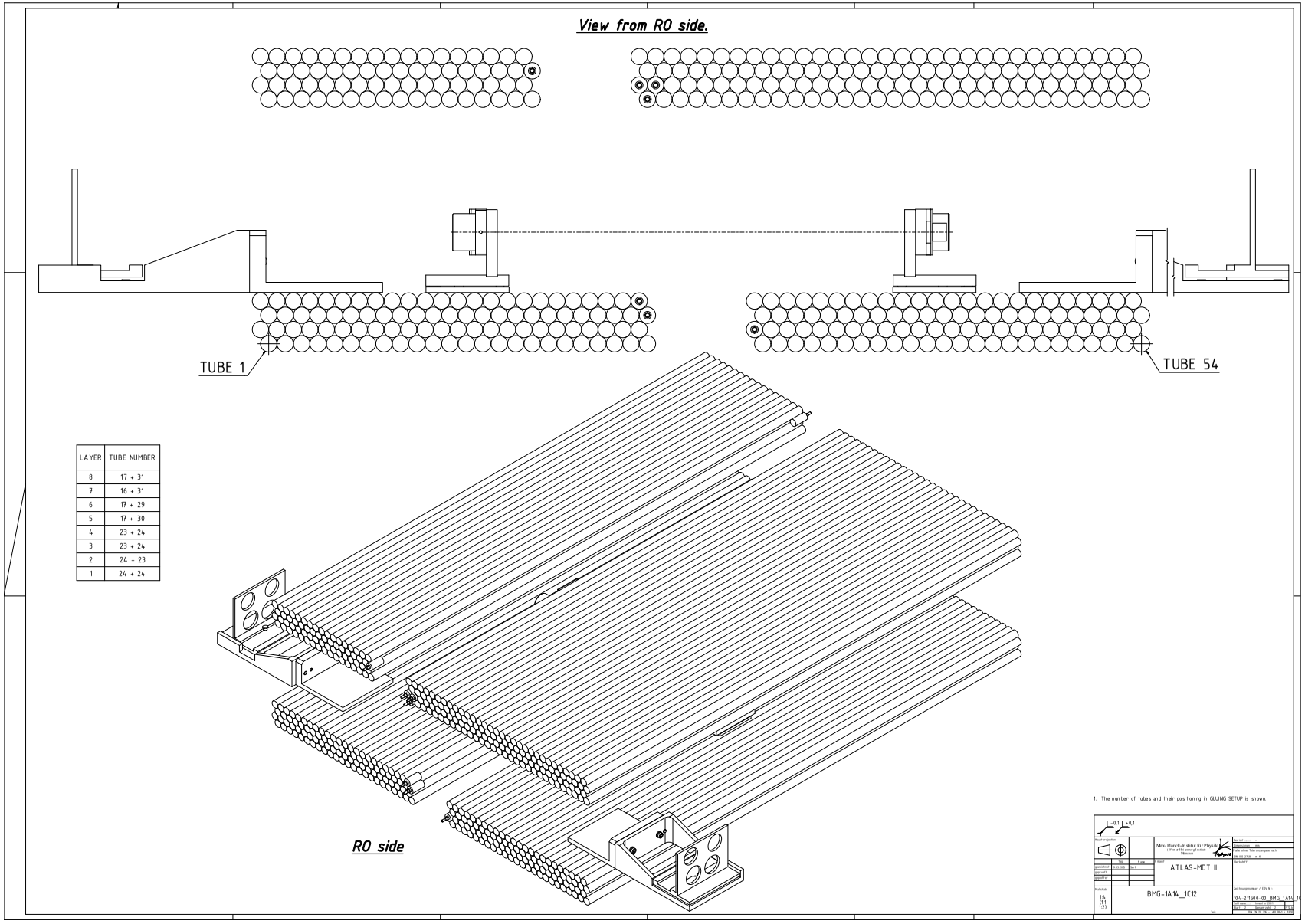

Figure 33: Schematic of the tube locations for BMG-1C-12 and BMG-1A-14.

Not reviewed, for internal circulation only

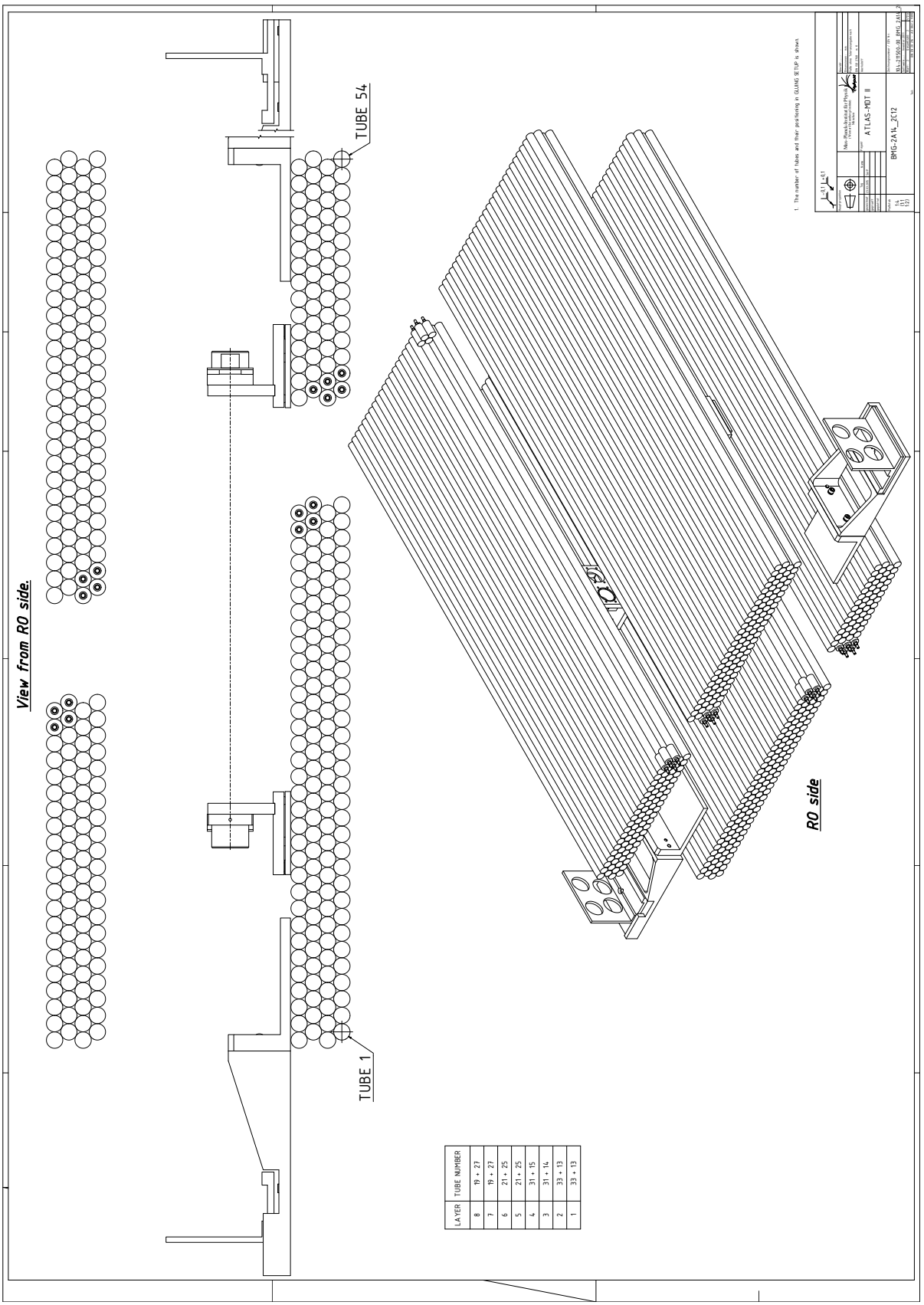

Figure 34: Schematic of the tube locations for BMG-2C-12 and BMG-2A-14.

Not reviewed, for internal circulation only

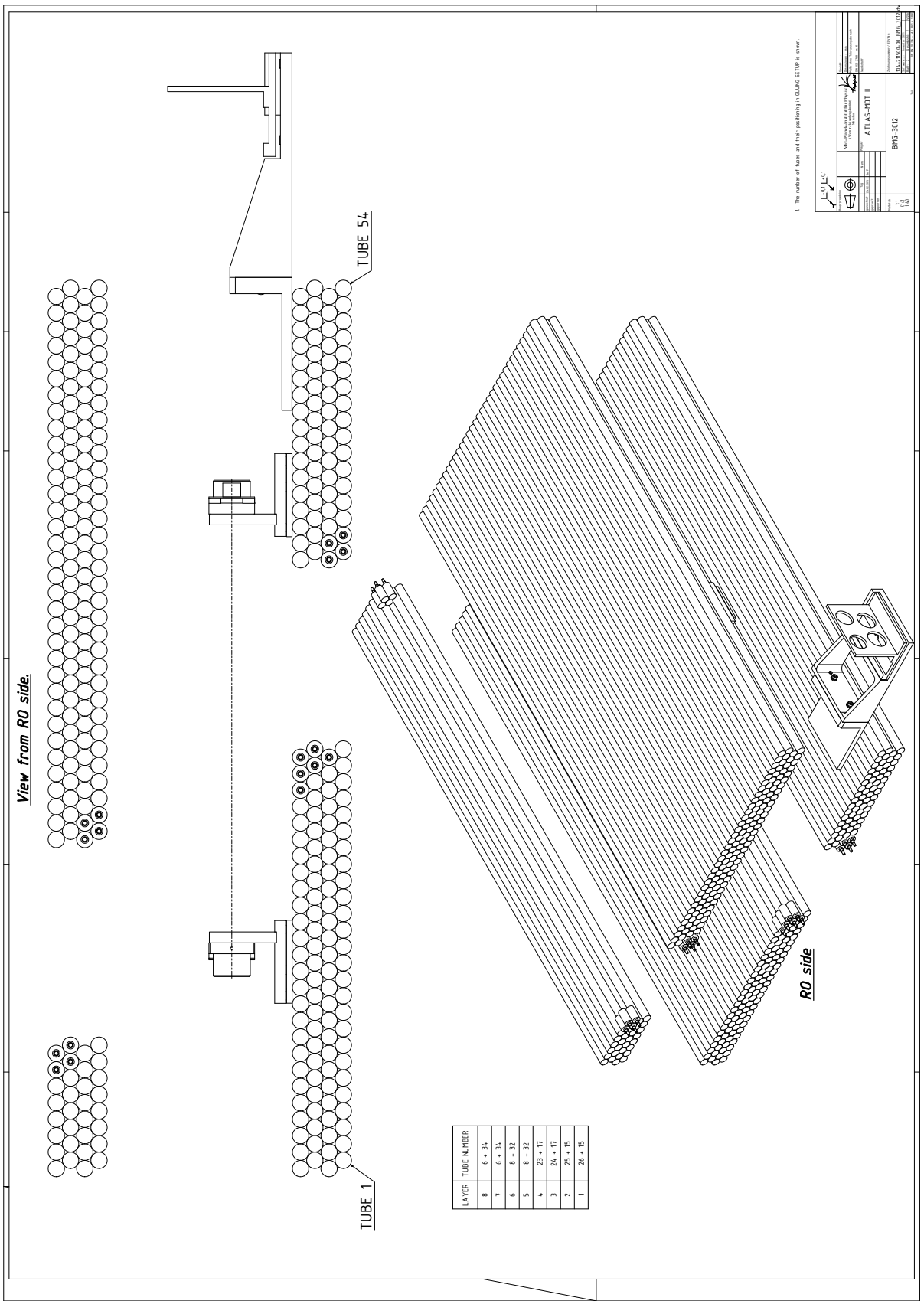

Figure 35: Schematic of the tube locations for BMG-3C-12.

Not reviewed, for internal circulation only

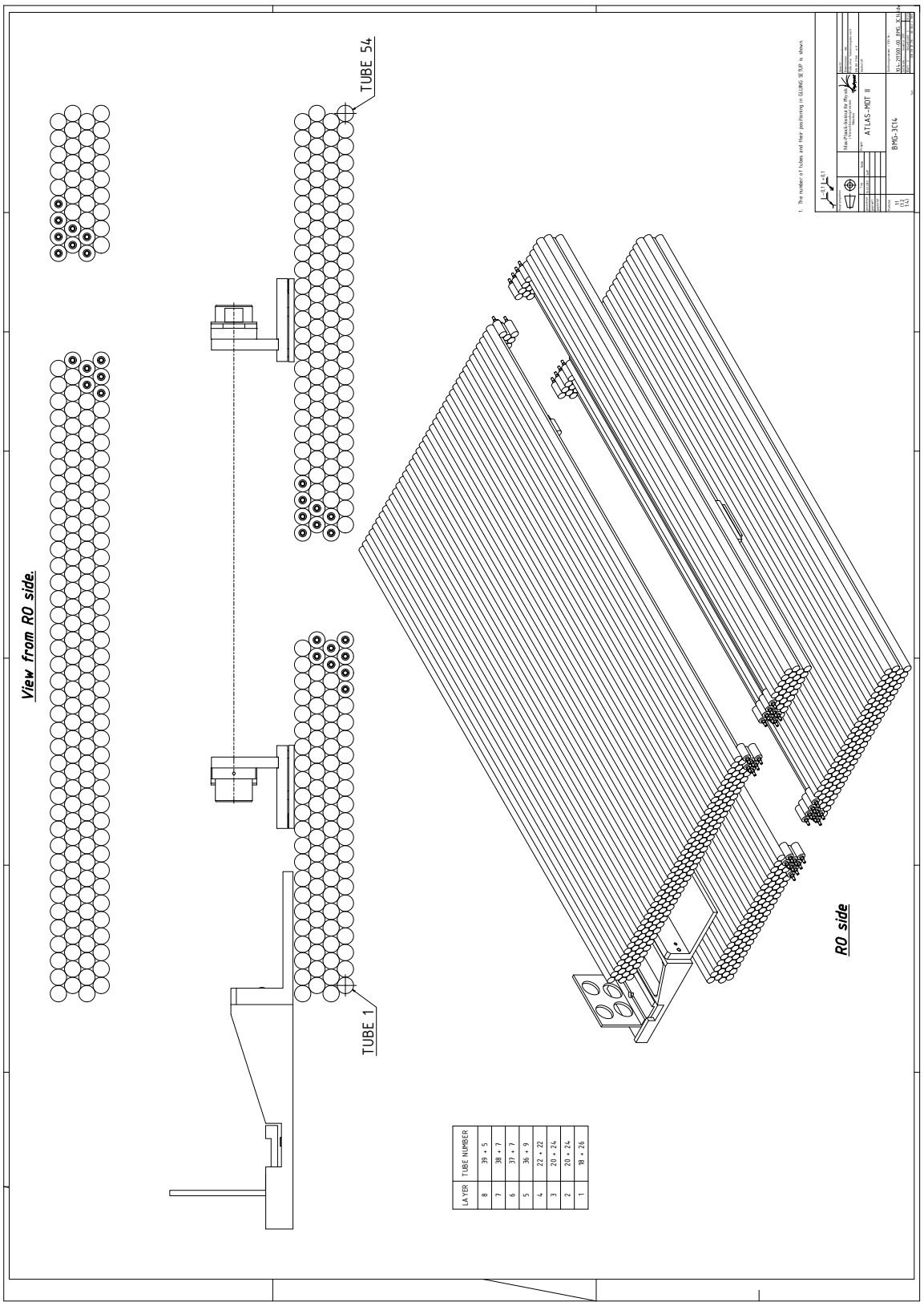

Figure 36: Schematic of the tube locations for BMG-3C-14.

Not reviewed, for internal circulation only

7 sMDT BMG Chamber Testing

Once the tubes have been installed, the physical parameters of the chamber are measured and confirmed to ensure that the chamber's detection is within specifications. After a chamber is confirmed to be within specified parameters, the electronics are installed and tested as well.

7.1 Wire Position Measurement and Fitting

The concentricity between the wire and the tube endplug allows for a measurement of the wire position by measuring the position of the endplug for each tube (see Fig. 37). This is then fit to the ideal grid positions of the wires. The measurement is done on both sides of the chamber (the RO and HV side). Each side is fit separately first, then a combined fit is done to check for any overall torsion on the chamber. The results of these fits can be seen in Tab. 8, the torsion on the chambers can be seen in Tab. 9, and the residuals can be seen in Tab. 10.

Important to this is a measurement of the grid created by the combs as well in the placement of the wires. These were also run through the fit to confirm that each side was within specifications. The fitted comb parameters can be seen in Tab. 6, and include the pitch in z, y, the size of the multilayer in y, the shift of the multilayer in z, and the RMS and σ of the z- and y-residuals. The RMS and σ of the z- and y-residuals of the fitted distributions are shown in Tab. 7.

The first constructed chamber, BMG-3C-12, has the largest spread in the y-, z-, and r-residuals (Tab. 10). As experience was gained in the layering of the tubes, the spread of the residuals decreased. By the seventh chamber (BMG-2C-14), the spread of the residuals decreased by almost a factor of two. Even the largest spread, however, has values which are all within the specified values for the sMDT chambers.

The fitted chamber parameters (Tab. 8), as with the combs, include the pitch in z, y, the size of the multilayer in y, the shift of the multilayer in z, and the RMS and σ of the z- and y-residuals. Every chamber constructed is within nominal values. The RMS and σ of the z- and y-residuals of the fitted distributions are shown in Tab. 10. Overall, the RMS and σ of these decrease as more chambers were constructed. The residuals for a combined fit over all chambers is shown in Fig. 11. A combined figure including all chambers can be seen in Figs. 38–40. The torsion on each chamber (Tab. 9) are well below the tolerances of ATLAS, and are also below 0.5 milliradians.

Furthermore, BMG-3C-12 (i.e., the first constructed chamber) utilized parts from the older chamber production run. For example, the gas seals were from a previous production of MDT chambers, and the tubes were cut down from older tubes which were 2130 mm in length. This chamber showed unacceptable chamber gas leak rates as well as noise rates in cosmic tests and is rejected. A new BMG-3C-12 was created instead, and the original (now called Module 0) is used for tests of the physical tolerances of the sMDT chambers.

Not reviewed, for internal circulation only

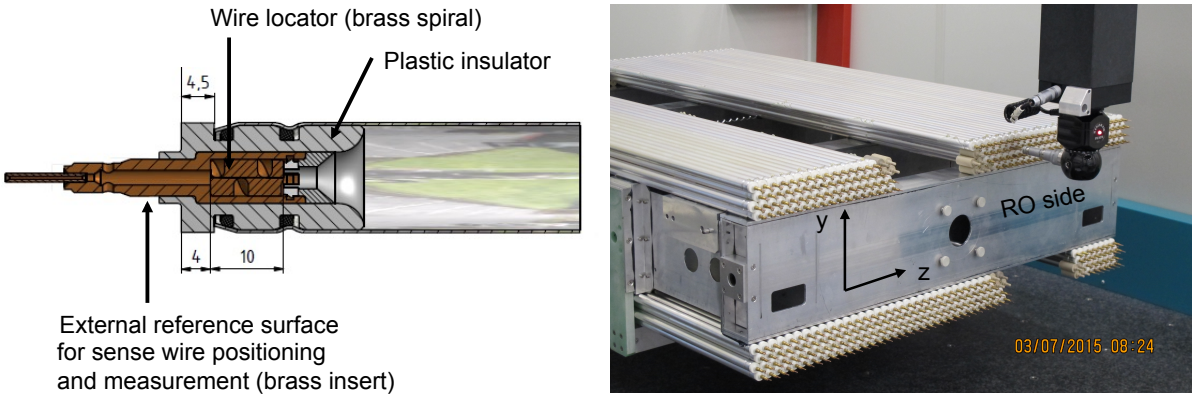

Figure 37: Cutaway of tube endplug (left), and wire measurement using endplugs (right).

Table 6: Fitted comb parameters.

	Comb Measurement
z pitch [mm]	15.0995 ± 0.00001
y pitch [mm]	13.0768 ± 0.0001
Multilayer Δz [mm]	−0.0148 ± 0.0003
Multilayer Δy [mm]	184.9930 ± 0.0006
RMS (σ) z [mm]	0.0066 (0.0066)
RMS (σ) y [mm]	0.0038 (0.0037)
RMS (σ) r [mm]	0.0059 (0.0058)

Not reviewed, for internal circulation only

Table 7: Combined fitted comb position residuals in z, y, and $r = \sqrt{z^2 + y^2}$.

	z-Residuals	y-Residuals	r-Residuals
Comb			

Not reviewed, for internal circulation only

Table 8: Fitted chamber parameters.

BMG-3C-14	RO-Side	HV-Side	RO and HV Combined Fit	Average
z pitch [mm]	15.0991 ± 0.00001	15.0990 ± 0.00001	15.0990 ± 0.00001	15.0991
y pitch [mm]	13.0790 ± 0.0002	13.0786 ± 0.0001	13.0788 ± 0.0001	13.082
Multilayer Δz [mm]	−0.0089 ± 0.0002	−0.0052 ± 0.0004	−0.0018 ± 0.0003	−0.006
Multilayer Δy [mm]	184.9870 ± 0.0004	184.9866 ± 0.0007	184.9868 ± 0.0005	184.980
RMS (σ) z [mm]	0.0047 (0.0039)	0.0057 (0.0050)	0.0061 (0.0052)	0.0076 (0.0062)
RMS (σ) y [mm]	0.0069 (0.0060)	0.0069 (0.0059)	0.0070 (0.0062)	0.0101 (0.0084)
RMS (σ) r [mm]	0.0050 (0.0041)	0.0053 (0.0044)	0.0056 (0.0049)	0.0105 (0.0069)
BMG-3C-12	RO-Side	HV-Side	RO and HV Combined Fit	Average
z pitch [mm]	15.0991 ± 0.00001	15.0990 ± 0.00001	15.0990 ± 0.00001	15.0991
y pitch [mm]	13.0792 ± 0.0002	13.0797 ± 0.0001	13.0795 ± 0.0001	13.082
Multilayer Δz [mm]	−0.0103 ± 0.0002	0.0052 ± 0.0004	−0.0026 ± 0.0003	−0.006
Multilayer Δy [mm]	184.9882 ± 0.0007	184.9967 ± 0.0007	184.9925 ± 0.0005	184.980
RMS (σ) z [mm]	0.0062 (0.0047)	0.0060 (0.0046)	0.0062 (0.0056)	0.0076 (0.0062)
RMS (σ) y [mm]	0.0080 (0.0045)	0.0078 (0.0062)	0.0080 (0.0056)	0.0101 (0.0084)
RMS (σ) r [mm]	0.0082 (0.0051)	0.0058 (0.0070)	0.0077 (0.0052)	0.0105 (0.0069)
BMG-3A-14	RO-Side	HV-Side	RO and HV Combined Fit	Average
z pitch [mm]	15.0993 ± 0.00001	15.0992 ± 0.00001	15.0992 ± 0.00001	15.0991
y pitch [mm]	13.0929 ± 0.0002	13.0838 ± 0.0001	13.0883 ± 0.0001	13.082
Multilayer Δz [mm]	−0.0117 ± 0.0002	−0.0044 ± 0.0004	−0.0081 ± 0.0003	−0.006
Multilayer Δy [mm]	184.9539 ± 0.0004	184.9758 ± 0.0007	184.9643 ± 0.0005	184.980
RMS (σ) z [mm]	0.0082 (0.0063)	0.0054 (0.0041)	0.0070 (0.0051)	0.0076 (0.0062)
RMS (σ) y [mm]	0.0190 (0.0146)	0.0092 (0.0067)	0.0153 (0.0110)	0.0101 (0.0084)
RMS (σ) r [mm]	0.0102 (0.0096)	0.0066 (0.0049)	0.0085 (0.0074)	0.0105 (0.0069)
BMG-3A-12	RO-Side	HV-Side	RO and HV Combined Fit	Average
z pitch [mm]	15.0991 ± 0.00001	15.0990 ± 0.00001	15.0990 ± 0.00001	15.0991
y pitch [mm]	13.0907 ± 0.0002	13.0841 ± 0.0001	13.0877 ± 0.0001	13.082
Multilayer Δz [mm]	−0.0164 ± 0.0002	−0.0005 ± 0.0004	−0.0085 ± 0.0003	−0.006
Multilayer Δy [mm]	184.9667 ± 0.0004	184.9731 ± 0.0007	184.9697 ± 0.0005	184.980
RMS (σ) z [mm]	0.0078 (0.0061)	0.0075 (0.0053)	0.0080 (0.0061)	0.0076 (0.0062)
RMS (σ) y [mm]	0.0143 (0.0100)	0.0111 (0.0101)	0.0126 (0.0112)	0.0101 (0.0084)
RMS (σ) r [mm]	0.0101 (0.0065)	0.0089 (0.0061)	0.0099 (0.0070)	0.0105 (0.0069)
BMG-2C-14	RO-Side	HV-Side	RO and HV Combined Fit	Average
z pitch [mm]	15.0993 ± 0.00001	15.0990 ± 0.00001	15.0992 ± 0.00001	15.0991
y pitch [mm]	13.0873 ± 0.0001	13.0805 ± 0.0001	13.0839 ± 0.0001	13.082
Multilayer Δz [mm]	−0.0068 ± 0.0002	−0.0050 ± 0.0004	−0.0059 ± 0.0003	−0.006
Multilayer Δy [mm]	184.9763 ± 0.0004	184.9855 ± 0.0007	184.9809 ± 0.0005	184.980
RMS (σ) z [mm]	0.0092 (0.0068)	0.0076 (0.0048)	0.0086 (0.0059)	0.0076 (0.0062)
RMS (σ) y [mm]	0.0124 (0.0100)	0.0078 (0.0054)	0.0110 (0.0085)	0.0101 (0.0084)
RMS (σ) r [mm]	0.0116 (0.0078)	0.0078 (0.0053)	0.0099 (0.0068)	0.0105 (0.0069)

Not reviewed, for internal circulation only

Table 8: Fitted chamber parameters (continued).

BMG-2C-12	RO-Side	HV-Side	RO and HV Combined Fit	Average
z pitch [mm]	15.0992 ± 0.00001	15.0991 ± 0.00001	15.0992 ± 0.00001	15.0991
y pitch [mm]	13.0819 ± 0.0001	13.0779 ± 0.0001	13.0799 ± 0.0001	13.082
Multilayer Δz [mm]	−0.0089 ± 0.0002	−0.0078 ± 0.0004	−0.0084 ± 0.0003	−0.006
Multilayer Δy [mm]	184.9849 ± 0.0004	184.9889 ± 0.0007	184.9869 ± 0.0005	184.980
RMS (σ) z [mm]	0.0084 (0.0075)	0.0046 (0.0038)	0.0068 (0.0055)	0.0076 (0.0062)
RMS (σ) y [mm]	0.0125 (0.0106)	0.0056 (0.0051)	0.0102 (0.0082)	0.0101 (0.0084)
RMS (σ) r [mm]	0.0098 (0.0084)	0.0048 (0.0043)	0.0079 (0.0065)	0.0105 (0.0069)
BMG-2A-14	RO-Side	HV-Side	RO and HV Combined Fit	Average
z pitch [mm]	15.0991 ± 0.00001	15.0991 ± 0.00001	15.0991 ± 0.00001	15.0991
y pitch [mm]	13.0794 ± 0.0002	13.0784 ± 0.0001	13.0790 ± 0.0001	13.082
Multilayer Δz [mm]	−0.0077 ± 0.0002	−0.0037 ± 0.0004	−0.0056 ± 0.0003	−0.006
Multilayer Δy [mm]	184.9834 ± 0.0004	184.9384 ± 0.0006	184.9610 ± 0.0005	184.980
RMS (σ) z [mm]	0.0079 (0.0064)	0.0063 (0.0042)	0.0079 (0.0064)	0.0076 (0.0062)
RMS (σ) y [mm]	0.0114 (0.0087)	0.0072 (0.0059)	0.0114 (0.0088)	0.0101 (0.0084)
RMS (σ) r [mm]	0.0098 (0.0075)	0.0060 (0.0044)	0.0099 (0.0076)	0.0105 (0.0069)
BMG-2A-12	RO-Side	HV-Side	RO and HV Combined Fit	Average
z pitch [mm]	15.0993 ± 0.00001	15.0992 ± 0.00001	15.0993 ± 0.00001	15.0991
y pitch [mm]	13.0834 ± 0.0002	13.0793 ± 0.0001	13.0814 ± 0.0001	13.082
Multilayer Δz [mm]	−0.0014 ± 0.0002	−0.0123 ± 0.0004	−0.0085 ± 0.0003	−0.006
Multilayer Δy [mm]	184.9840 ± 0.0004	184.9784 ± 0.0007	184.9812 ± 0.0005	184.980
RMS (σ) z [mm]	0.0063 (0.0058)	0.0081 (0.0072)	0.0072 (0.0062)	0.0076 (0.0062)
RMS (σ) y [mm]	0.0095 (0.0078)	0.0098 (0.0067)	0.0111 (0.0090)	0.0101 (0.0084)
RMS (σ) r [mm]	0.0079 (0.0070)	0.0109 (0.0076)	0.0102 (0.0071)	0.0105 (0.0069)
BMG-1C-14	RO-Side	HV-Side	RO and HV Combined Fit	Average
z pitch [mm]	15.0992 ± 0.00001	15.0991 ± 0.00001	15.0992 ± 0.00001	15.0991
y pitch [mm]	13.0816 ± 0.0002	13.0802 ± 0.0001	13.0809 ± 0.0001	13.082
Multilayer Δz [mm]	−0.0308 ± 0.0002	0.0126 ± 0.0004	−0.0091 ± 0.0003	−0.006
Multilayer Δy [mm]	184.9766 ± 0.0004	184.9882 ± 0.0007	184.9819 ± 0.0005	184.980
RMS (σ) z [mm]	0.0085 (0.0076)	0.0052 (0.0047)	0.0111 (0.0108)	0.0076 (0.0062)
RMS (σ) y [mm]	0.0102 (0.0089)	0.0066 (0.0056)	0.0098 (0.0094)	0.0101 (0.0084)
RMS (σ) r [mm]	0.0090 (0.0074)	0.065 (0.0046)	0.0118 (0.0109)	0.0105 (0.0069)
BMG-1C-12	RO-Side	HV-Side	RO and HV Combined Fit	Average
z pitch [mm]	15.0994 ± 0.00001	15.0992 ± 0.00001	15.0993 ± 0.00001	15.0991
y pitch [mm]	13.0834 ± 0.0002	13.0793 ± 0.0001	13.0814 ± 0.0001	13.082
Multilayer Δz [mm]	−0.0089 ± 0.0002	0.0015 ± 0.0004	−0.0037 ± 0.0003	−0.006
Multilayer Δy [mm]	184.9874 ± 0.0004	184.9823 ± 0.0006	184.9844 ± 0.0005	184.980
RMS (σ) z [mm]	0.0066 (0.0054)	0.0062 (0.0043)	0.0068 (0.0054)	0.0076 (0.0062)
RMS (σ) y [mm]	0.0111 (0.0090)	0.0075 (0.0072)	0.0108 (0.0098)	0.0101 (0.0084)
RMS (σ) r [mm]	0.0084 (0.0075)	0.0060 (0.0046)	0.0077 (0.0063)	0.0105 (0.0069)

Not reviewed, for internal circulation only

Table 8: Fitted chamber parameters (continued).

BMG-1A-14	RO-Side	HV-Side	RO and HV Combined Fit	Average
z pitch [mm]	15.0994 ± 0.00001	15.0993 ± 0.00001	15.0993 ± 0.00001	15.0991
y pitch [mm]	13.0839 ± 0.0002	13.0886 ± 0.0001	13.0862 ± 0.0001	13.082
Multilayer Δz [mm]	−0.0082 ± 0.0002	0.0377 ± 0.0004	0.0148 ± 0.0003	−0.006
Multilayer Δy [mm]	184.9739 ± 0.0004	184.9986 ± 0.0007	184.9862 ± 0.0005	184.980
RMS (σ) z [mm]	0.0105 (0.0069)	0.0130 (0.0142)	0.0148 (0.0152)	0.0076 (0.0062)
RMS (σ) y [mm]	0.0164 (0.0141)	0.0090 (0.0072)	0.0172 (0.0166)	0.0101 (0.0084)
RMS (σ) r [mm]	0.0128 (0.0095)	0.0124 (0.0122)	0.0170 (0.0159)	0.0105 (0.0069)
BMG-1A-12	RO-Side	HV-Side	RO and HV Combined Fit	Average
z pitch [mm]	15.0991 ± 0.00001	15.0991 ± 0.00001	15.0991 ± 0.00001	15.0991
y pitch [mm]	13.0776 ± 0.0002	13.0819 ± 0.0001	13.0798 ± 0.0001	13.082
Multilayer Δz [mm]	−0.0126 ± 0.0002	−0.0007 ± 0.0004	−0.0067 ± 0.0003	−0.006
Multilayer Δy [mm]	184.9886 ± 0.0004	184.9669 ± 0.0006	184.9778 ± 0.0005	184.980
RMS (σ) z [mm]	0.0082 (0.0051)	0.0064 (0.0050)	0.0079 (0.0058)	0.0076 (0.0062)
RMS (σ) y [mm]	0.0101 (0.0056)	0.0091 (0.0086)	0.0102 (0.0081)	0.0101 (0.0084)
RMS (σ) r [mm]	0.0102 (0.0054)	0.0080 (0.0051)	0.0098 (0.0059)	0.0105 (0.0069)

Table 9: Chamber torsion measurements, measure as the rotation of the HV side with respect to the RO side. Positive indicates a counter-clockwise rotation, as seen from RO side with the chamber in the upright position.

Chamber	RMS, r [μm]	$\sigma\, r$ [μm]	Torsion [mrad]
BMG-3C-14	5.6	4.9	0.198
BMG-3C-12	7.7	5.2	0.036
BMG-3A-14	8.5	7.4	0.184
BMG-3A-12	9.9	7.0	0.059
BMG-2C-14	9.9	6.8	0.108
BMG-2C-12	7.9	6.5	0.172
BMG-2A-14	9.9	7.6	0.290
BMG-2A-12	10.2	7.1	0.406
BMG-1C-14	11.8	10.9	-0.023
BMG-1C-12	7.7	6.3	0.178
BMG-1A-14	17.0	15.9	-0.178
BMG-1A-12	9.8	5.9	-0.012

Not reviewed, for internal circulation only

DRAFT

Table 10: Fitted wire position residuals in z, y, and $r = \sqrt{z^2 + y^2}$.

Chamber	z-Residuals	y-Residuals	r-Residuals
BMG-3C-14	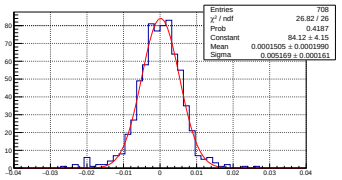	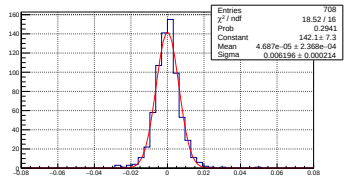	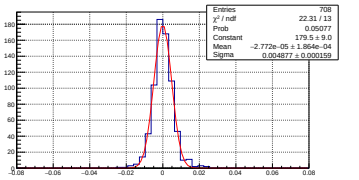
BMG-3C-12	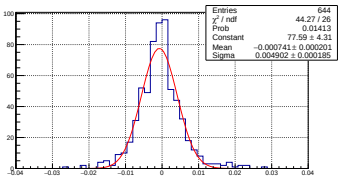	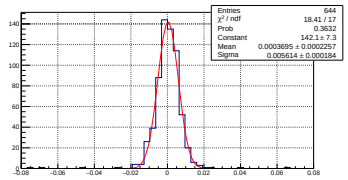	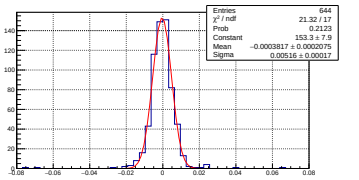
BMG-3A-14	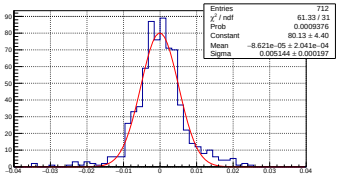	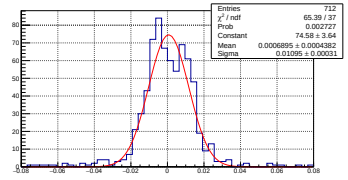	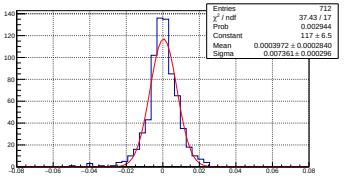
BMG-3A-12	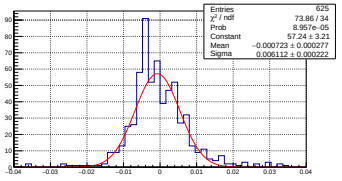	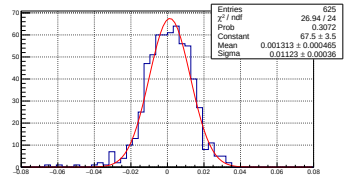	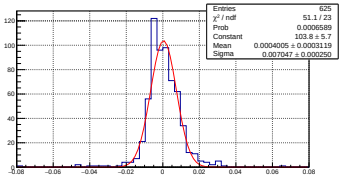
BMG-2C-14	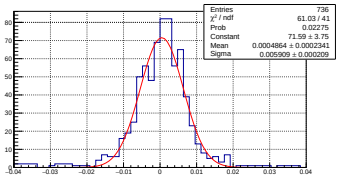	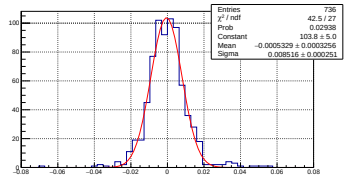	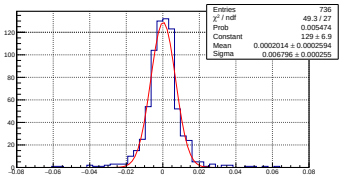

Not reviewed, for internal circulation only

Table 10: Fitted wire position residuals in z, y, and $r = \sqrt{z^2 + y^2}$ (continued).

Chamber	z-Residuals	y-Residuals	r-Residuals
BMG-2C-12	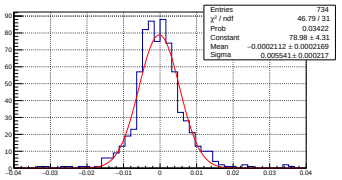	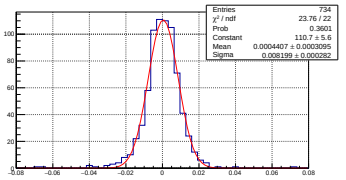	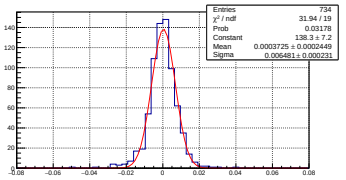
BMG-2A-14	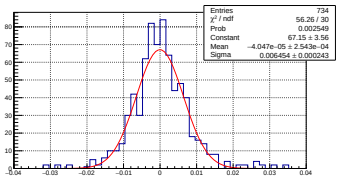	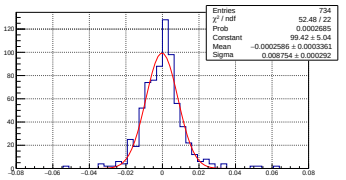	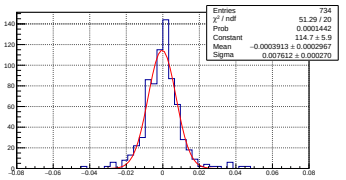
BMG-2A-12	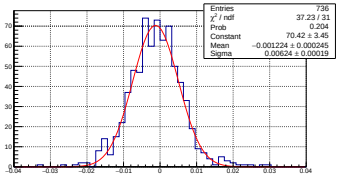	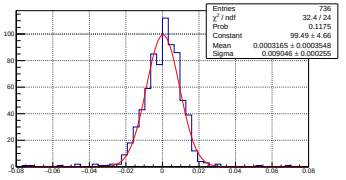	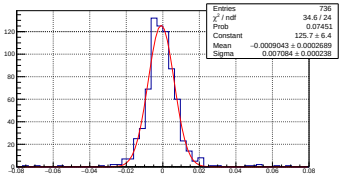
BMG-1C-14	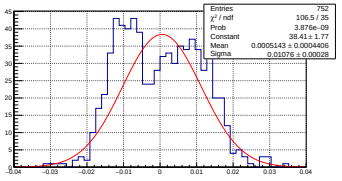	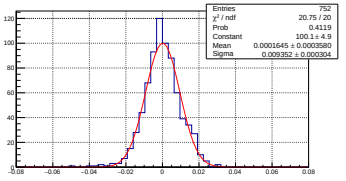	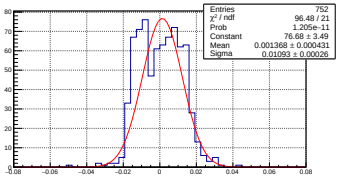
BMG-1C-12	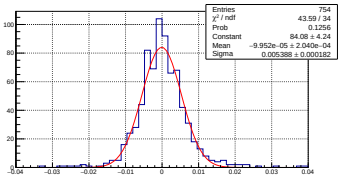	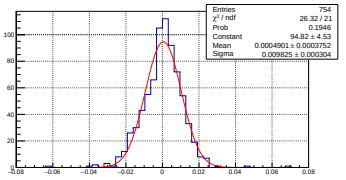	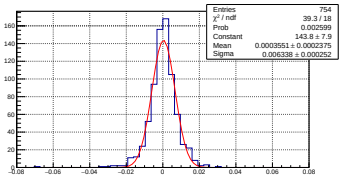

Not reviewed, for internal circulation only

Table 10: Fitted wire position residuals in z, y, and $r = \sqrt{z^2 + y^2}$ (continued).

Chamber	z-Residuals	y-Residuals	r-Residuals
BMG-1A-14			
BMG-1A-12			

Not reviewed, for internal circulation only

Table 11: Combined fitted wire position residuals in z, y, and $r = \sqrt{z^2 + y^2}$.

HV/RO/Combined	z-Residuals	y-Residuals	r-Residuals
HV	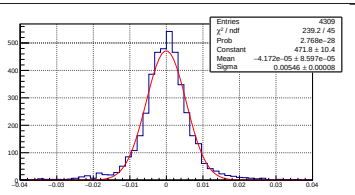	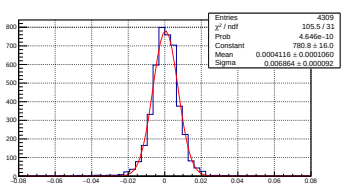	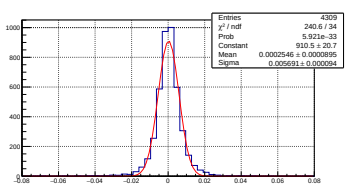
RO	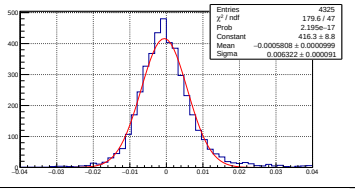	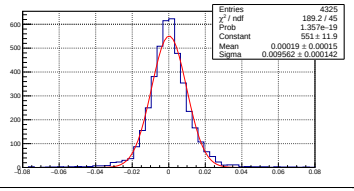	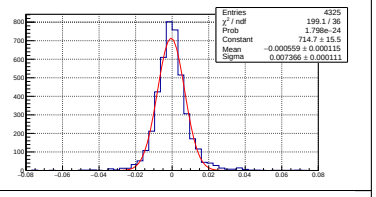
Combined RO and HV	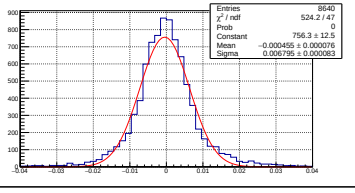	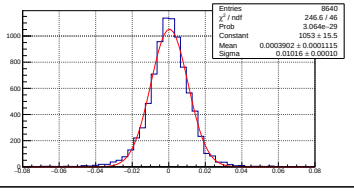	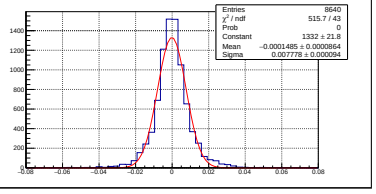

DRAFT

Not reviewed, for internal circulation only

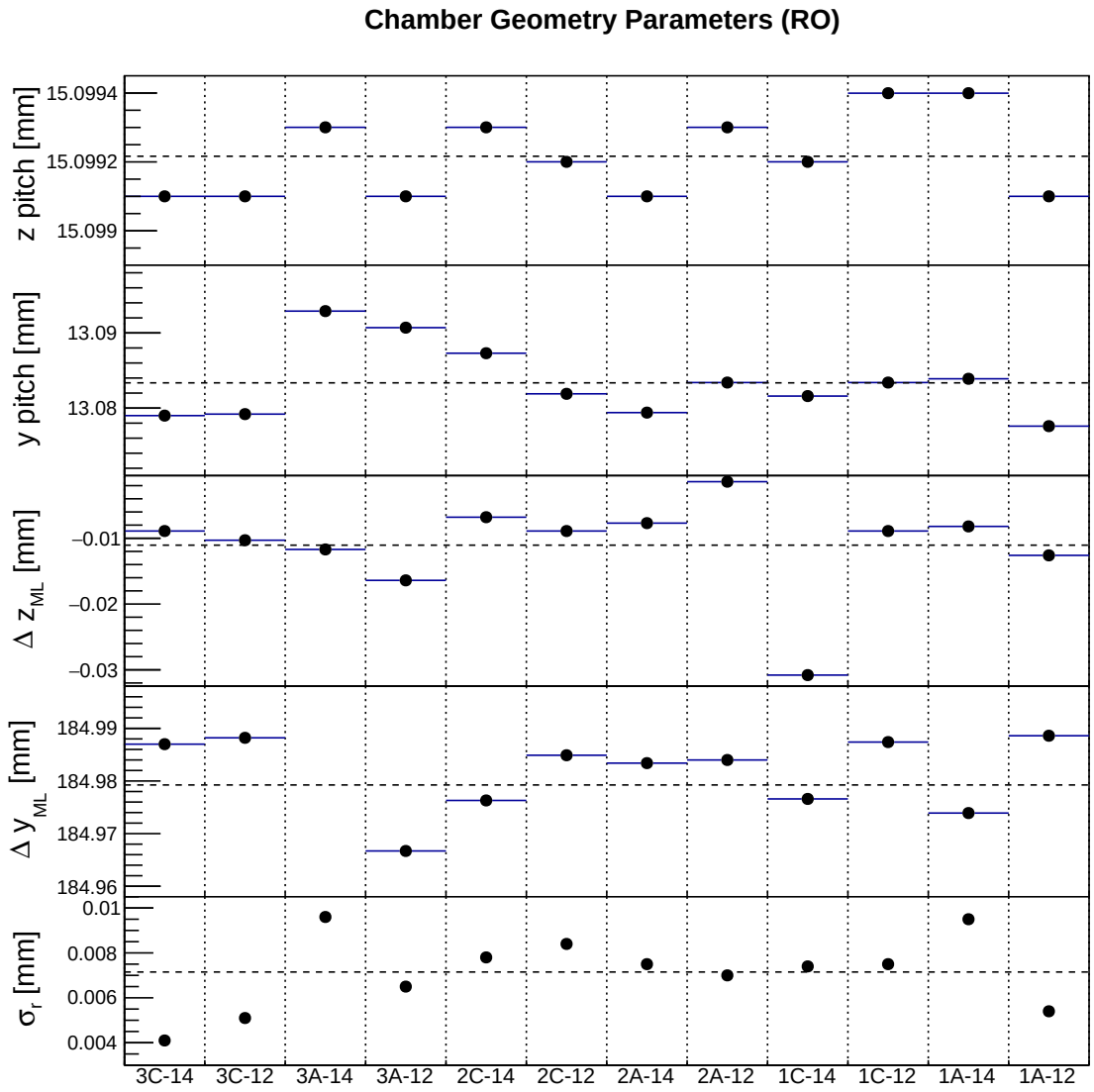

Figure 38: Chamber geometry parameters from all chambers for the RO side. The dotted line denotes the average across all chambers.

7.1.1 Wire Position Repeatability

In order to confirm the repeatability of the measurements and the accuracy of the measuring machine, one chamber's wire positions, BMG-3C-14, were measured and fitted a second time. The differences in the raw measurements were plotted (see Fig. 41). Overall, the average difference is less than 0.01 mm, and the majority of the points are clustered around zero. An analysis of the wire positions was also done to re-calculate the fitting parameters. This also showed a negligible difference in the final fit parameters, lending confidence to the measurement and fitting of the wire positions within the chambers.

Not reviewed, for internal circulation only

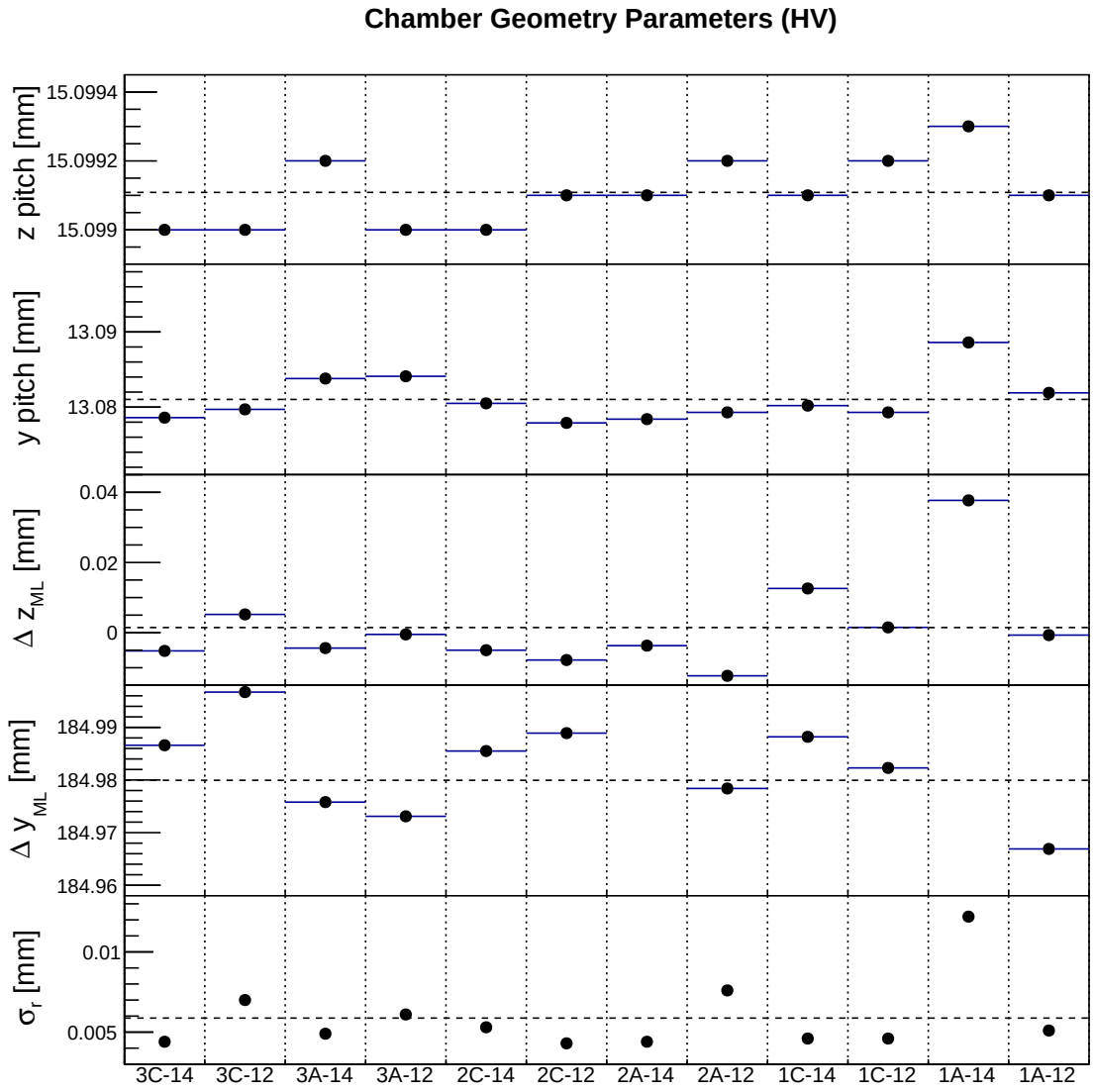

Figure 39: Chamber geometry parameters from all chambers for the HV side. The dotted line denotes the average across all chambers.

Not reviewed, for internal circulation only

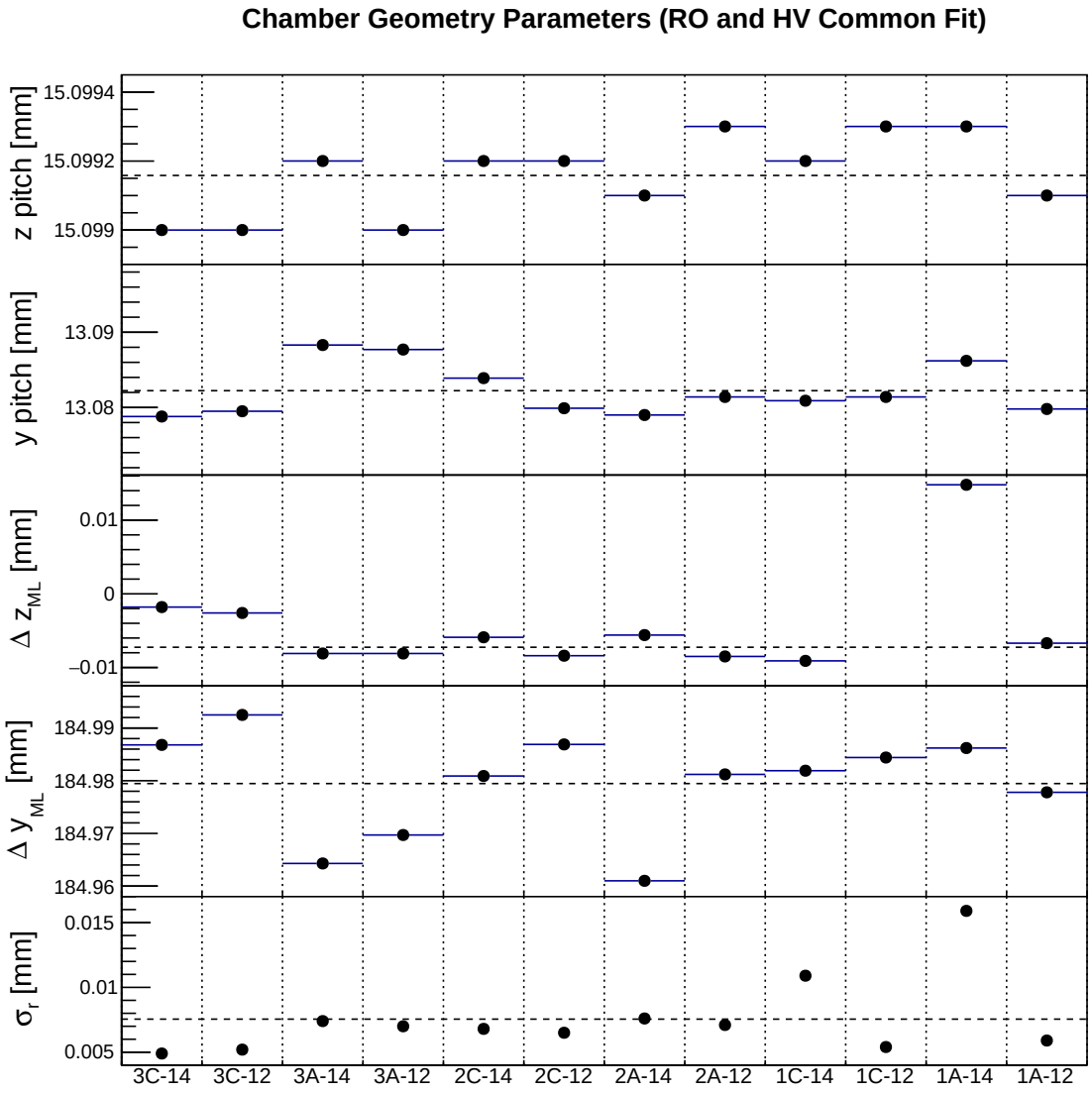

Figure 40: Chamber geometry parameters from all chambers for the combined RO and HV sides. The dotted line denotes the average across all chambers.

Not reviewed, for internal circulation only

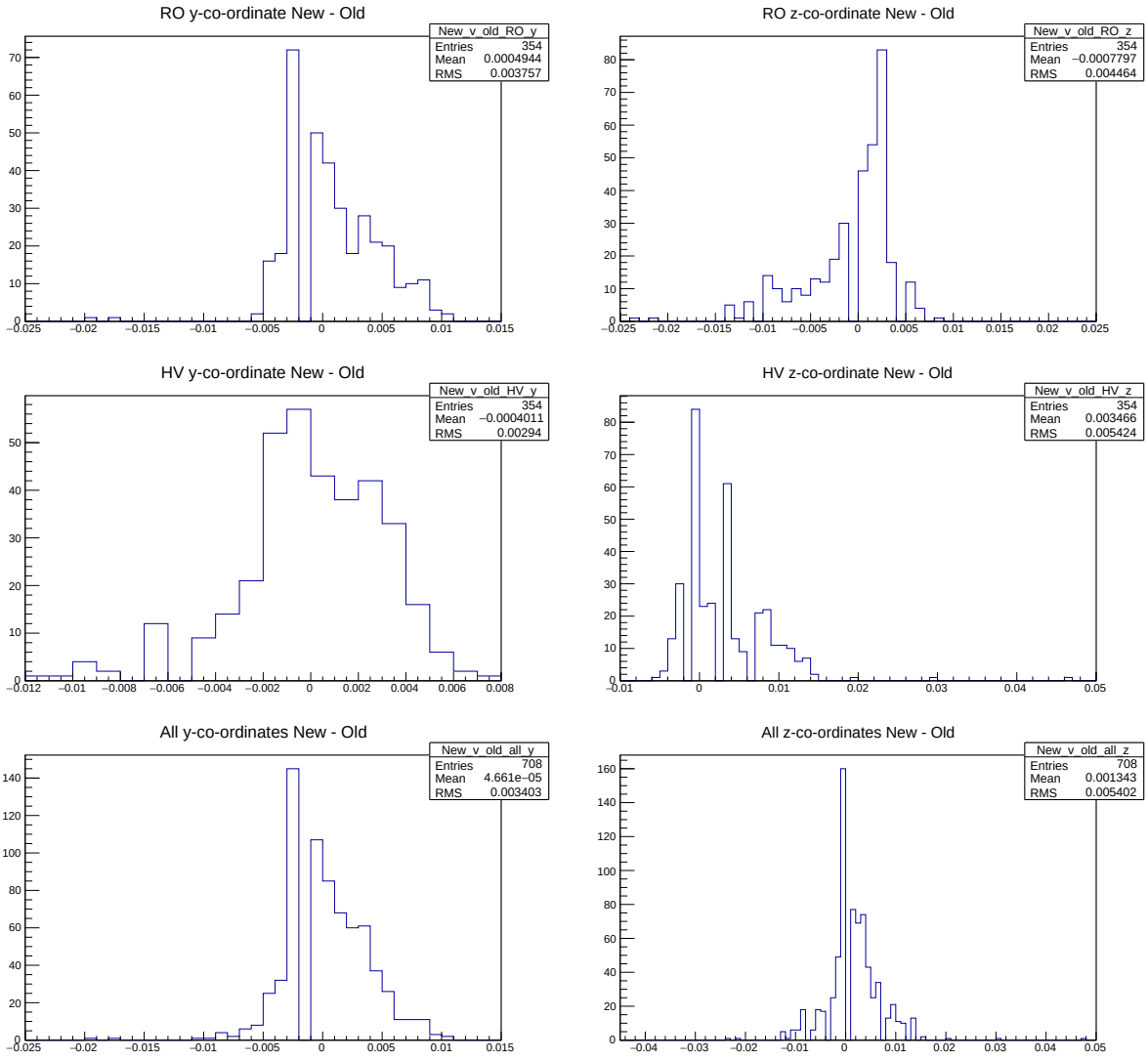

Figure 41: Difference between the repeated wire position measurements. The left column is the y-coordinate, while the right is the z-coordinate. The top row is the RO side, the middle row is the HV side, and the bottom row is the combination.

Not reviewed, for internal circulation only

7.2 Gas, HV, and Electronics Installation

While the fits are done, the on-chamber electronics and gas systems are installed. This includes the high voltage connections to the wires, the electronics to read a signal from each tube and Faraday cages to reduce noise on the electronics. The basic schematic for the readout, HV, and gas system is similar to an MDT tube (see Fig. 3 for a basic schematic). For more details about the electronics boards, see [2].

The gas system is first installed, with inputs on the RO side and outputs on the HV side. The gas manifold runs across the width of the chamber, and distributes the gas in columns of four tubes per multilayer. Each multilayer has one pair of gas bars, one for input and one for output. On the RO side, gas is filled, while on the HV side, the gas is drawn out of the tubes. These are then connected to the input and output valves installed on the RO side of the chamber. A wire-frame of the gas system can be seen in Fig. 42. A cutaway of the gas distribution into four tubes can be seen in Fig. 43. The connection of one tube to the gas system can be seen in the lower left of Fig. 10.

Two boards are installed for the readout of the tubes on the RO side. First, a signal hedgehog board, which connects directly to the tubes, is installed. These boards read the signals from up to 24 tubes. Depending on the chamber, there are locations where these hedgehog boards are not installed. These correspond to the cutouts in the tubes for the ATLAS alignment system.

On top of the hedgehog board is an aluminum plate to reduce the noise seen from the chamber. A mezzanine board (seen in Fig. 49) is installed above this, and connected directly to the hedgehog boards. These can read out the same number of tubes (24) as the hedgehog boards underneath. There are also mezzanine cards not installed which correspond to the cutouts in the chamber (see Fig. 46). These are connected to the CSM on the top of the chamber. The CSM provides communication between the chamber and the ATLAS system, providing the triggers to the chamber and delivering data from the chamber via optical fiber.

On the opposite (HV) side, the components for high voltage distribution are installed. The HV hedgehog cards, like the readout hedgehog boards, provide high voltage for up to 24 tubes. These are connected together via jumpers at five points: one for each of the four layers plus an additional for the ground. One card has an additional connection to the high voltage distribution box mounted on top of the chamber. The voltage distribution box takes two high voltage inputs, one for each multilayer, and distributes them, with one output cable per layer in the chamber and one last cable for ground.

Throughout the chamber, 14 temperature sensors are installed to ensure the chambers are at nominal temperature. These are connected to the MDT-DCS board on top of the chamber. This MDT-DCS board also takes input from the CSM (and thus from the mezzanine cards), providing parameters to the CSM and mezzanine cards for operation. The MDT-DCS board also provides for status and error monitoring of the CSM and mezzanine cards. Finally, Faraday cages are installed around the HV and RO electronics, and the boards on top of the chamber (CSM, DCS and HV distribution board) are also covered. A schematic of the Faraday cages can be seen in Fig. 44.

The completed chamber can be seen in Figs. 45–47. The physical parameters of the completed chambers can be seen in Tabs. 12 and 13. The chamber is then run though the final set of tests.

Not reviewed, for internal circulation only

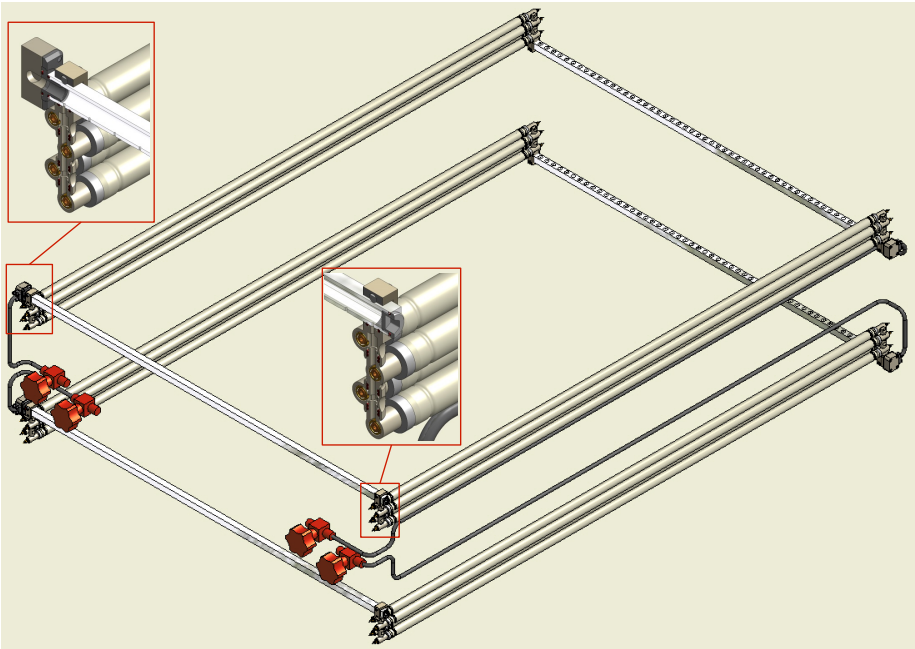

Figure 42: A wire-frame view of the gas system on the BMG chambers. Inset are closeups of the distribution of the gas over a vertical column of four tubes on the RO side. A similar setup is on the HV is used to consolidate the gas outputs in each multilayer.

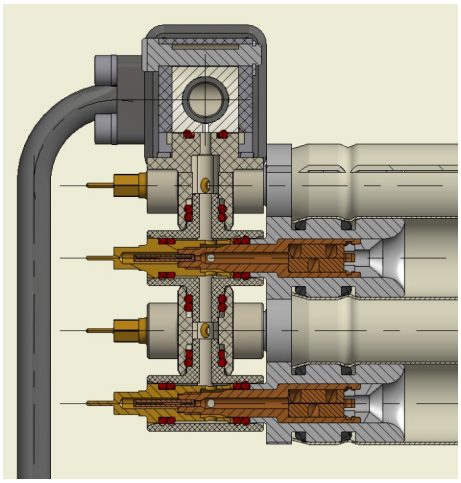

Figure 43: A side-view cutaway of the distribution of the gas over a vertical column of four tubes.

Not reviewed, for internal circulation only

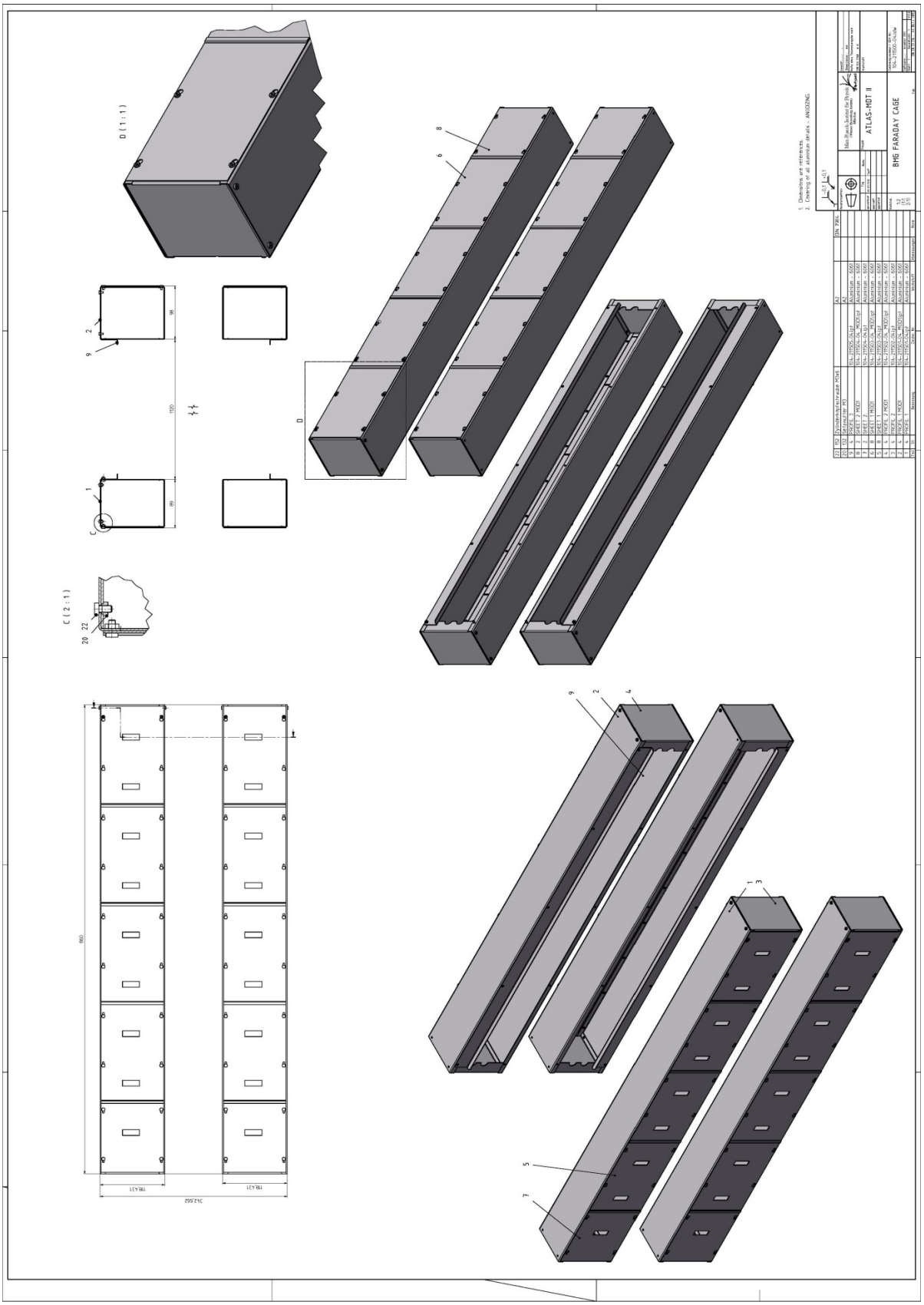

Figure 44: A schematic of the Faraday cages which cover the RO and HV sides of the chamber. The bottom left shows the cages as seen from the RO side, the lower right as seen from the HV side. The top row show various additional views of the Faraday cages.

Not reviewed, for internal circulation only

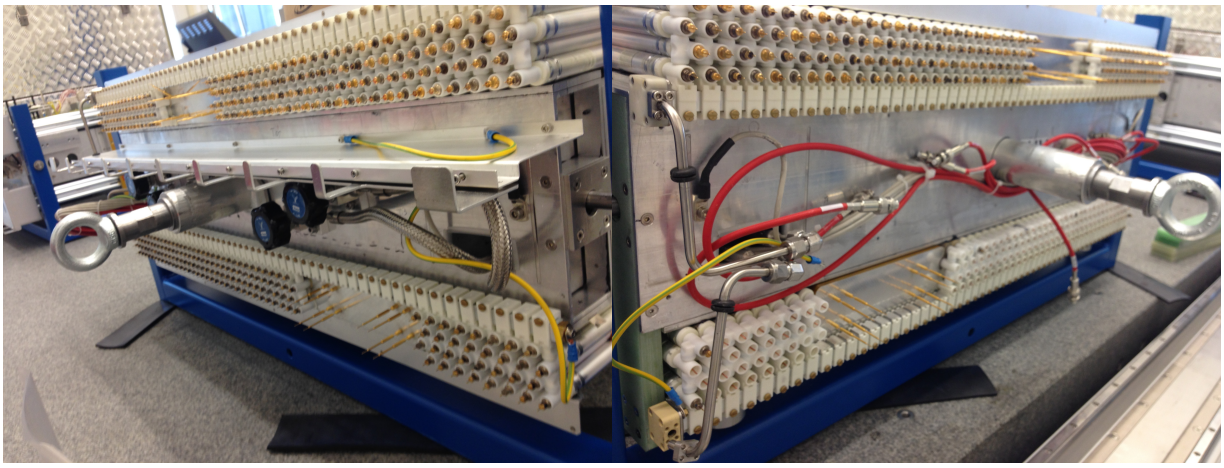

Figure 45: Chamber seen from HV side (right) and RO side (left) with gas and HV system installed.

Figure 46: Chamber with readout system installed. Note: the two gaps correspond to the cutouts required for the ATLAS alignment system. In the center are the four valves, two for gas in (left side of the chamber) and two for gas out (right side of the chamber).

Not reviewed, for internal circulation only

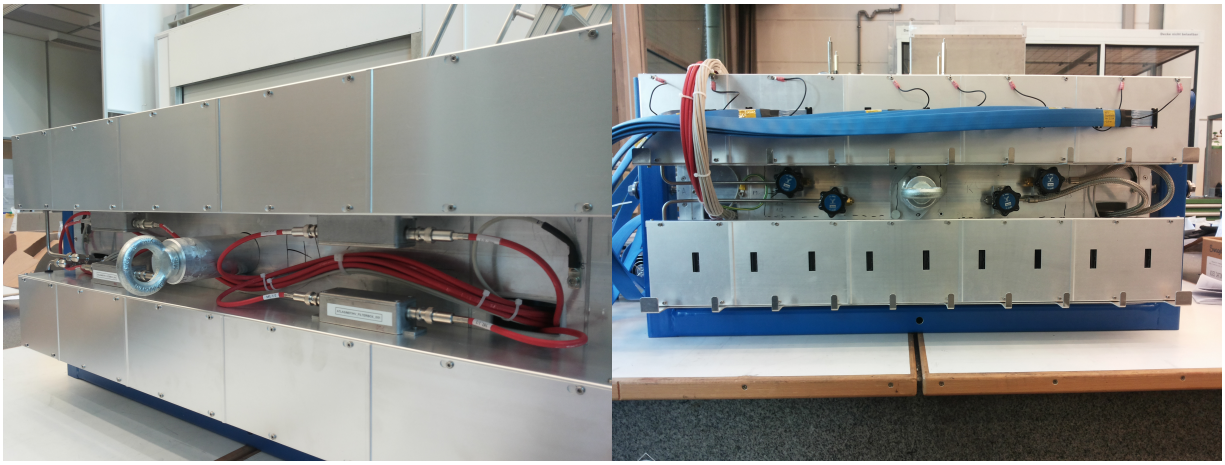

Figure 47: Completed chamber with Faraday cages seen from HV side (left) and RO side (right).

Not reviewed, for internal circulation only

Table 12: Physical chamber parameters for all completed chambers (I)

Type	BMG-2A12	BMG-2C12	BMG-2A14	BMG-2C14	BMG-4A12	BMG-4C12
Radial distance from beam (mm)	8095	8095	8095	8095	8095	8095
Chamber width in z (mm)	860	860	860	860	860	860
Tubes width in z (mm)	823	823	823	823	823	823
Chamber length in x (mm)	1307	1307	1307	1307	1307	1307
Aluminum tube length (mm)	1120	1120	1120	1120	1120	1120
Assembled tube length (mm)	1129	1129	1129	1129	1129	1129
Tube layers	2×4	2×4	2×4	2×4	2×4	2×4
Tube positions/layer	54	54	54	54	54	54
Tube positions/chamber	432	432	432	432	432	432
Tubes/top ML	188	189	189	188	184	183
Tubes/bottom ML	188	188	188	188	184	184
Tubes/chamber	376	377	377	376	368	367
Spacer height (mm)	184.965	184.965	184.965	184.965	184.965	184.965
Tubes height (mm)	271	271	271	271	271	271
Chamber height (mm)	358	358	358	358	358	358
Gas volume/chamber (l)	67.2	67.4	67.4	67.2	65.8	65.6
Chamber weight (kg)	95	95	95	95	95	95
Mezz. cards (24 ch.)/chamber	18	17	17	18	18	18
Temperature sensors/chamber	14	14	14	14	14	14
Praxial alignment platforms	4	4	4	4	4	4
Survey targets	4	4	4	4	4	4

DRAFT

Not reviewed, for internal circulation only

Table 13: Physical chamber parameters for all completed chambers (II)

Type	BMG-4A14	BMG-4C14	BMG-6A12	BMG-6C12	BMG-6A14	BMG-6C14
Radial distance from beam (mm)	8095	8095	8095	8095	8095	8095
Chamber width in z (mm)	860	860	860	860	860	860
Tubes width in z (mm)	823	823	823	823	823	823
Chamber length in x (mm)	1307	1307	1307	1307	1307	1307
Aluminum tube length (mm)	1120	1120	1120	1120	1120	1120
Assembled tube length (mm)	1129	1129	1129	1129	1129	1129
Tube layers	2×4	2×4	2×4	2×4	2×4	2×4
Tube positions/layer	54	54	54	54	54	54
Tube positions/chamber	432	432	432	432	432	432
Tubes/top ML	183	184	160	166	178	176
Tubes/bottom ML	184	184	160	162	190	178
Tubes/chamber	367	368	320	328	368	354
Spacer height (mm)	184.965	184.965	184.965	184.965	184.965	184.965
Tubes height (mm)	271	271	271	271	271	271
Chamber height (mm)	358	358	358	358	358	358
Gas volume/chamber (l)	65.6	65.8	57.2	58.6	65.8	63.3
Chamber weight (kg)	95	95	95	95	95	95
Mezz. cards (24 ch.)/chamber	18	18	16	16	18	18
Temperature sensors/chamber	14	14	14	14	14	14
Praxial alignment platforms	4	4	4	4	4	4
Survey targets	4	4	4	4	4	4

Not reviewed, for internal circulation only

8 Cosmic Ray Testing

For each chamber, the noise and response of the electronics are tested using cosmic rays. The chamber is connected to readout electronics with an external trigger in a similar setup as what will be found in the ATLAS detector. The chamber is tested once at MPI before it is shipped to CERN. After the chamber arrives at CERN, another test is run to ensure the chamber suffered no damage during transportation before installation in the ATLAS detector.

8.1 Testing at MPI

As the sMDT BMG chambers do not have an internal trigger, the noise and cosmic ray tests require an external trigger for the chamber. To do this, a scintillator is positioned above and below the chamber. A coincidence window of approximately 20 ns is used. A pre-mixed gas bottle, with 93% Ar, 3% CO_2, is connected, via a flow regulator, to the chamber. At the output, a pressure sensor and flow monitor is connected. The flow monitor ensures that the gas is recycled at a rate of approximately 10 l/h, and the pressure sensor ensures that the internal pressure of the chamber is the operating value (3 bar absolute). The readout from the flow monitor and pressure sensor is used to automatically adjust the flow on the intake. The chamber is then connected to a HV source. The distribution of HV is done on-chamber, but requires two inputs at 2,370 V. The chamber is then brought to operating conditions, with appropriate pressure, gas flow rate, and high voltage. The chamber is then used to read out cosmic ray hits. The readout window for the channels is approximately 1.3 μs. Two methods were employed to read out the data. The first was to use a GLIB (Gigabit Link Interface Board), which can read out a maximum of six boards at once. One readout is required for timing and triggering from the scintillators, allowing for five cards to be read out at the same time. The other method is to use the on-chamber CSM (Chamber Service Module) which can read out all 18 boards on a chamber simultaneously. However, for these tests (as was the case for the GLIB), one input slot was initially needed for triggering and timing from the scintillator. Later tests utilized a full VME crate which allowed for the readout of the maximum number of boards (6 or 18 from GLIB or CSM, respectively).

8.1.1 Testing Results from MPI

The chambers were completely installed with new mezzanine cards. A photo of the card can be seen in Fig. 49. During the design, some noise was seen on the ASD chips from the power line so the input was redesigned slightly (Fig. 48). The noise spectrum of these redesigned chips compared to the older boards used in MDTs can be see in Fig. 50.

The setup was also modified to better reflect the final setup to be used in the ATLAS Muon Spectrometer. Firstly, the GLIB board was not used. Instead, the on-chamber CSM was used to read out the boards. Secondly, a dedicated triggering and timing board was used off chamber, allowing for all mezzanine cards to be read out simultaneously. The numbering of the chambers were also changed to reflect their final positions in the ATLAS Muon Spectrometer. This amounts to the leading digit being increased by a factor of two, i.e., BMG-1X-XX becomes BMG-2X-XX, BMG-2X-XX becomes BMG-4X-XX, and BMG-3X-XX becomes BMG-6X-XX).

The chambers were then triggered using the scintillators placed above and below the chamber. An `OR` coincidence was required for the noise tests, to increase statistics, while an `AND` was used for the cosmic

Not reviewed, for internal circulation only

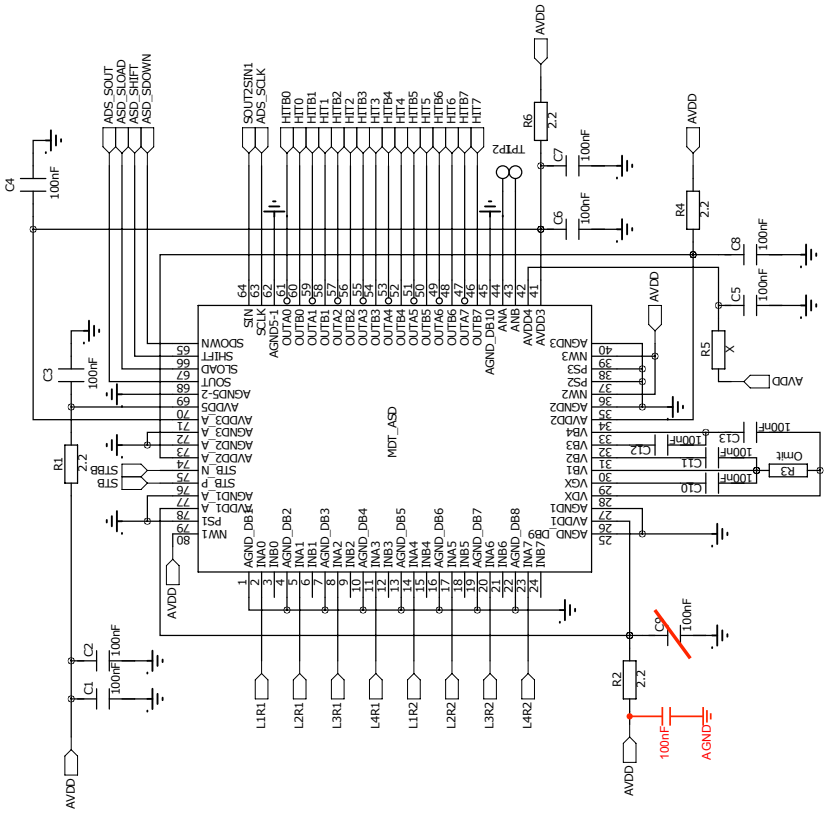

Figure 48: Circuit diagram of the ASD chip before (left) and after (right) the power supply modification tested at MPI.

Not reviewed, for internal circulation only

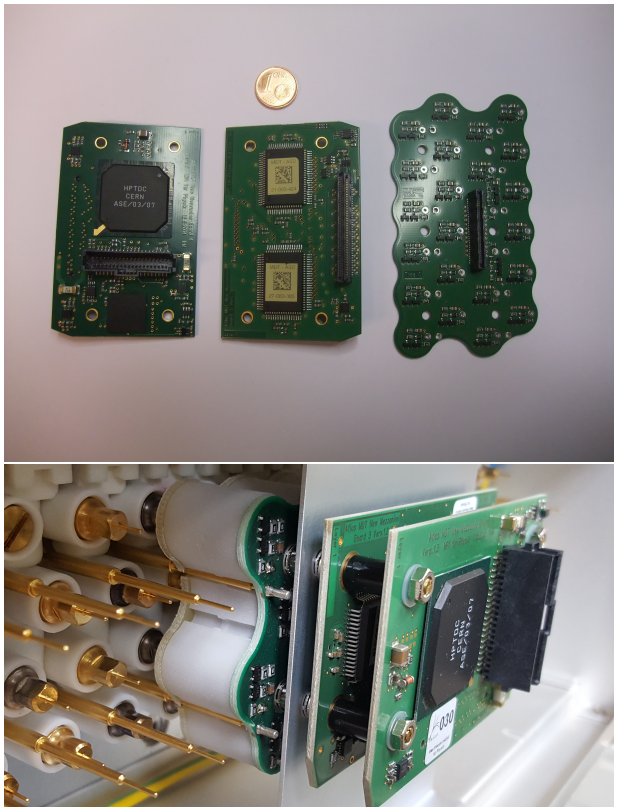

Figure 49: The two layers of the new stacked sMDT mezzanine card (with €0.01 coin for scale, ⌀ = 16.25 mm) beside the hedgehog board (top image, boards from left to right). Mezzanine and hedgehog boards assembled with aluminum plate for noise reduction and installed on chamber (bottom).

tests. This was done to restrict the triggering of the chamber to hits with tracks which go through the chamber. The noise tests and cosmic tests were done with nominal operating parameters, in particular the ADC threshold. The chamber was then isolated from the gas system and its pressure loss over at least 10 hours was measured to ensure that there were no large leaks in the gas structure installed on the chamber. This pressure measurement was temperature corrected. Each multilayer is recorded separately. The target leak rate was 0.4 mbar/hr per multilayer. The results of the chamber gas leak test done at MPI are shown in Tab. 14. While the final leak rates were higher than the target, they are low enough such that data taking will be unaffected.

The source of the slight leakage was determined to be from the hedgehog boards installed on the chamber: they were touching neighboring boards putting stress on the O-rings in the tubes (Fig. 51). As the final leak rate was low enough, the boards were not re-printed, but rather the design of future boards will be changed to reduce stress on the gas seals.

A sample ADC and drift time spectrum can be seen in Figs. 53. All chambers showed nominal spectra and distributions. The noise rate on the operational chambers was seen to be less than 5 kHz overall (e.g., Fig. 52). The average accidental hit rate (noise rate) for all chambers can be seen in Fig. 54. Some chambers were found to have slightly higher noise rates in individual tubes (Tab. 15), but these were caused by bad grounding connection in these tubes. This is due to the fact that these noisy tubes are all edge tubes (tubes at either the edge of a layer or the edge of a cutout), and the grounding of the tubes

Not reviewed, for internal circulation only

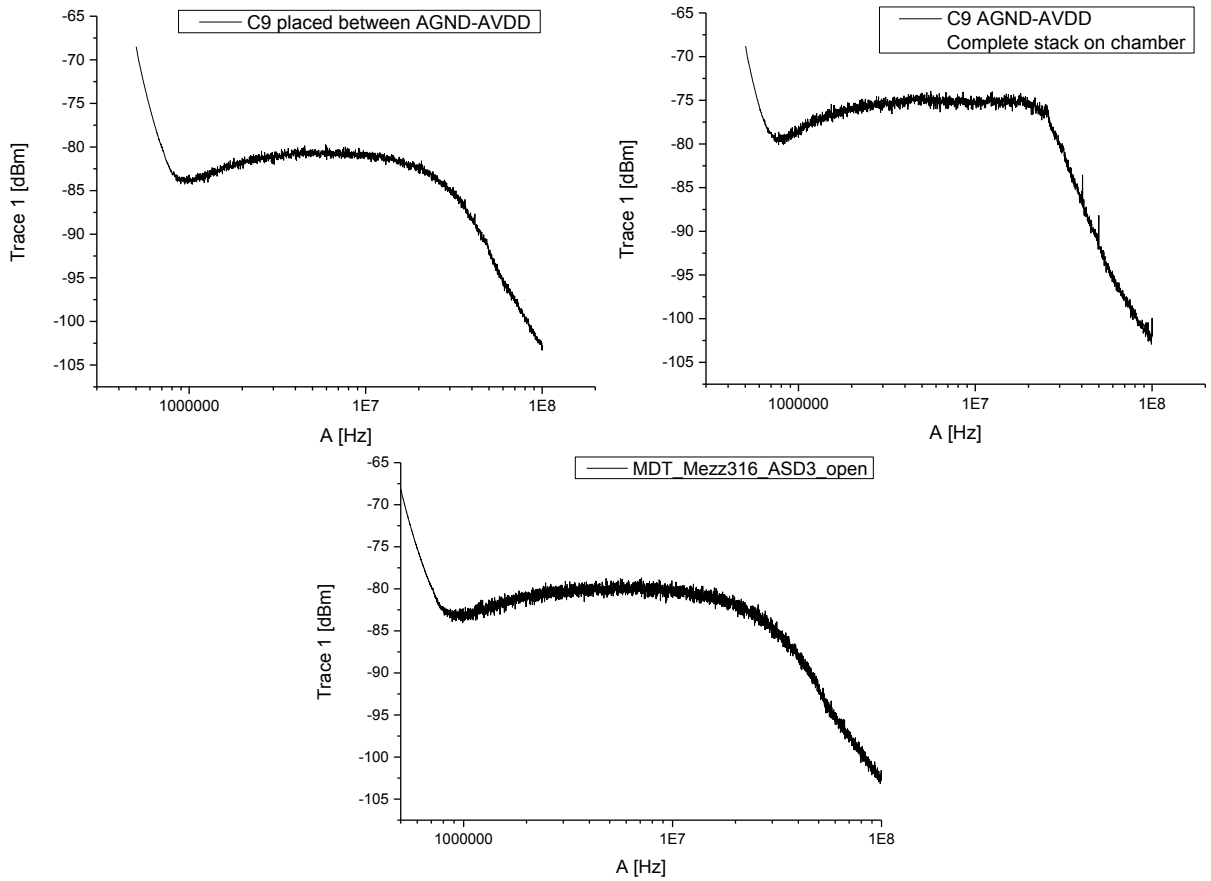

Figure 50: Noise spectrum of the new boards with (top left) and without (top right) tubes. The noise spectrum of the old type cards is on bottom.

Figure 51: Image of two neighboring mezzanine cards. They are in contact, putting stress on the gas seals inside the chamber.

Not reviewed, for internal circulation only

Table 14: Measured gas leak rates for all completed chambers as tested at MPI in mbar/h. Multiples of target ATLAS leak rate (0.4 mbar/hr per multilayer) is listed in parenthesis. BMG-2A-14 was sent to CERN before the gas leak rate was measured at MPI. The measurements were taking before and after electronics were installed. The pressure measurement with electronics were temperature corrected, but the measurement without electronics was not temperature corrected.

Chamber	Top Multilayer w/ electronics	Bottom Multilayer w/ electronics	Top Multilayer w/o electronics	Bottom Multilayer w/o electronics
BMG-2A-12	0.7 (1.7)	1.0 (2.5)	< 0.2 (0.5)	< 0.2 (0.5)
BMG-2C-12	3.8 (9.3)	0.3 (0.6)	< 0.2 (0.5)	< 0.2 (0.5)
BMG-2C-14	1.6 (3.9)	3.1 (7.6)	< 0.2 (0.5)	< 0.2 (0.5)
BMG-4A-12	0.7 (1.6)	0.8 (1.9)	< 0.2 (0.5)	< 0.2 (0.5)
BMG-4A-14	0.6 (1.5)	0.3 (0.8)	< 0.2 (0.5)	< 0.2 (0.5)
BMG-4C-12	1.2 (2.9)	0.8 (2.0)	< 0.2 (0.5)	< 0.2 (0.5)
BMG-4C-14	2.8 (6.8)	2.6 (6.2)	< 0.2 (0.5)	< 0.2 (0.5)
BMG-6A-12	1.7 (4.1)	4.2 (10)	< 0.2 (0.5)	< 0.2 (0.5)
BMG-6A-14	3.5 (8.6)	0.2 (0.4)	< 0.2 (0.5)	< 0.2 (0.5)
BMG-6C-12	1.0 (2.3)	3.2 (7.7)	< 0.2 (0.5)	< 0.2 (0.5)
BMG-6C-14	3.5 (8.5)	1.5 (3.8)	< 0.2 (0.5)	< 0.2 (0.5)

is done with a screw located in between tubes (see Fig. 55). This means that edge tubes can become ungrounded. Conducting glue and tape were used to reduce ground these edge tubes. The noise spectra of one chamber with HV on and ASD threshold set to the operational value of 108 can be seen in Tab. 17 (the remaining chamber results can be found in the Appendix, Tab. 22). The overall noise after this change is summarized in Tab. 16, with two chambers (BMG-2C12 and BMG-4A12) now showing no tubes with high noise. All plots shown are the final tests run, i.e., after all modifications, including the addition of any conducting glue and tape.

The cosmic ray hits spectra for one chamber can be seen in Tab. 18 (the remaining chamber results can be found in the Appendix, in Tab. 23). The red distribution in each plot corresponds to the hits associated with cosmic tracks. The distributions show the expected "bulge" in the middle. Clearly seen in each distribution is also the cutout, which manifests as a large gap in hits in the chamber.

8.2 Testing at CERN

The completed chambers were shipped to CERN for an abbreviated test to confirm the chambers were undamaged during transport. Tests were conducted at the BB5 facility using a second, similar setup. The chambers were stacked two high, with scintillators placed above and below the chamber. A coincidence between the two scintillators was used as a trigger (either set to `OR` for noise runs or `AND` for cosmic runs as at MPI). The chamber's gas input was then connected to a vacuum pump and gas bottle with the appropriate gas mixture with a switching valve. This time, however, only a pressure sensor was connected at the output. The gas was purged from the system, using a vacuum pump. When the chamber was evacuated, it was then filled with gas until the tubes had an internal pressure of 3 bar. The noise test was run to check the accidental hit rate in the chamber. The cosmic test was then run in parallel to the gas leak test.

Not reviewed, for internal circulation only

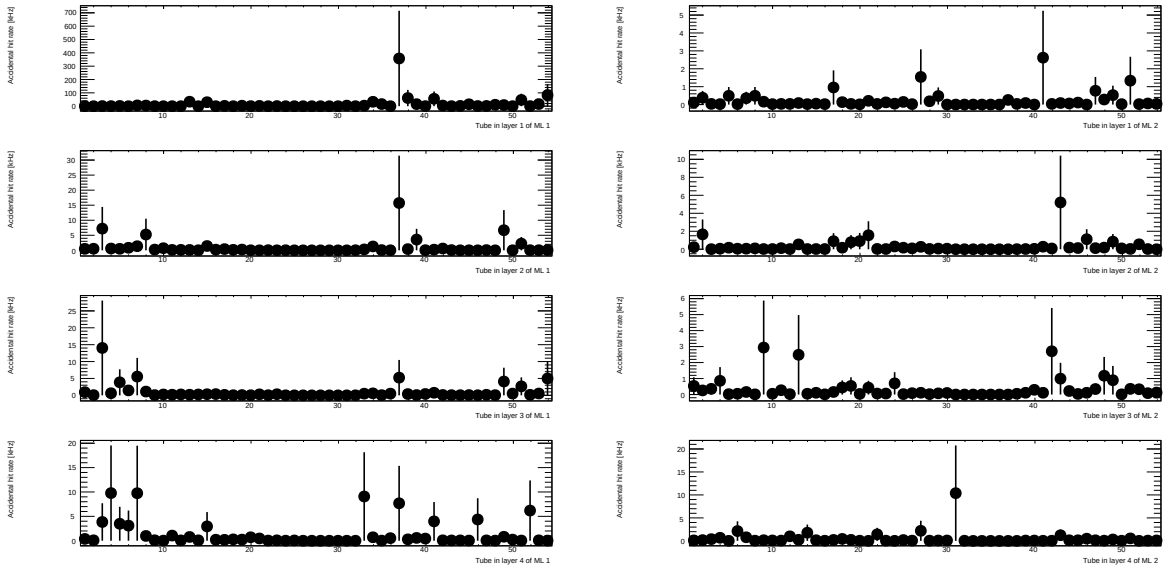

Figure 52: Noise from a complete chamber (BMG-2C-14) using the new stacked mezzanine boards tested at MPI. The chamber was brought to nominal operation values and recorded 400,000 cosmic ray events. The accidental noise rate is displayed per layer in the upper (left column) and lower (right column) multilayers. The four plots in each column, from top to bottom, correspond to the four layers of tubes in each multilayer.

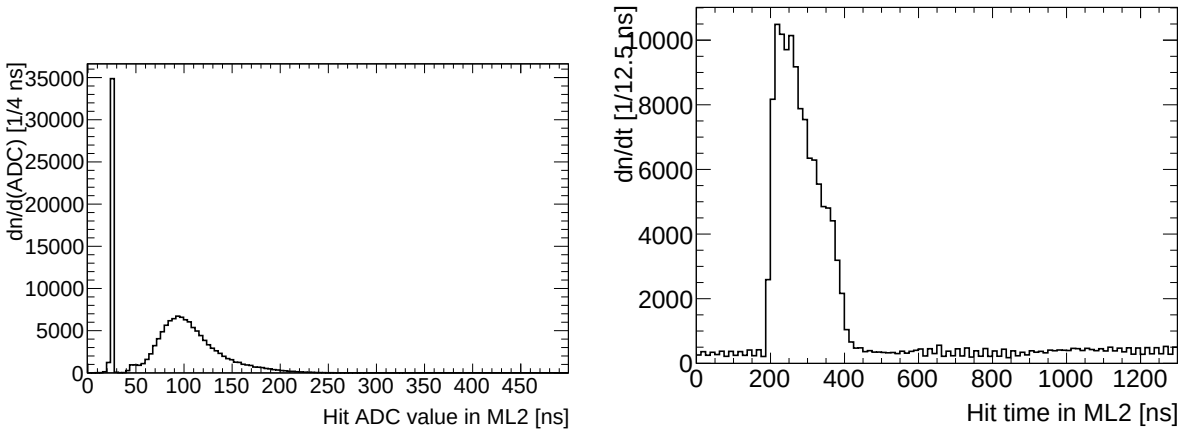

Figure 53: Sample ADC spectrum (left) and TDC spectrum (right) from multilayer 2 of chamber BMG-2A-12 tested at MPI.

Not reviewed, for internal circulation only

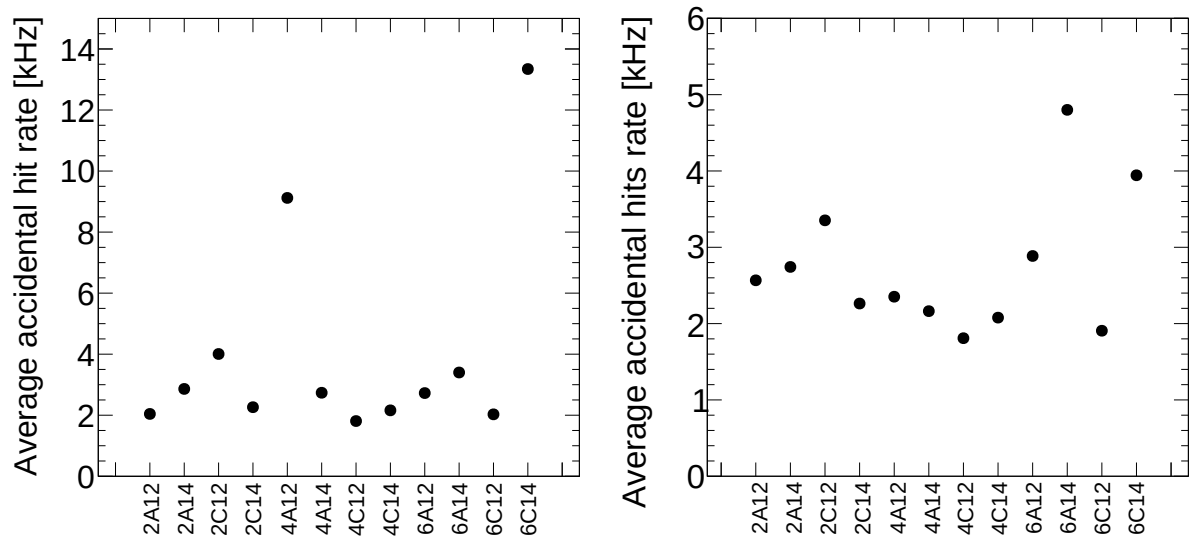

Figure 54: Average noise rates for each chamber tested at MPI before (left) and after (right) the grounding for the tubes was modified.

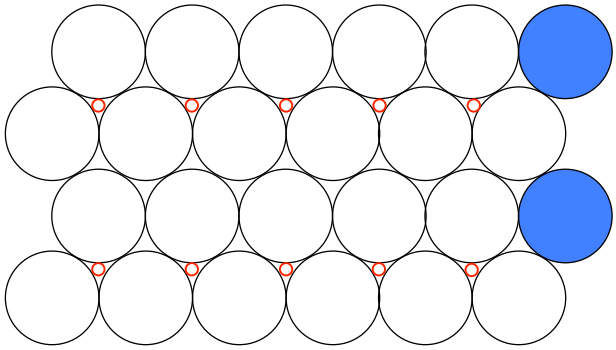

Figure 55: Diagram showing grounding of tubes in a multilayer. Red shows the location of grounding pins. Tubes which do not contact grounding pins are highlighted in blue.

Not reviewed, for internal circulation only

Table 15: Chambers with specific tubes with high noise rates, highlighted in red, with the measured noise rates tested at MPI.

BMG-2A-14	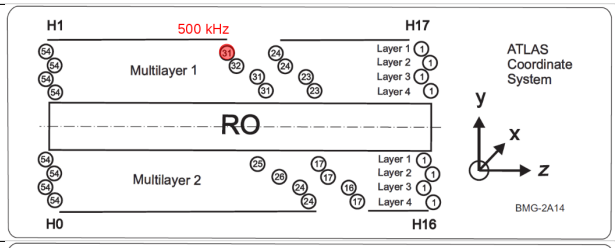
BMG-2C-12	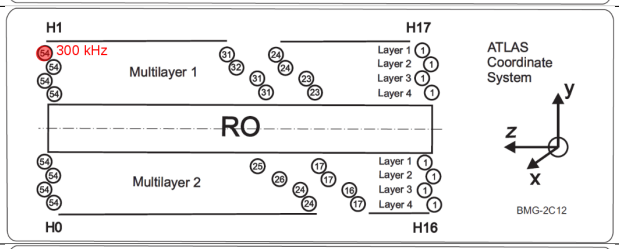
BMG-4A-12	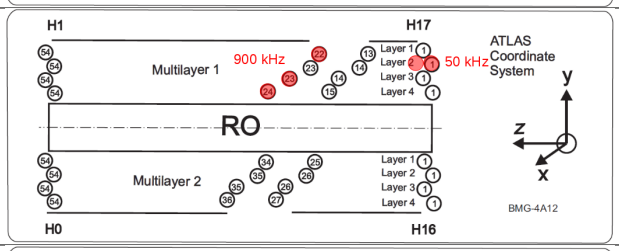
BMG-6A-14	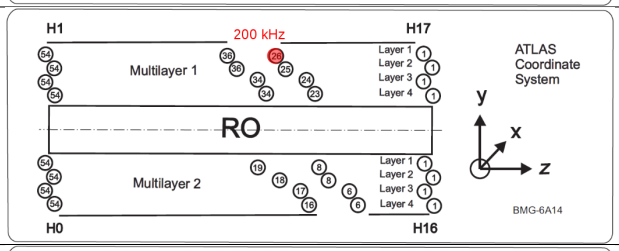
BMG-6C-14	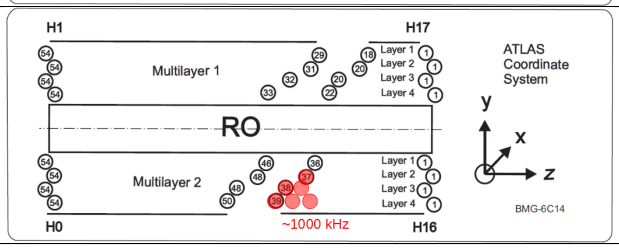

8.2.1 Testing Results from CERN

The noise on each chamber is checked to ensure that no noisy channels were introduced during shipment to CERN. The noise spectra are measured with the HV on (at 2,370 V) and off, as well as with five different ASD threshold levels: 103, 106, 108 (nominal), 110, and 112, which correspond to a threshold of -49 mV, -43 mV, -39 mV, -35 mV, and -31 mV, respectively. In all, ten noise runs were taken in total. These were undertaken to test the effects of the high voltage as well as the different thresholds on the noise seen on the electronics. The noise spectra of one chamber with HV on and ASD threshold set to the operational value of 108 can be seen in Tab. 19 (the remaining chamber results and runs with HV on, off, and ASD thresholds changed, can be found in the Appendix, Tabs. 24–33). The rates seen in this nominal case are

Not reviewed, for internal circulation only

Table 16: Chambers with specific tubes with high noise rates, highlighted in red, with the measured noise rates tested at MPI after edge tube grounding modification.

BMG-2A-14	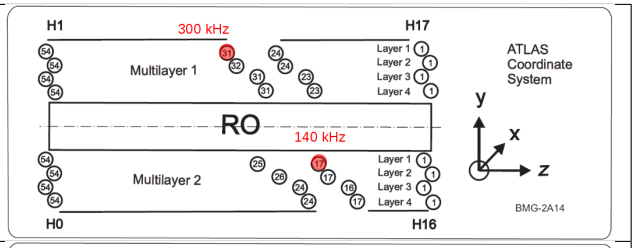
BMG-6A-14	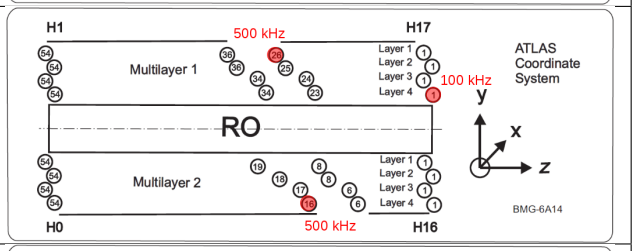
BMG-6C-14	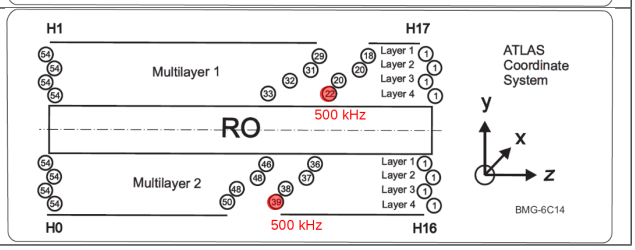

as expected - the rates were at most 20 kHz, with the exception of the tubes noted in Tab. 16. No new noisy tubes were introduced during transport from MPI to CERN.

Then, a cosmic ray test was run overnight to ensure that the drift time spectra are still as expected, and that the response to hits throughout the chamber were still within expectations. In parallel, a gas leak test was run to ensure that no multilayer showed excessive leaking in comparison to the tests conducted at MPI. Again, this run was required to be at least 10 hours long. The cosmic ray hits spectra for one chamber can be seen in Tab. 20 (the remaining chamber results can be found in the Appendix, in Tab. 34). The red distribution in each plot corresponds to the hits associated with cosmic tracks. The distributions show the expected “bulge” in the middle, as was seen in MPI. Clearly seen in each distribution is also the cutout, which manifests as a large gap in hits in the chamber. Furthermore, there are no additional tubes which show no hits or no noise, indicating that no connections between the tubes, readout electronics, or high voltage systems were damaged during transport.

The gas leak test results are seen in Tab. 21. These also show that no significant damage was done during transport to the gas system of the chambers.

Not reviewed, for internal circulation only

Table 17: Measured noise rates for BMG-4C-14 at MPI with HV on and the ASD threshold of 108 (or 39 mV, the operational value). As before, the left column corresponds to the upper multilayer, and the right column corresponds to the lower multilayer. The four plots in each column, from top to bottom, correspond to the four layers of tubes in each multilayer.

Chamber	
BMG-4C-14	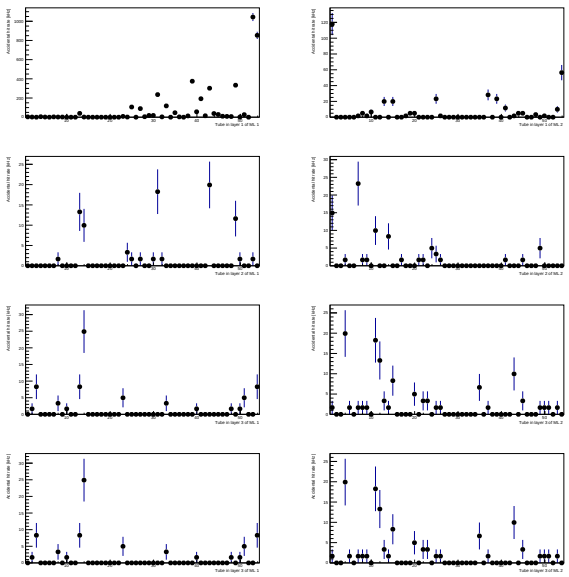

Table 18: Measured cosmic hit rates spectra for for BMG-4A-14 at MPI. The total hits per tube is shown in black, and the hits associated with cosmic tracks are shown in red. As before, the left column corresponds to the upper multilayer, and the right column corresponds to the lower multilayer. The four plots in each column, from top to bottom, correspond to the four layers of tubes in each multilayer.

Chamber	
BMG-4A-14	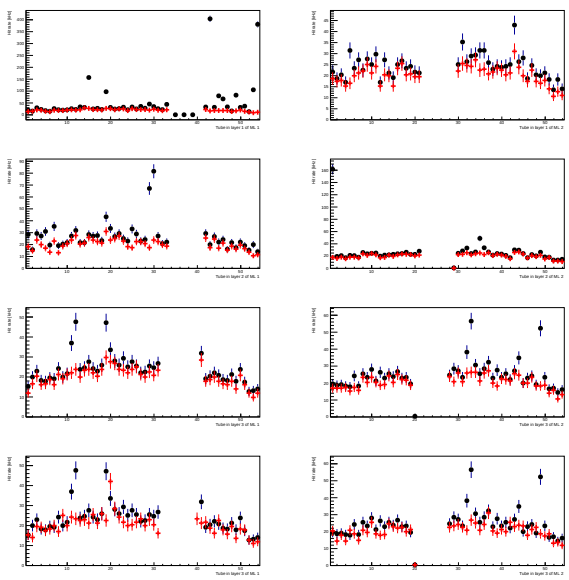

Not reviewed, for internal circulation only

Table 19: Measured noise rates for BMG-4C-14 at CERN with HV on and the ASD threshold of 108 (or 39 mV, the operational value). As before, the left column corresponds to the upper multilayer, and the right column corresponds to the lower multilayer. The four plots in each column, from top to bottom, correspond to the four layers of tubes in each multilayer.

Chamber	
BMG-4C-14	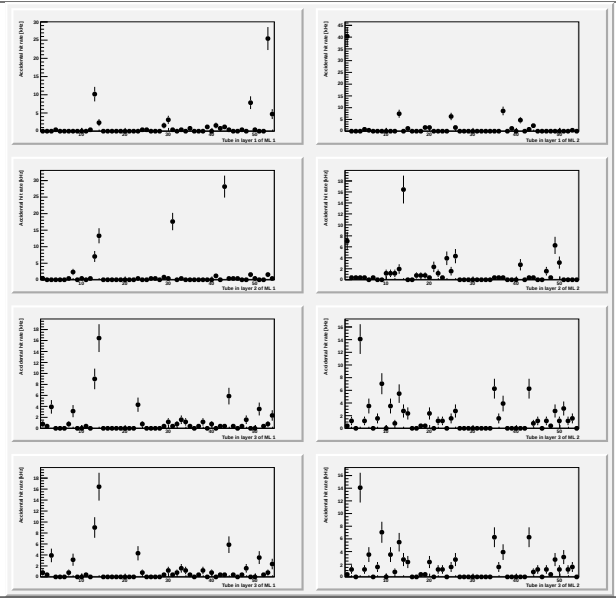

Table 20: Measured cosmic hit rates spectra for for BMG-4A-14 at CERN. The total hits per tube is shown in black, and the hits associated with cosmic tracks are shown in red. As before, the left column corresponds to the upper multilayer, and the right column corresponds to the lower multilayer. The four plots in each column, from top to bottom, correspond to the four layers of tubes in each multilayer.

Chamber	
BMG-4A-14	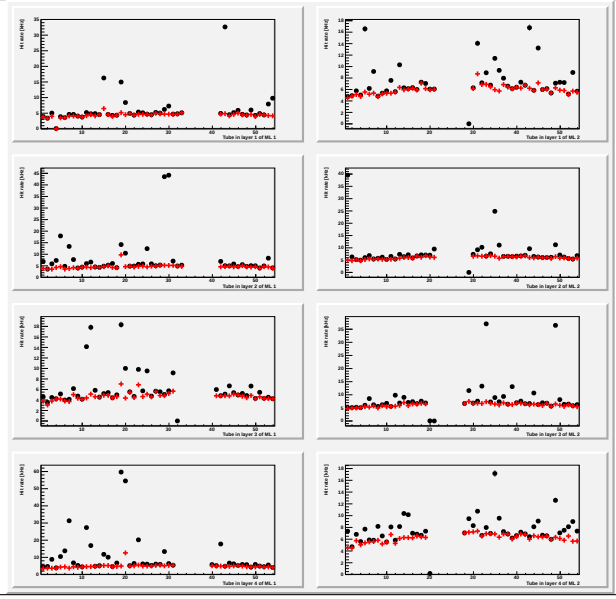

Not reviewed, for internal circulation only

Table 21: Measured gas leak rates for all completed chambers as tested at BB5 in mbar/h. Multiples of target ATLAS leak rate (0.4 mbar/hr per multilayer) is listed in parenthesis.

Chamber	Top Multilayer	Bottom Multilayer
BMG-2A-12	0.02 (0.05)	0.3 (0.7)
BMG-2A-14	6.6 (16)	2.8 (6.8)
BMG-2C-12	6.0 (15)	0.2 (0.4)
BMG-2C-14	1.7 (4.0)	3.0 (7.3)
BMG-4A-12	2.1 (5.1)	1.5 (3.7)
BMG-4A-14	0.5 (1.2)	0.1 (0.2)
BMG-4C-12	1.4 (3.4)	1.0 (2.5)
BMG-4C-14	2.4 (5.9)	2.7 (6.7)
BMG-6A-12	4.9 (12)	6.4 (15)
BMG-6A-14	4.4 (11)	0.9 (1.4)
BMG-6C-12	2.8 (6.8)	5.0 (12)
BMG-6C-14	3.5 (8.6)	2.0 (4.9)

Not reviewed, for internal circulation only

9 Conclusions

Testing conducted at MPI showed that tubes could be consistently constructed to within acceptable specifications: the tubes were gas-tight and sealed properly; the tubes had the proper tension on the wires; the wires did not loosen over time to unacceptable levels; and the tubes did not draw excessive current when brought to (and even above) their operating voltage. In the end, almost 90% of the constructed tubes pass all tests (See Tab. 4). Furthermore, this allows for spare tubes (10% of the required number) should any tubes become damaged.

The chambers were constructed using these tubes, and once completed, were themselves tested. In particular, the chambers were tested for their gas tightness, noise, and response to cosmic rays.

Initially, the chambers were found to be noisy and had large cross talk. As such, the ASD chips were redesigned and conductive tape and glue added to better ground the electronics on the chamber. These modifications reduced the noise seen on the chamber (aside from the individual tubes noted in Tab. 16). When subsequently tested with cosmic rays, the response of the chamber was as expected. No dead tubes were found, nor did any have unexpectedly high or low occupancy.

The gas testing revealed some problems with the gas systems of the chambers. Unfortunately, the installed gas systems showed leakage (Tab. 14). However, it was determined that the rates, while high, were acceptable for transport to CERN and for installation in the ATLAS Muon Spectrometer.

After transportation to CERN, an abbreviated test was conducted on the 12 BMG chambers, namely gas leak test, noise rate test, and cosmic ray test. One change was made to the noise rate test: noise rate measurements were taken with the HV both on and off, as well as with five different ASD thresholds.

The noise test revealed no unexpected results. The chambers had the expected noise rate, and there were still isolated tubes with higher noise rates as was seen at MPI (Tab. 19). The cosmic test also revealed no problems in the occupancy of the chambers (Tab. 20). In particular, there were no dead tubes (i.e., broken connections) introduced during transportation.

The gas leak test, however, again showed high gas leak rates (Tab. 21). The source of this is unknown, but the leak rates were determined to be low enough for installation in the ATLAS Muon Spectrometer, especially given the low noise rate and good occupancy of the chambers.

The chambers were therefore installed in the ATLAS Muon Spectrometer in January of 2017. The expertise gained in the construction of these chambers is being applied to the BIS7/8 project currently underway.

Not reviewed, for internal circulation only

References

[1] *ATLAS muon spectrometer: Technical Design Report*, Technical Design Report ATLAS, CERN, 1997, URL: http://cds.cern.ch/record/331068.

[2] Y. Arai et al., *ATLAS Muon Drift Tube Electronics*, Journal of Instrumentation **3** (2008) P09001, URL: http://stacks.iop.org/1748-0221/3/i=09/a=P09001.

[3] Oracle Corporation, *MySQL 5.5 Reference Manual*, URL: https://downloads.mysql.com/docs/refman-5.5-en.a4.pdf.

[4] O. Korter et al., *Construction, Testing, and Installation of New sMDT Chambers for the BME Elevator-region Upgrade*.

[5] B. Bittner et al., *Development of Muon Drift-Tube Detectors for High-Luminosity Upgrades of the Large Hadron Collider*, Nucl. Instrum. Meth. **A617** (2010) 169, arXiv: 1603.09504 [physics.ins-det].

[6] H. Kroha et al., *Construction and test of a full prototype drift-tube chamber for the upgrade of the ATLAS muon spectrometer at high LHC luminosities*, Nucl. Instrum. Meth. **A718** (2013) 427.

[7] G Aielli et al., 'Proposal for the Upgrade of the Elevator Regions in the ATLAS Barrel Muon Spectrometer', tech. rep. ATL-MUON-INT-2014-001, CERN, 2014, URL: https://cds.cern.ch/record/1642793.

[8] C. Ferretti and H. Kroha, *Upgrades of the ATLAS Muon Spectrometer with sMDT Chambers*, Nucl. Instrum. Meth. **A824** (2016) 538, arXiv: 1603.09544 [physics.ins-det].

[9] H. Kroha et al., *Construction and Test of New Precision Drift-Tube Chambers for the ATLAS Muon Spectrometer*, Nucl. Instrum. Meth. **A845** (2017) 244, arXiv: 1603.08760 [physics.ins-det].

[10] H. Kroha, 'Proposal for the Improvement of the ATLAS Muon Spectrometer Momentum Resolution in Barrel Sectors 12 and 14', tech. rep. ATL-MUON-INT-2015-001, CERN, 2015, URL: https://cds.cern.ch/record/1984472.

[11] G. Aielli et al., 'The ATLAS BIS78 Project', tech. rep. ATL-COM-MUON-2016-018, CERN, 2015, URL: https://cds.cern.ch/record/2156994.

[12] M. Deile et al., *Resolution and Efficiency of the ATLAS Muon Drift-Tube Chambers at High Background Rates*, Nucl. Instrum. Meth. **A535** (2004) 212, arXiv: 1603.09572 [physics.ins-det].

[13] S. Horvat et al., *Operation of the ATLAS muon drift-tube chambers at high background rates and in magnetic fields*, IEEE Transactions on Nuclear Science **53** (2006) 562, ISSN: 0018-9499.

[14] B. Bittner, H. Kroha and O. Kortner, 'Development and Characterisation of New High-Rate Muon Drift Tube Detectors', Presented 30 Jul 2012, PhD thesis: Munich, Tech. U., 2012, URL: https://cds.cern.ch/record/1479585.

[15] P. Schwegler and H. Kroha, 'High-Rate Performance of Muon Drift Tube Detectors', Presented 14 07 2014, PhD thesis: Munich, Tech. U., 2014, URL: https://cds.cern.ch/record/1746370.

Not reviewed, for internal circulation only

[16] B. Bittner et al.,
Performance of drift-tube detectors at high counting rates for high-luminosity LHC upgrades,
Nucl. Instrum. Meth. **A732** (2013) 250, arXiv: 1603.09508 [physics.ins-det].

[17] O. Kortner et al., *Precision muon tracking detectors and read-out electronics for operation at very high background rates at future colliders*, Nucl. Instrum. Meth. **A824** (2016) 556.

[18] P. Schwegler et al.,
'Optimization of the front-end electronics of Drift Tube chambers for high-rate operation',
2014 IEEE Nuclear Science Symposium and Medical Imaging Conference (NSS/MIC), 2014 1.

[19] S. Nowak et al., 'Optimisation of the Read-out Electronics of Muon Drift-Tube Chambers for Very High Background Rates at HL-LHC and Future Colliders', tech. rep., 2016 7581815,
arXiv: 1603.08841 [physics.ins-det],
URL: https://inspirehep.net/record/1436364/files/arXiv:1603.08841.pdf.

[20] J Christiansen, 'HPTDC High Performance Time to Digital Converter', tech. rep.,
Version 2.2 for HPTDC version 1.3: CERN, 2004,
URL: https://cds.cern.ch/record/1067476.

Not reviewed, for internal circulation only

Auxiliary material

A sMDT BMG Tests at MPI

A.1 sMDT BMG Noise Rates

The measured noise rates for the chambers at MPI with the HV on and with the ASD threshold at 108 are below.

Table 22: Measured noise rates for completed chambers at MPI with HV on and the ASD threshold of 108 (or 39 mV, the operational value). As before, the left column corresponds to the upper multilayer, and the right column corresponds to the lower multilayer. The four plots in each column, from top to bottom, correspond to the four layers of tubes in each multilayer.

Chamber	
BMG-6C-12	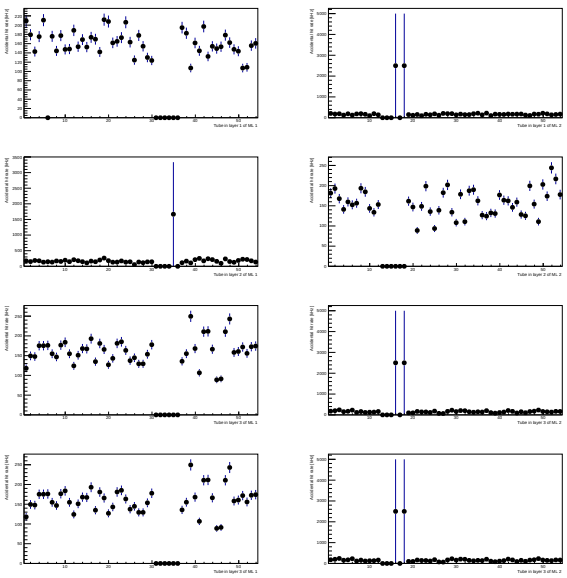

Not reviewed, for internal circulation only

Table 22: Measured noise rates for completed chambers at MPI with HV on and the ASD threshold of 108 (continued).

Chamber	
BMG-6C-14	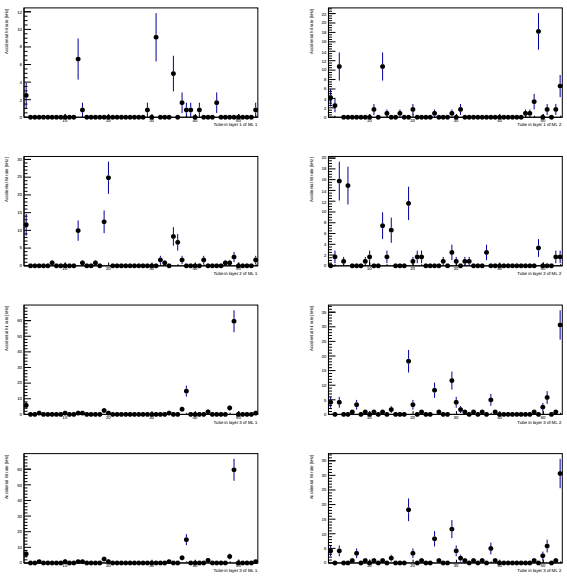
BMG-6A-12	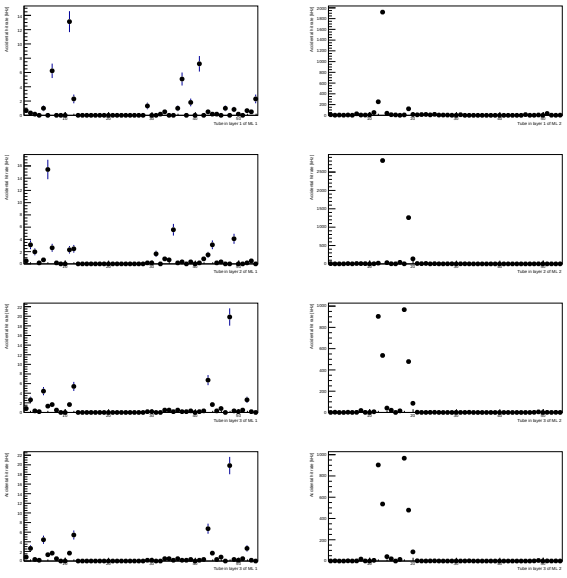

Not reviewed, for internal circulation only

Table 22: Measured noise rates for completed chambers at MPI with HV on and the ASD threshold of 108 (continued).

Chamber	
BMG-6A-14	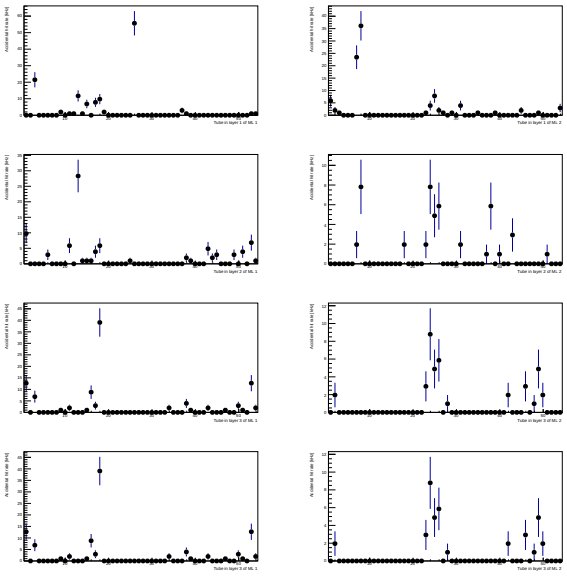
BMG-4C-12	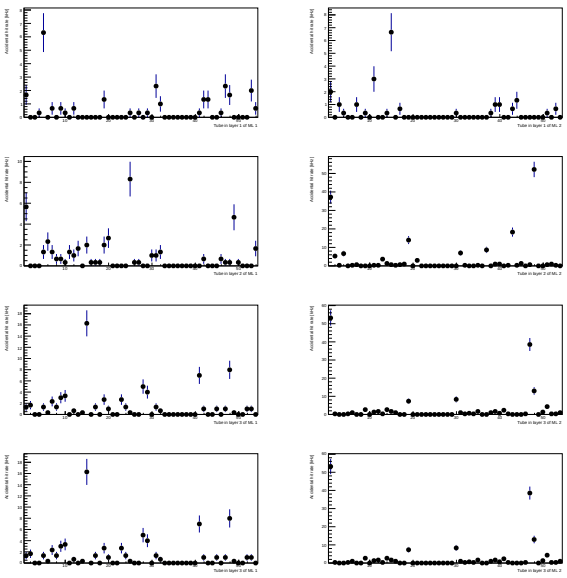

Not reviewed, for internal circulation only

Table 22: Measured noise rates for completed chambers at MPI with HV on and the ASD threshold of 108 (continued).

Chamber	
BMG-4C-14	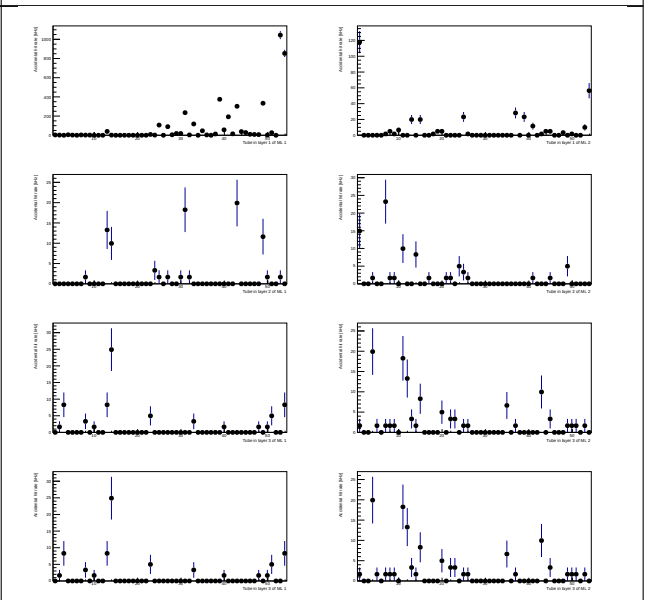
BMG-4A-14	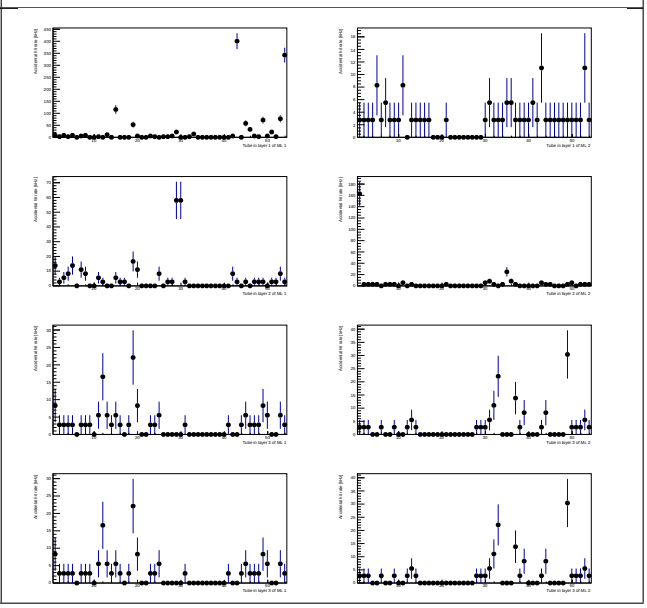

Not reviewed, for internal circulation only

Table 22: Measured noise rates for completed chambers at MPI with HV on and the ASD threshold of 108 (continued).

Chamber	
BMG-4A-12	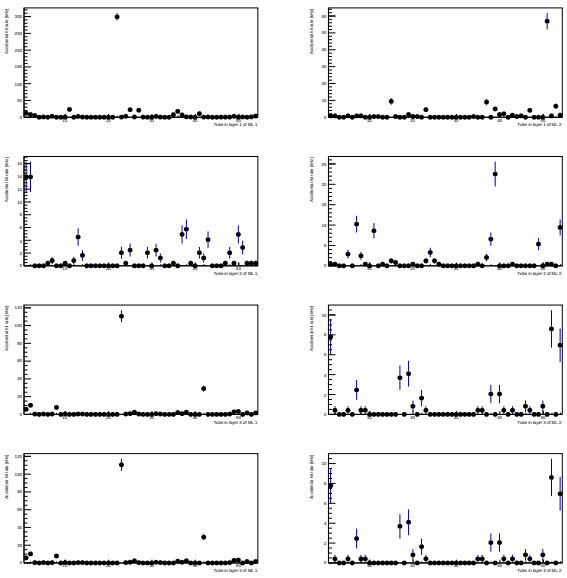
BMG-2C-12	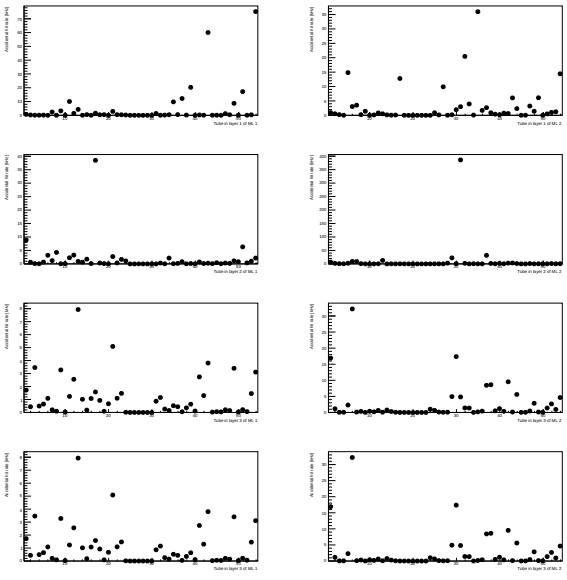

Not reviewed, for internal circulation only

Table 22: Measured noise rates for completed chambers at MPI with HV on and the ASD threshold of 108 (continued).

Chamber	
BMG-2C-14	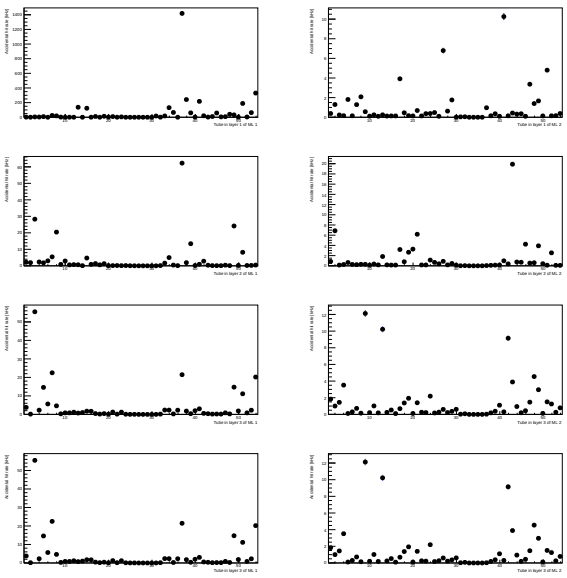
BMG-2A-12	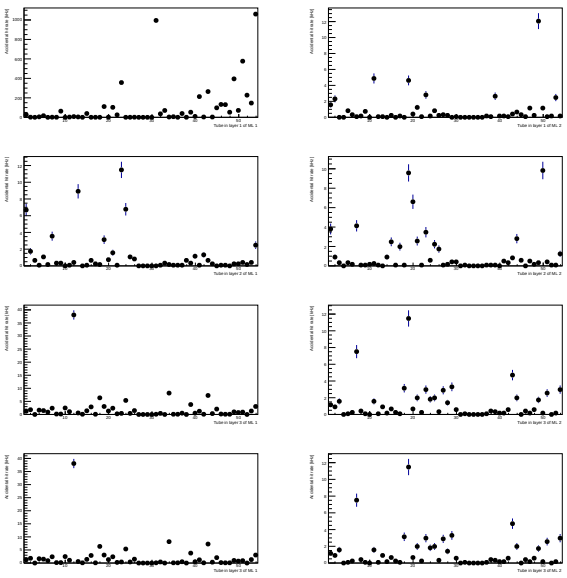

A.2 sMDT BMG Cosmic Ray Results

The measured cosmic ray hits for the chambers at MPI with the HV on and the ASD threshold at 108 are below.

Not reviewed, for internal circulation only

Table 23: Measured cosmic hit rates spectra for completed chambers at MPI. The total hits per tube is shown in black, and the hits associated with cosmic tracks are shown in red. As before, the left column corresponds to the upper multilayer, and the right column corresponds to the lower multilayer. The four plots in each column, from top to bottom, correspond to the four layers of tubes in each multilayer.

Chamber	
BMG-6C-12	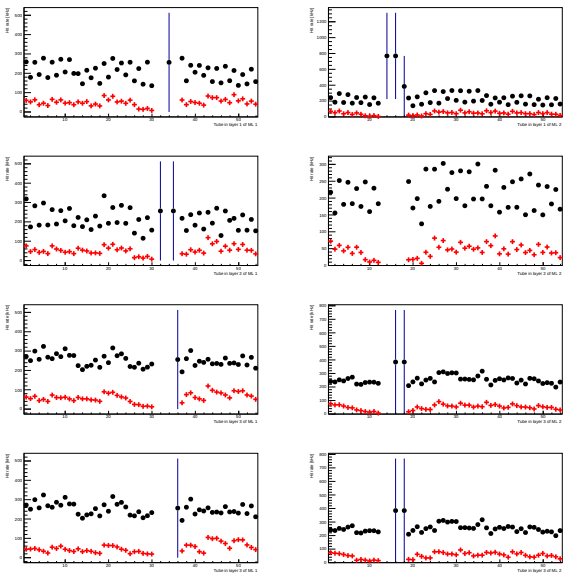
BMG-6A-12	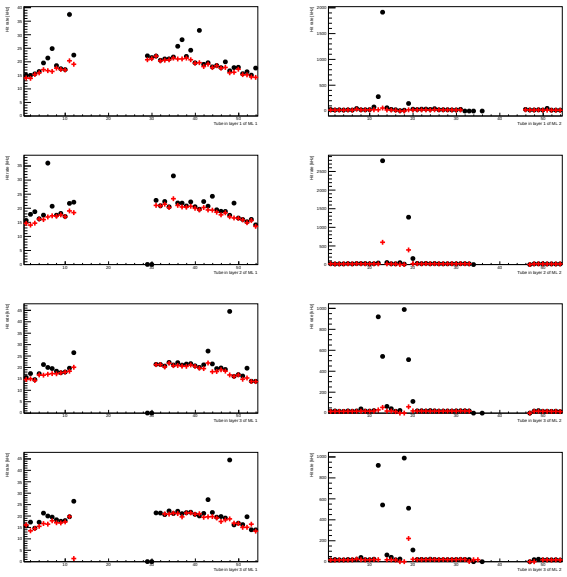

Not reviewed, for internal circulation only

Table 23: Measured cosmic hit rates spectra for completed chambers at MPI (continued).

Chamber	
BMG-6A-14	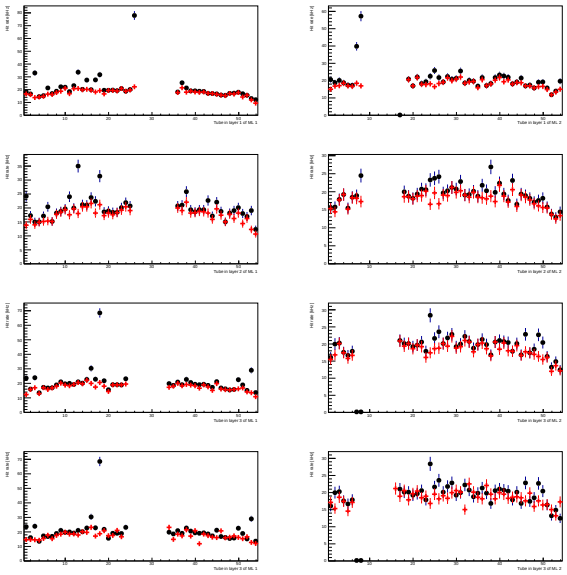
BMG-6C-14	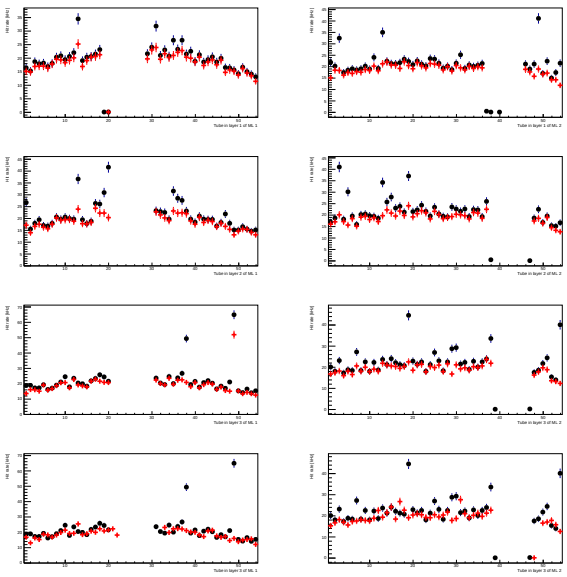

Not reviewed, for internal circulation only

Table 23: Measured cosmic hit rates spectra for completed chambers at MPI (continued).

Chamber	
BMG-4C-12	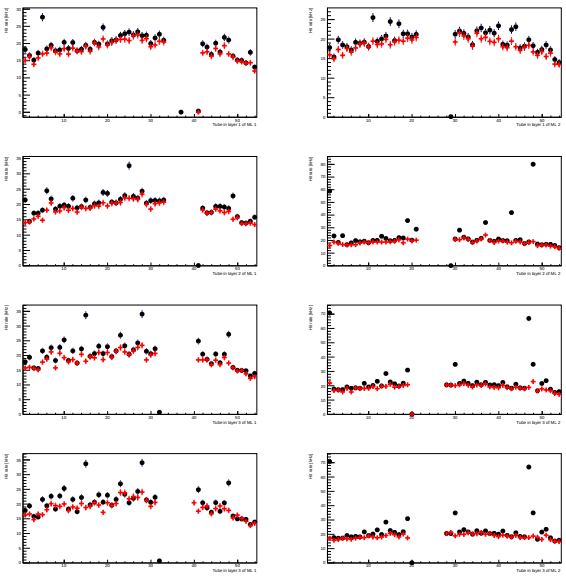
BMG-4C-14	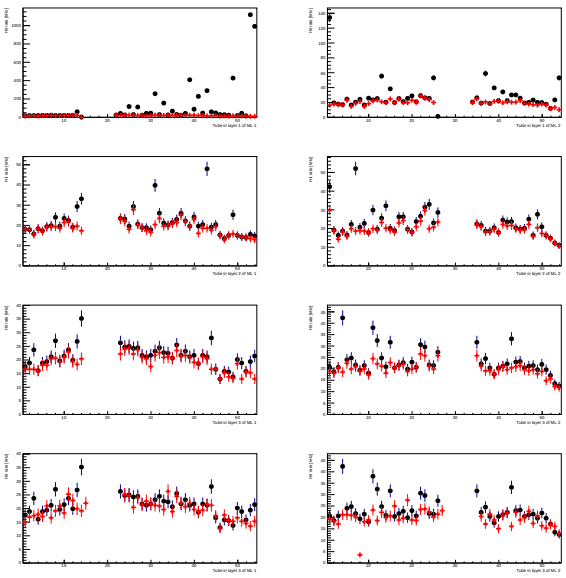

Not reviewed, for internal circulation only

Table 23: Measured cosmic hit rates spectra for completed chambers at MPI (continued).

Chamber	
BMG-4A-14	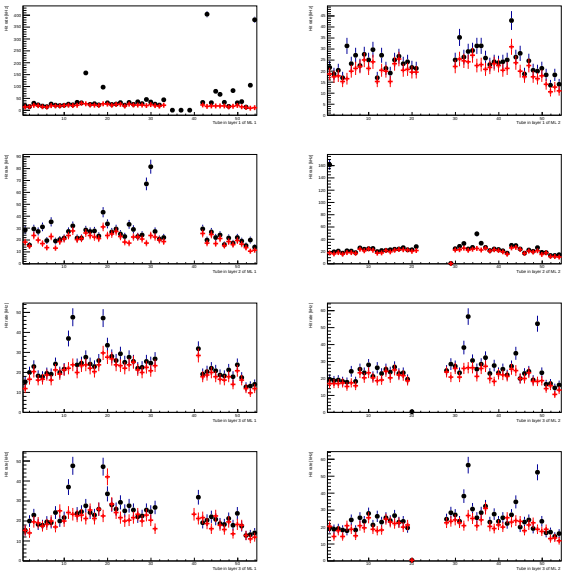
BMG-4A-12	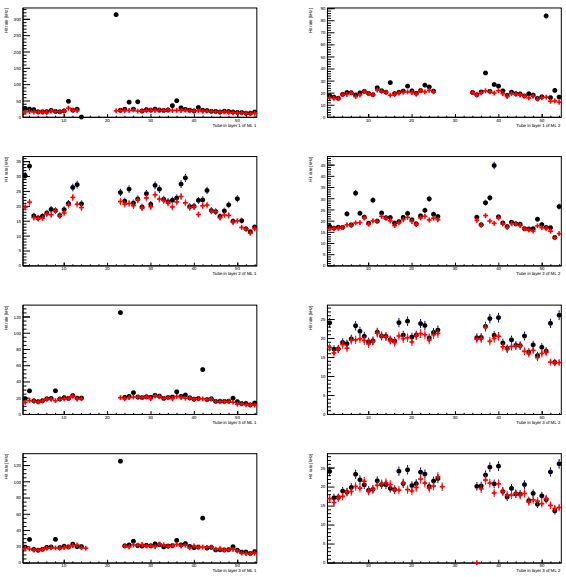

Not reviewed, for internal circulation only

Table 23: Measured cosmic hit rates spectra for completed chambers at MPI (continued).

Chamber	
BMG-2C-12	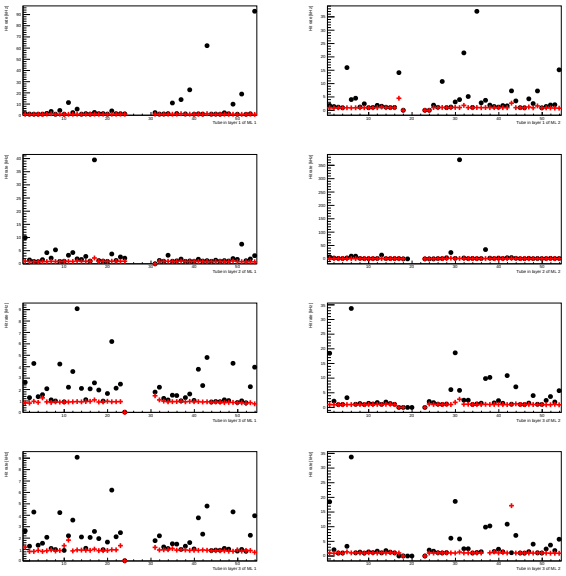
BMG-2C-14	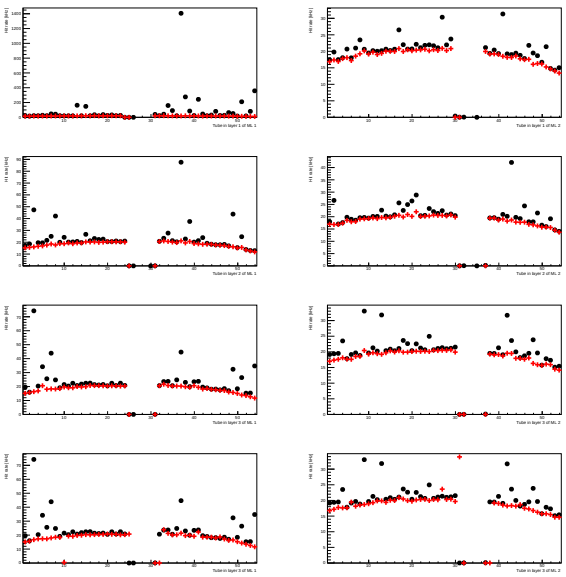

Not reviewed, for internal circulation only

Table 23: Measured cosmic hit rates spectra for completed chambers at MPI (continued).

Chamber	
BMG-2A-12	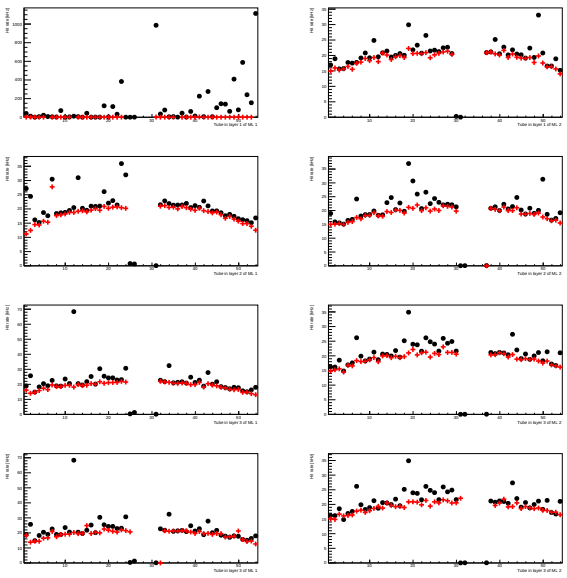

B sMDT BMG Tests at CERN

B.1 sMDT BMG Noise Rates

The measured noise rates for the chambers at CERN with the HV on and off, with the ASD threshold varied between 103, 106, 108, 110, and 112 are below.

Not reviewed, for internal circulation only

Table 24: Measured noise rates for completed chambers at CERN with HV on and the ASD threshold of 103

Chamber	
BMG-6C-12	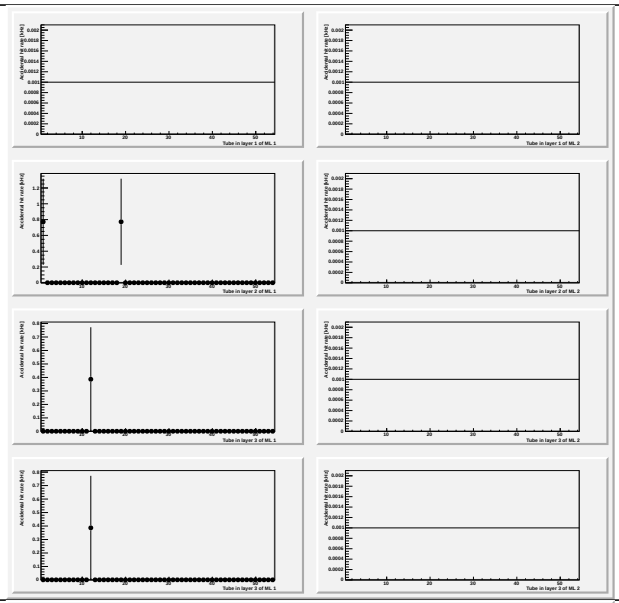
BMG-6A-12	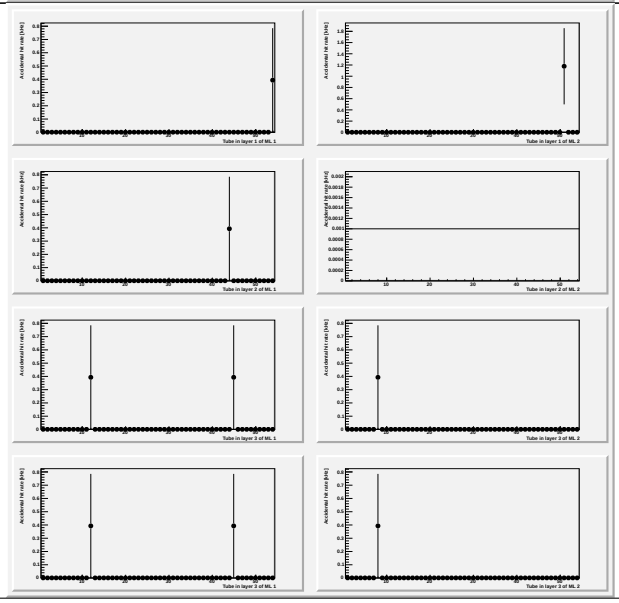

Not reviewed, for internal circulation only

Table 24: Measured noise rates for completed chambers at CERN with HV on and the ASD threshold of 103 (continued)

Chamber	
BMG-6A-14	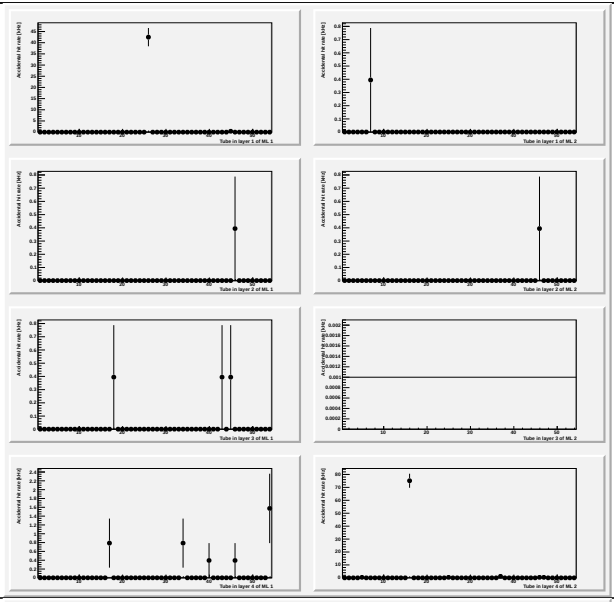
BMG-6C-14	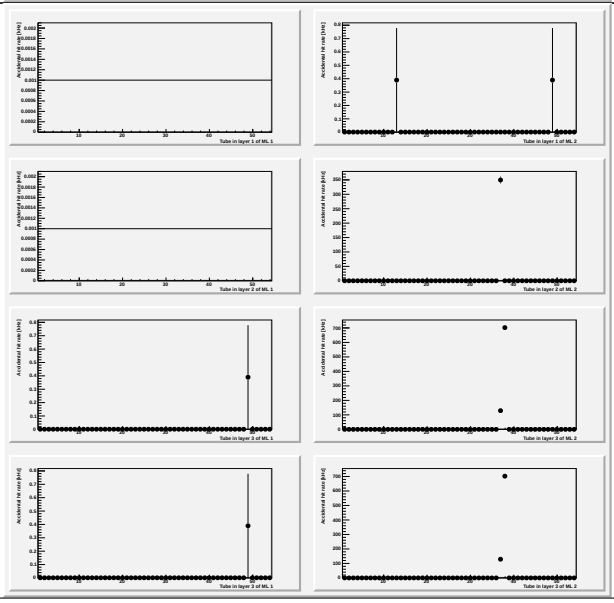

Not reviewed, for internal circulation only

Table 24: Measured noise rates for completed chambers at CERN with HV on and the ASD threshold of 103 (continued)

Chamber	
BMG-4C-12	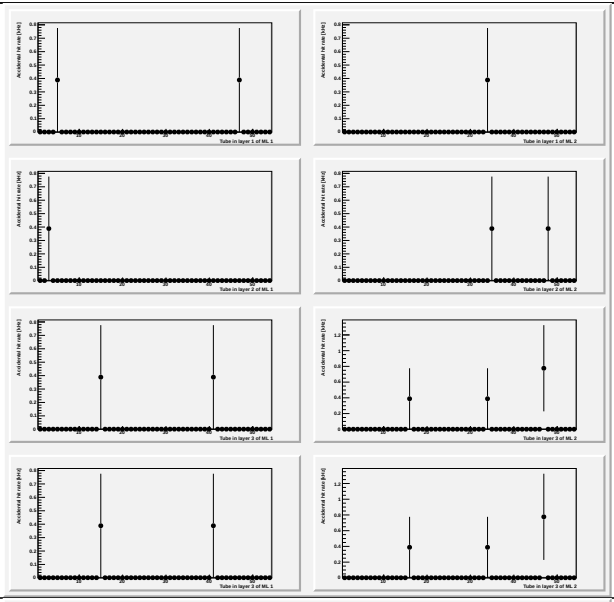
BMG-4C-14	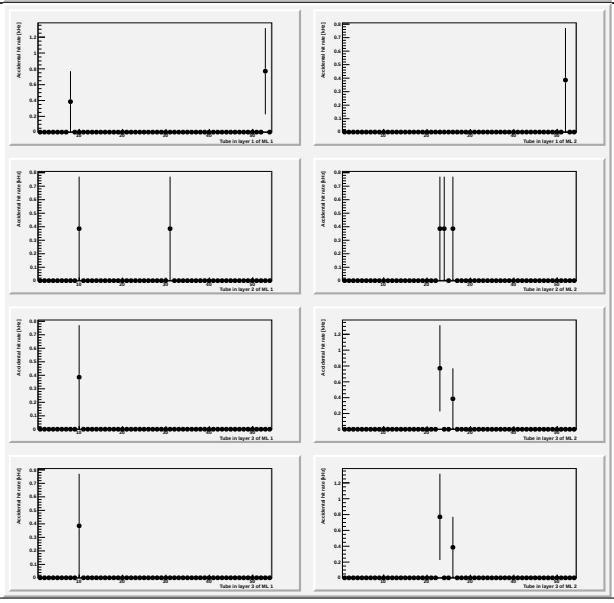

Not reviewed, for internal circulation only

Table 24: Measured noise rates for completed chambers at CERN with HV on and the ASD threshold of 103 (continued)

Chamber	
BMG-4A-14	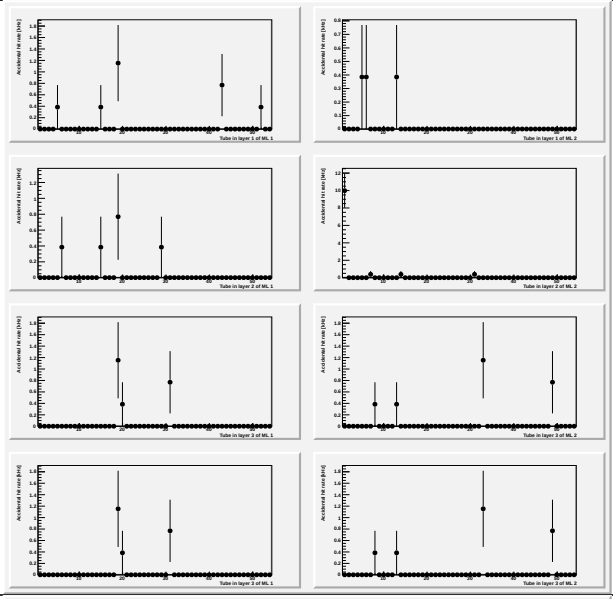
BMG-4A-12	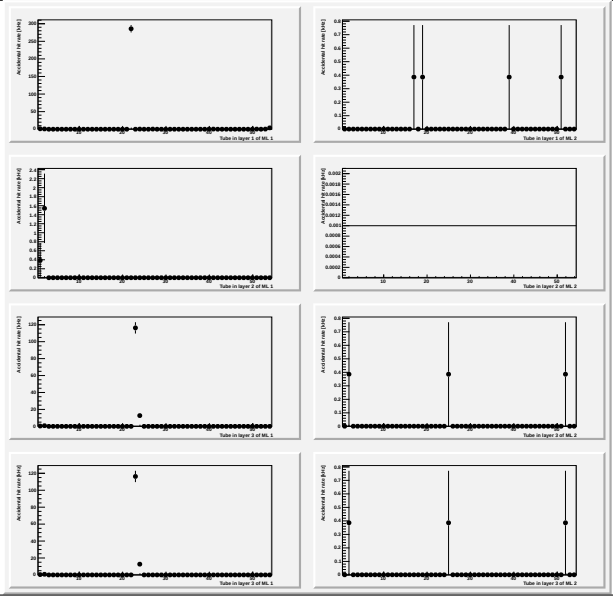

Not reviewed, for internal circulation only

Table 24: Measured noise rates for completed chambers at CERN with HV on and the ASD threshold of 103 (continued)

Chamber	
BMG-2C-12	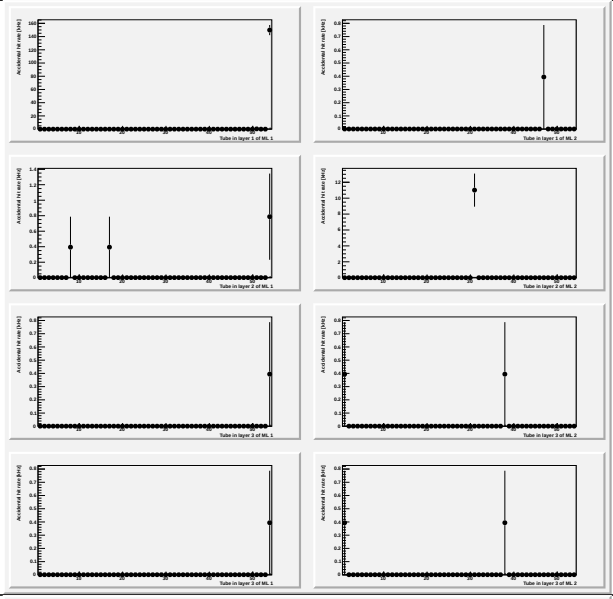
BMG-2A-14	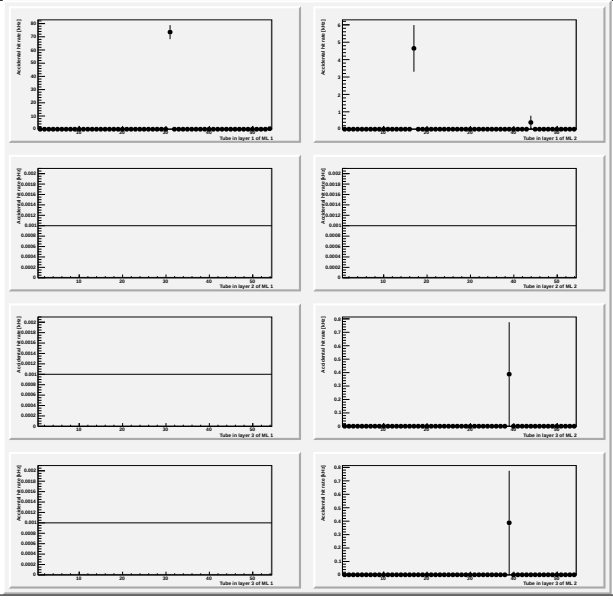

Not reviewed, for internal circulation only

Table 24: Measured noise rates for completed chambers at CERN with HV on and the ASD threshold of 103 (continued)

Chamber	
BMG-2C-14	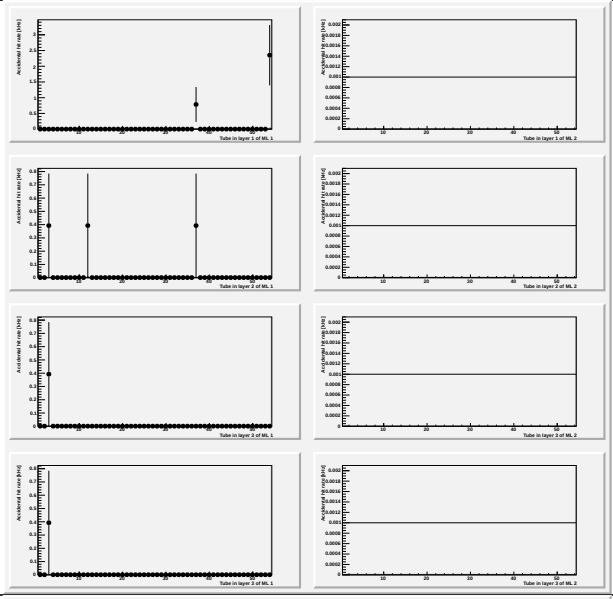
BMG-2A-12	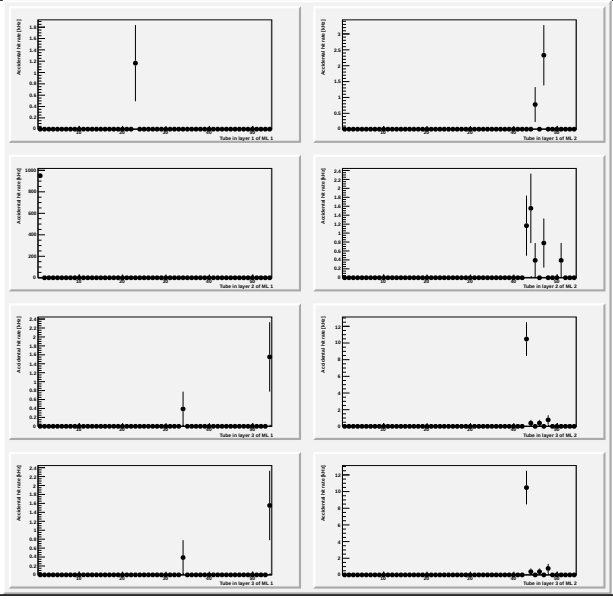

Not reviewed, for internal circulation only

Table 25: Measured noise rates for completed chambers at CERN with HV on and the ASD threshold of 106

Chamber	
BMG-6C-12	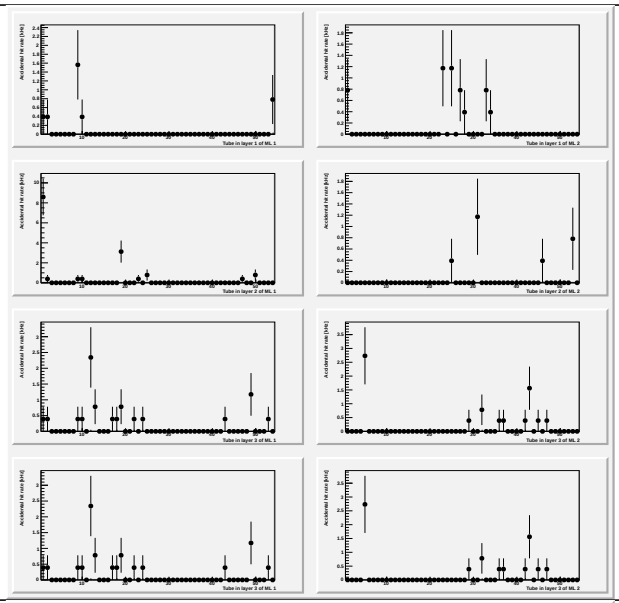
BMG-6A-12	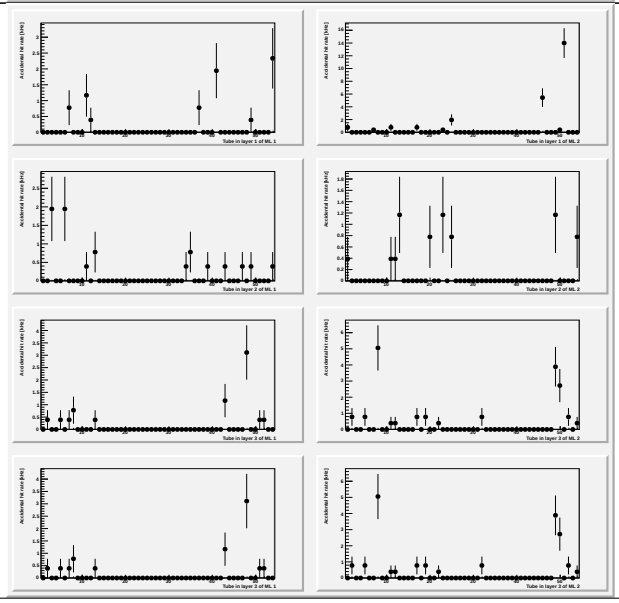

Not reviewed, for internal circulation only

Table 25: Measured noise rates for completed chambers at CERN with HV on and the ASD threshold of 106 (continued)

Chamber	
BMG-6A-14	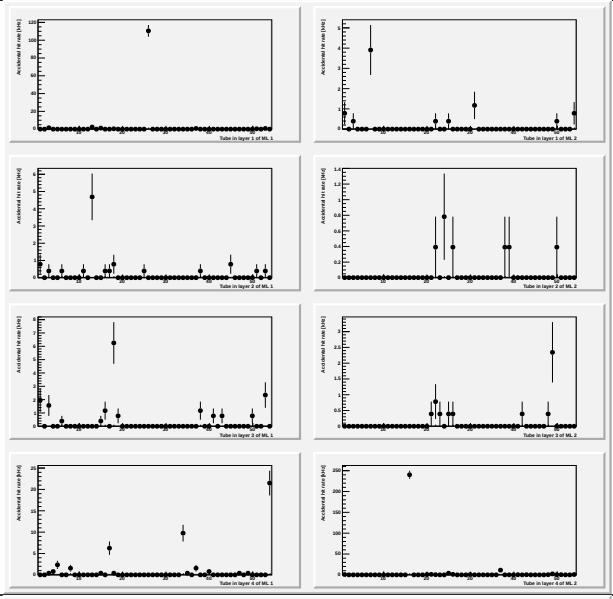
BMG-6C-14	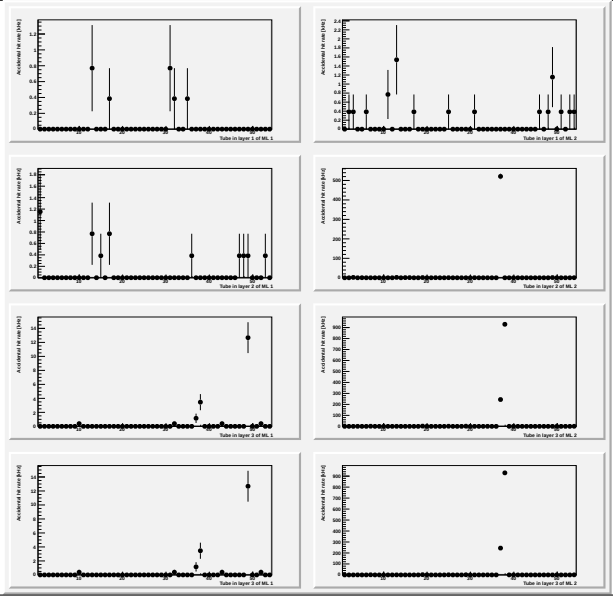

Not reviewed, for internal circulation only

Table 25: Measured noise rates for completed chambers at CERN with HV on and the ASD threshold of 106 (continued)

Chamber	
BMG-4C-12	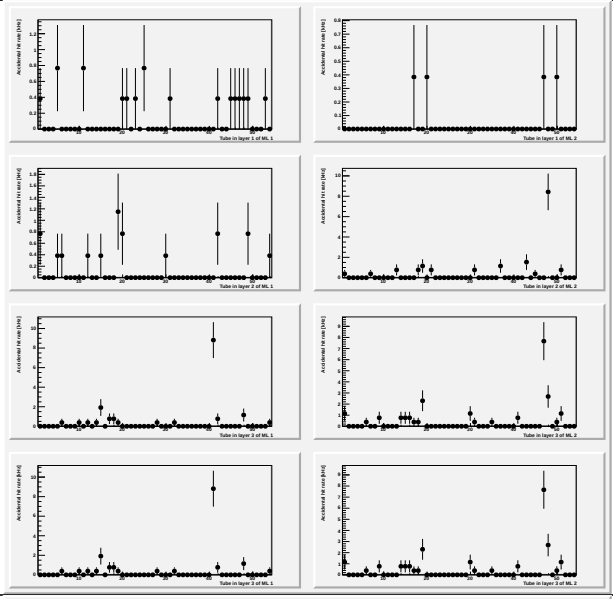
BMG-4C-14	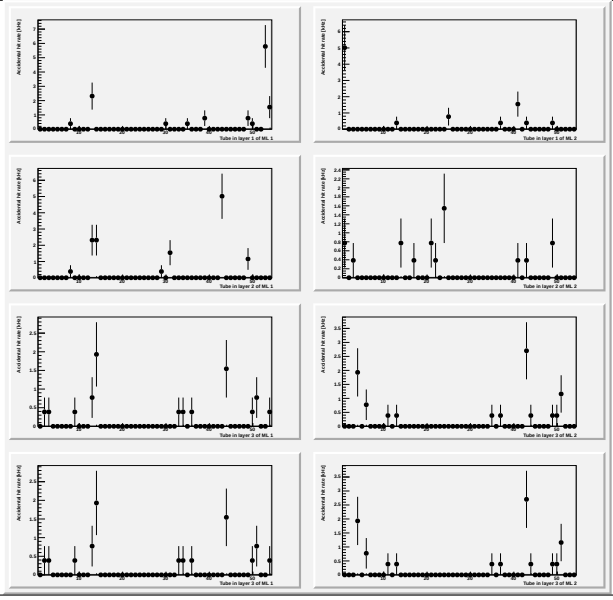

Not reviewed, for internal circulation only

Table 25: Measured noise rates for completed chambers at CERN with HV on and the ASD threshold of 106 (continued)

Chamber	
BMG-4A-14	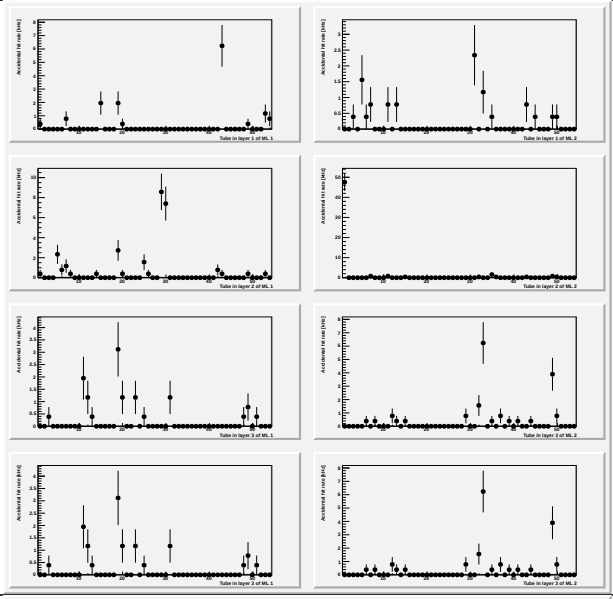
BMG-4A-12	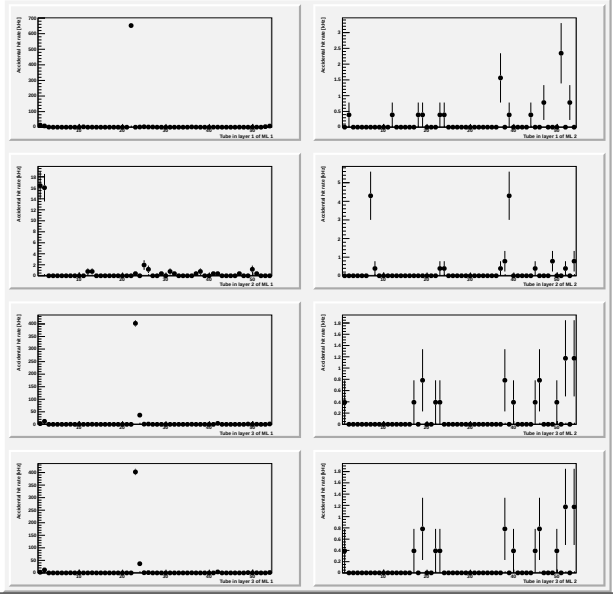

Not reviewed, for internal circulation only

Table 25: Measured noise rates for completed chambers at CERN with HV on and the ASD threshold of 106 (continued)

Chamber	
BMG-2C-12	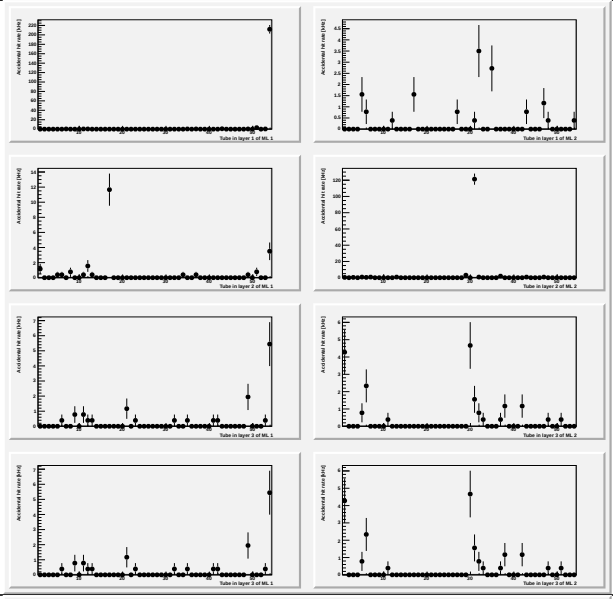
BMG-2A-14	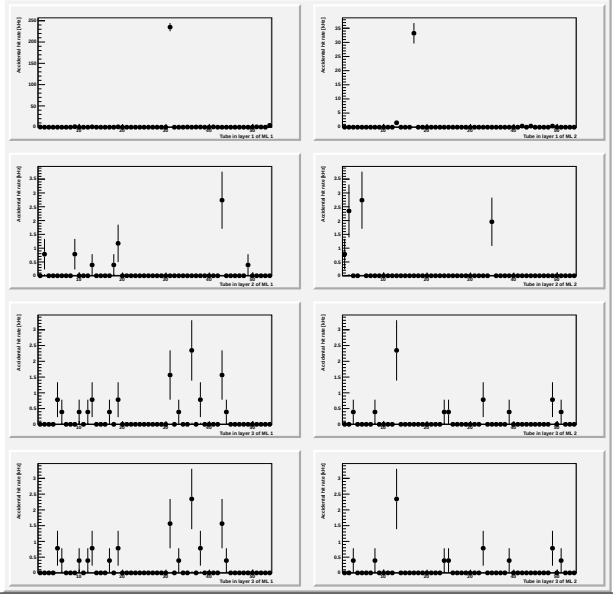

Not reviewed, for internal circulation only

Table 25: Measured noise rates for completed chambers at CERN with HV on and the ASD threshold of 106 (continued)

Chamber	
BMG-2C-14	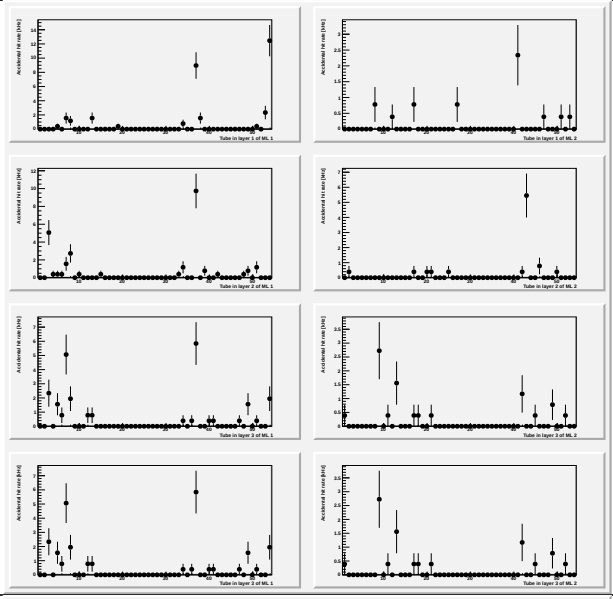
BMG-2A-12	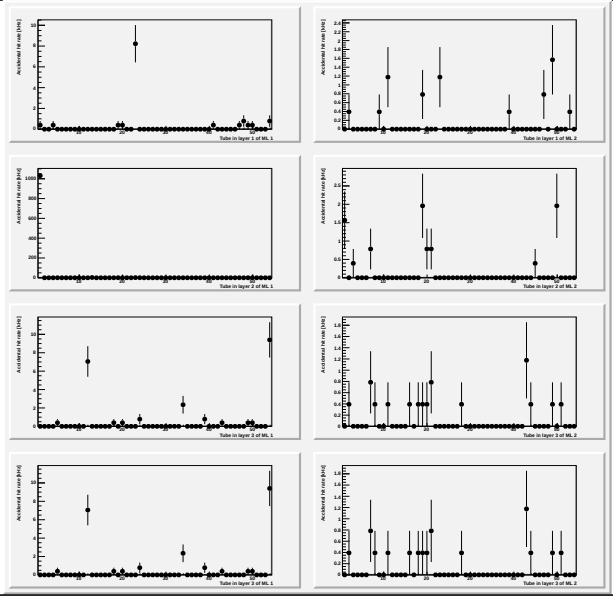

Not reviewed, for internal circulation only

Table 26: Measured noise rates for completed chambers at CERN with HV on and the ASD threshold of 108 (or 39 mV, the operational value). As before, the left column corresponds to the upper multilayer, and the right column corresponds to the lower multilayer. The four plots in each column, from top to bottom, correspond to the four layers of tubes in each multilayer.

Chamber	
BMG-6C-12	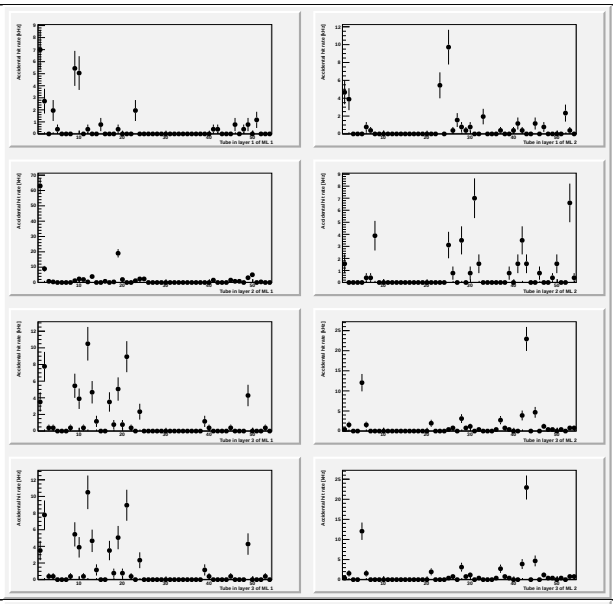
BMG-6C-14	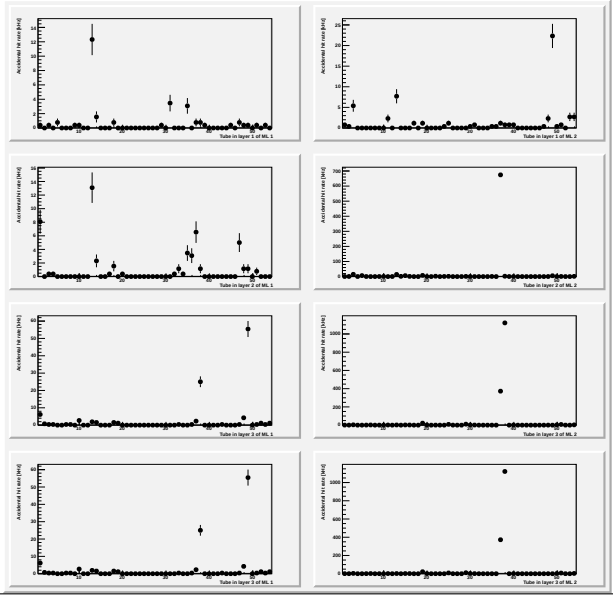

Not reviewed, for internal circulation only

Table 26: Measured noise rates for completed chambers at CERN with HV on and the ASD threshold of 108 (continued).

Chamber	
BMG-6A-12	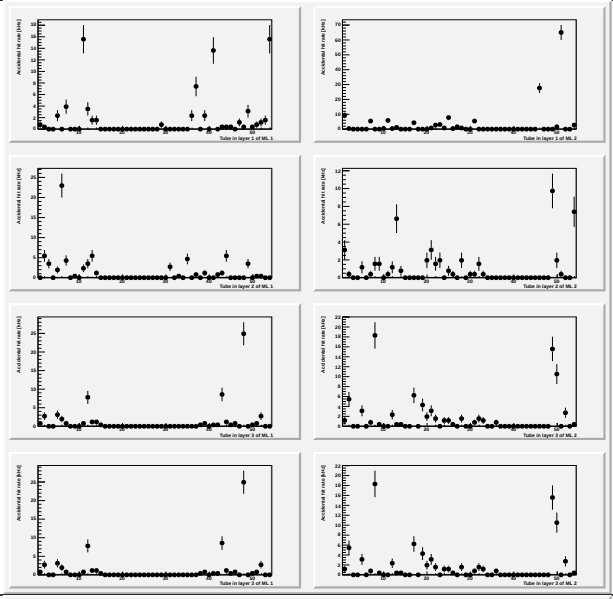
BMG-6A-14	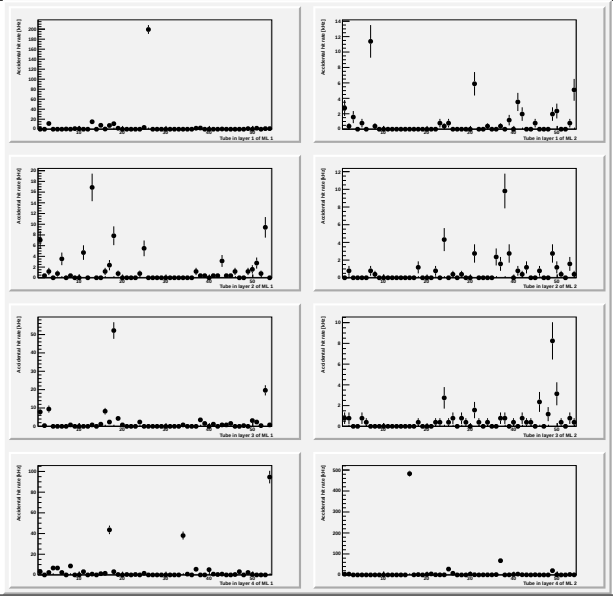

Not reviewed, for internal circulation only

Table 26: Measured noise rates for completed chambers at CERN with HV on and the ASD threshold of 108 (continued).

Chamber	
BMG-4C-12	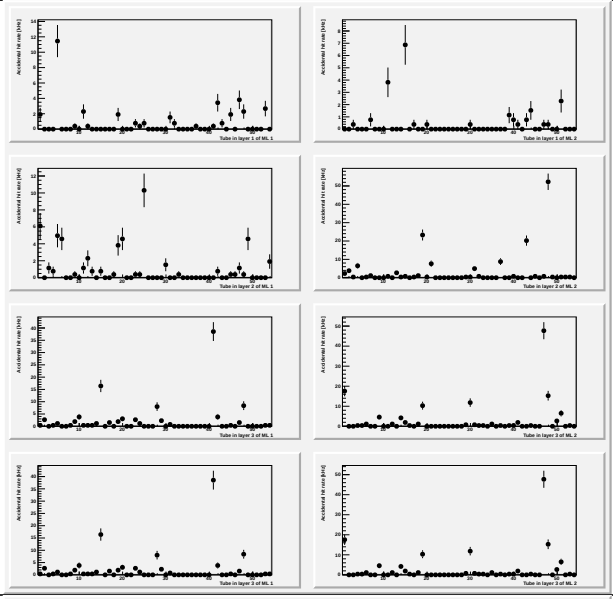
BMG-4C-14	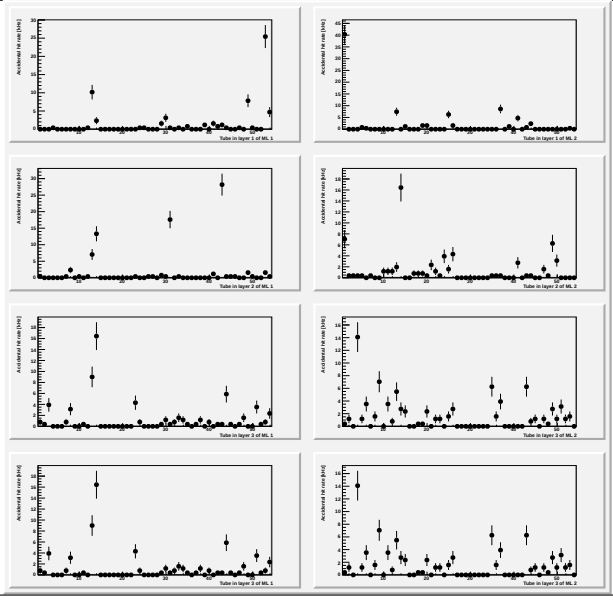

Not reviewed, for internal circulation only

Table 26: Measured noise rates for completed chambers at CERN with HV on and the ASD threshold of 108 (continued).

Chamber	
BMG-4A-14	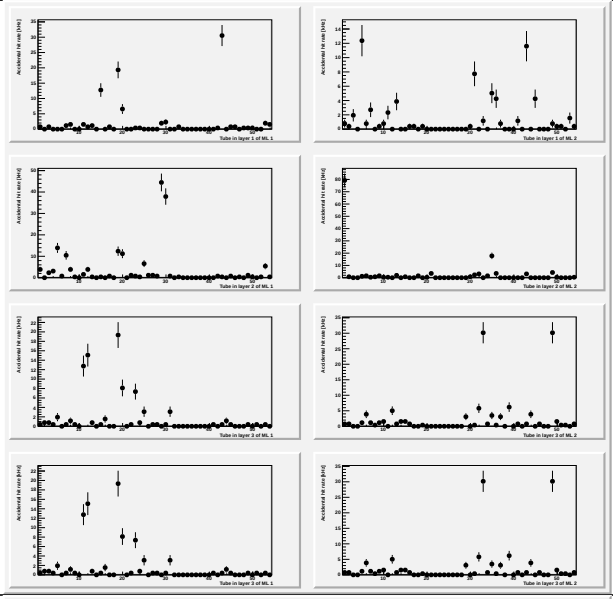
BMG-4A-12	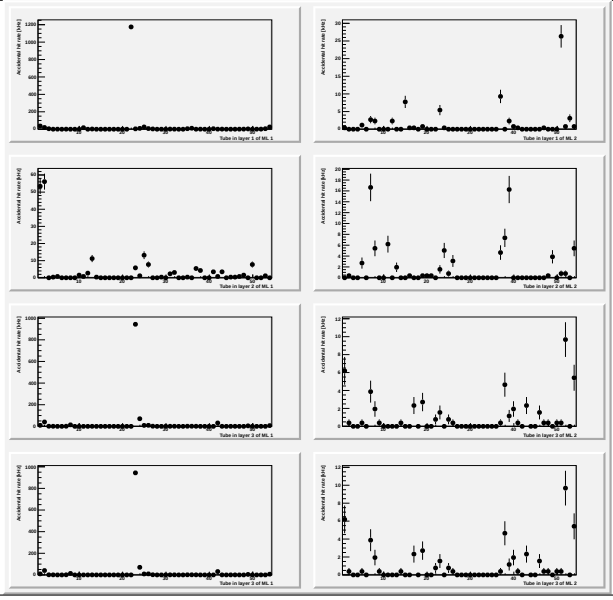

Not reviewed, for internal circulation only

Table 26: Measured noise rates for completed chambers at CERN with HV on and the ASD threshold of 108 (continued).

Chamber	
BMG-2C-12	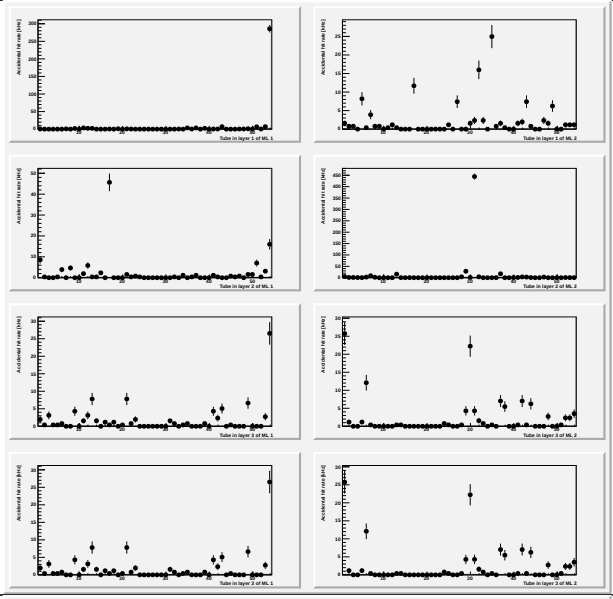
BMG-2A-14	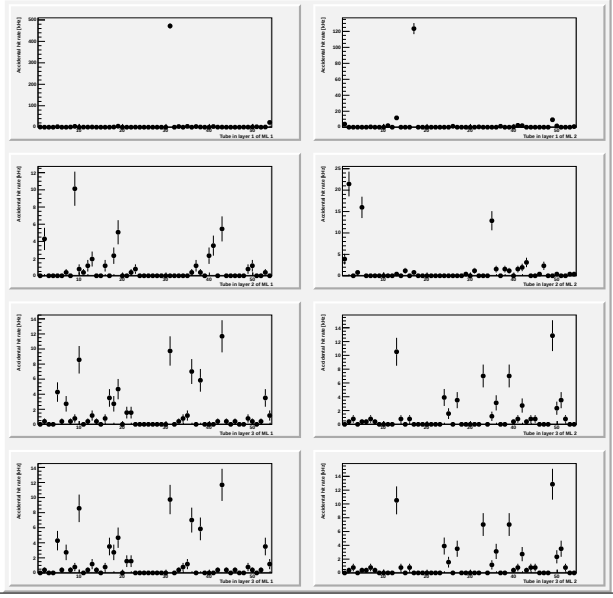

Not reviewed, for internal circulation only

Table 26: Measured noise rates for completed chambers at CERN with HV on and the ASD threshold of 108 (continued).

Chamber	
BMG-2C-14	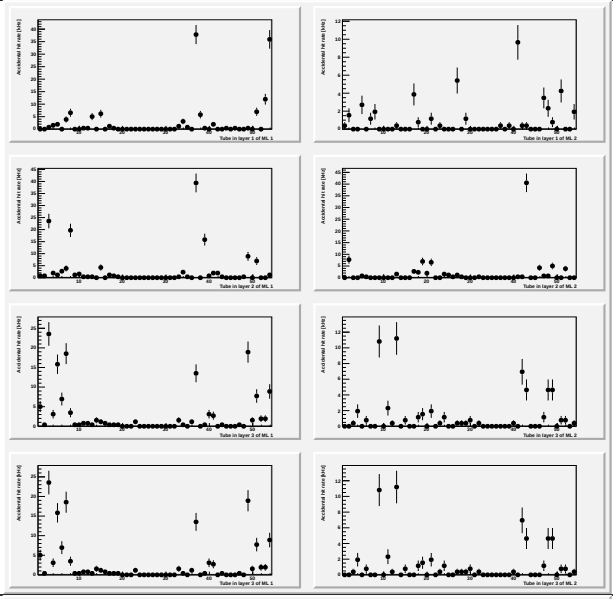
BMG-2A-12	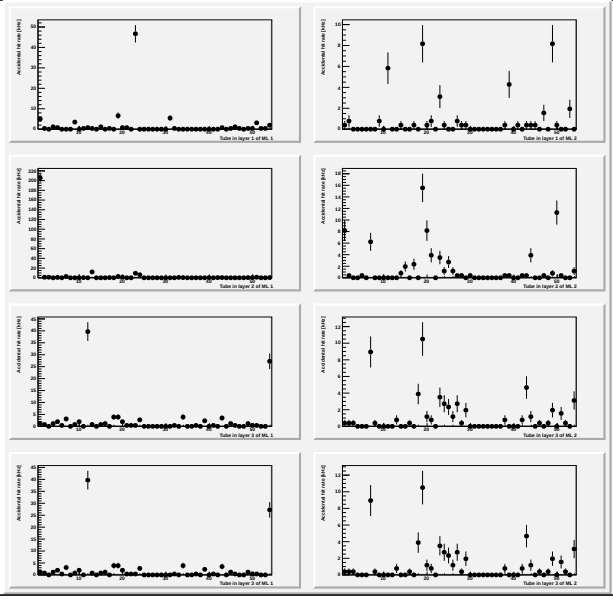

Not reviewed, for internal circulation only

Table 27: Measured noise rates for completed chambers at CERN with HV on and the ASD threshold of 110

Chamber	
BMG-6C-12	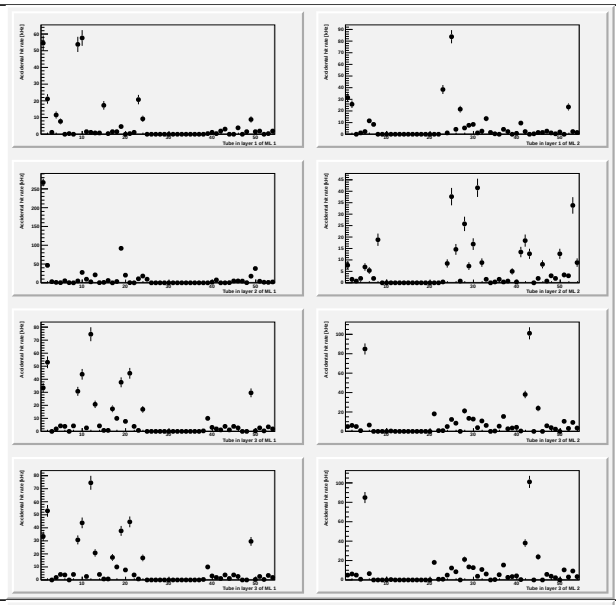
BMG-6A-12	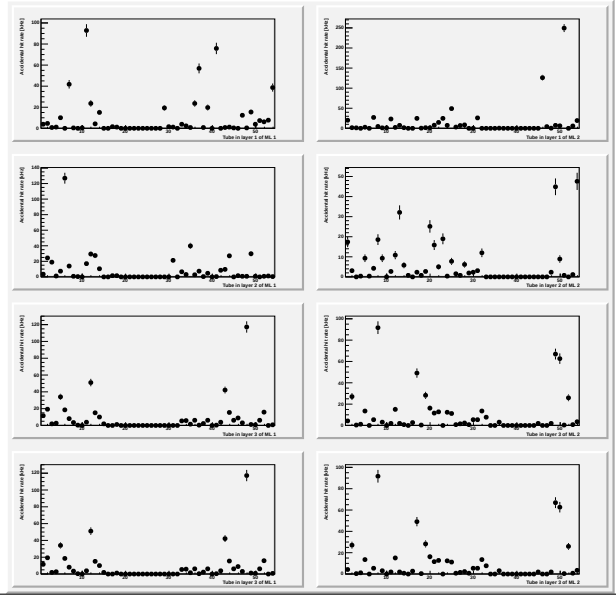

Not reviewed, for internal circulation only

Table 27: Measured noise rates for completed chambers at CERN with HV on and the ASD threshold of 110 (continued)

Chamber	
BMG-6A-14	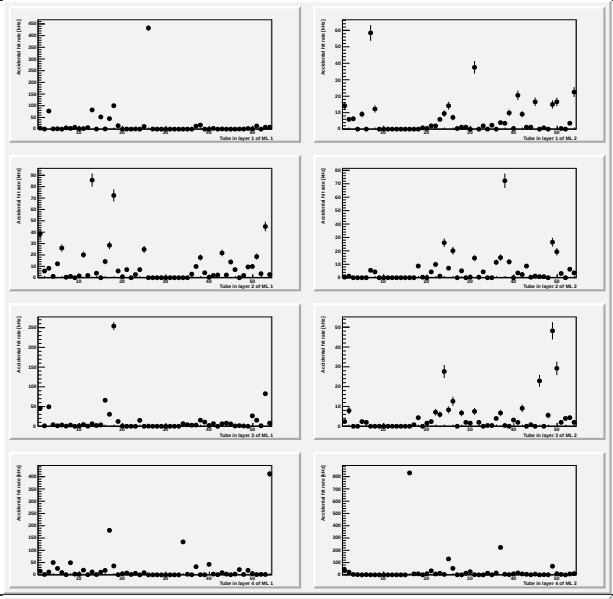
BMG-6C-14	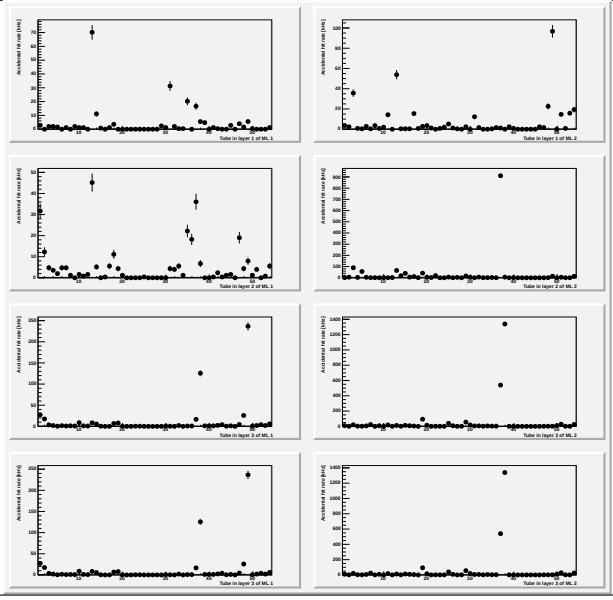

Not reviewed, for internal circulation only

Table 27: Measured noise rates for completed chambers at CERN with HV on and the ASD threshold of 110 (continued)

Chamber	
BMG-4C-12	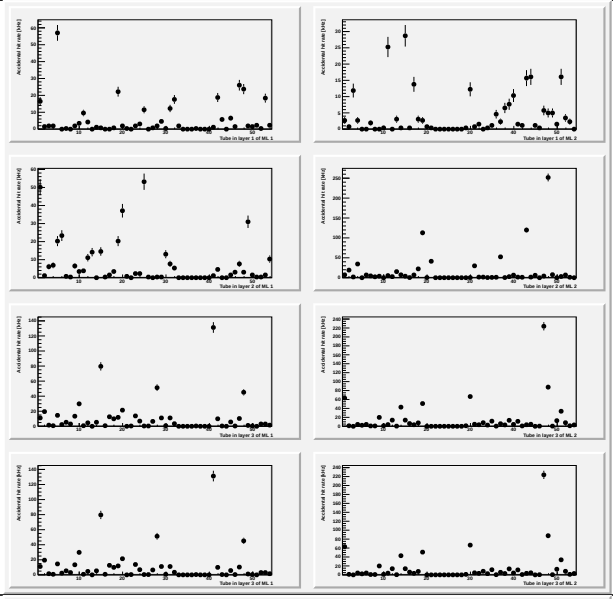
BMG-4C-14	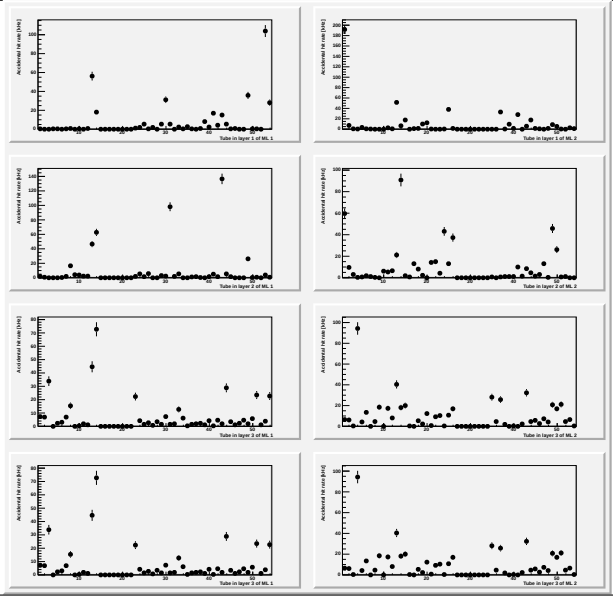

Not reviewed, for internal circulation only

Table 27: Measured noise rates for completed chambers at CERN with HV on and the ASD threshold of 110 (continued)

Chamber	
BMG-4A-14	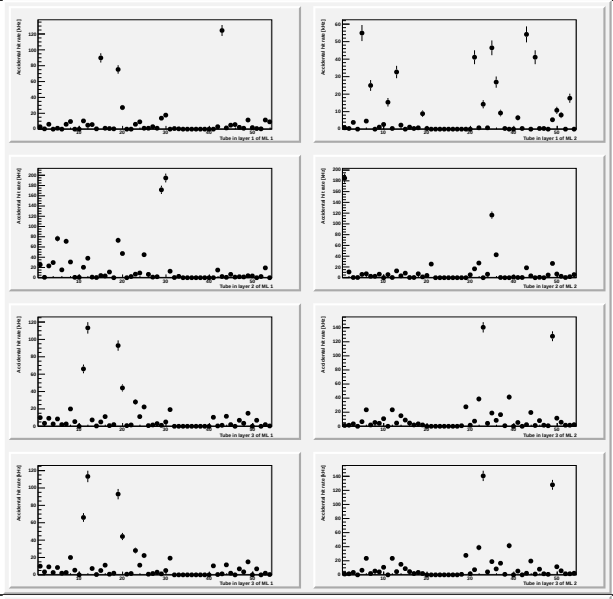
BMG-4A-12	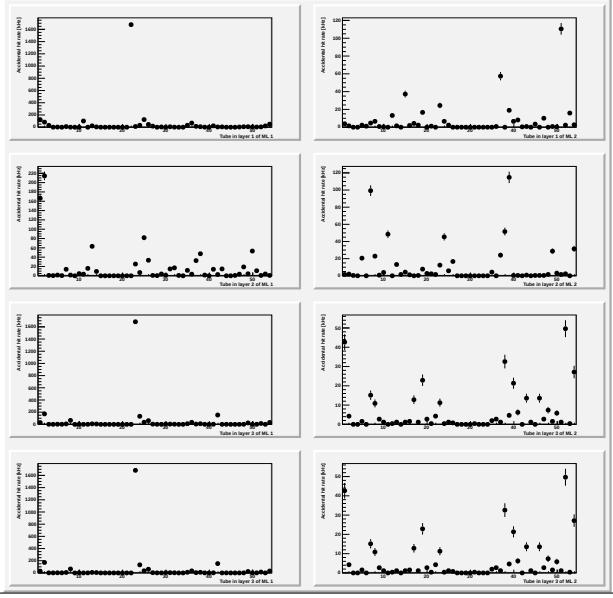

Not reviewed, for internal circulation only

Table 27: Measured noise rates for completed chambers at CERN with HV on and the ASD threshold of 110 (continued)

Chamber	
BMG-2C-12	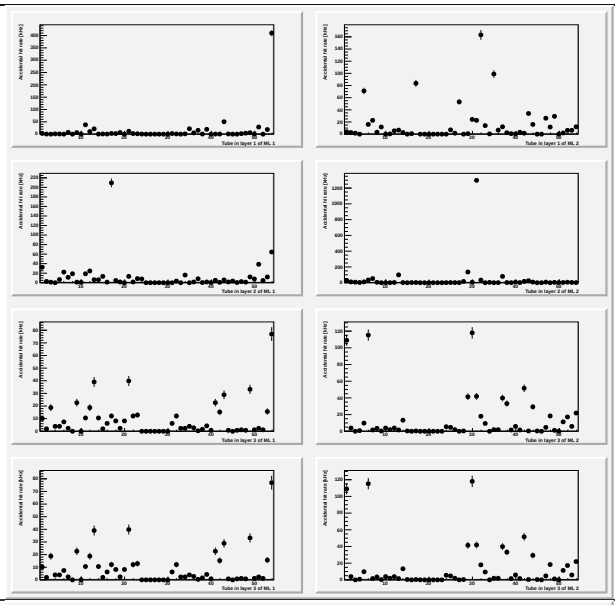
BMG-2A-14	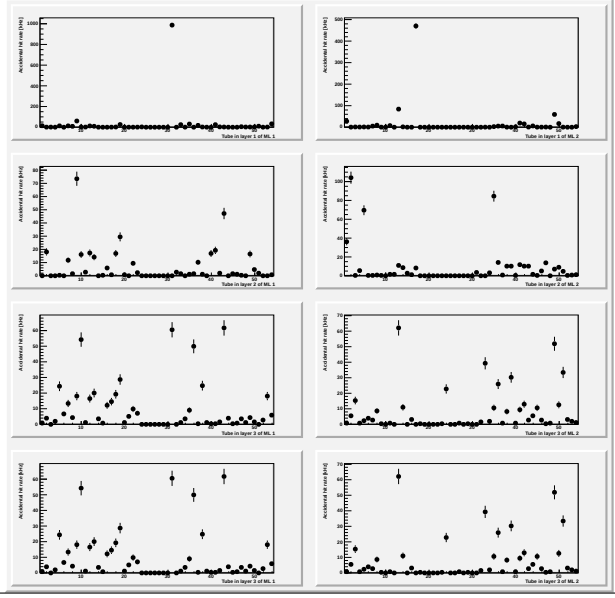

Not reviewed, for internal circulation only

Table 27: Measured noise rates for completed chambers at CERN with HV on and the ASD threshold of 110 (continued)

Chamber	
BMG-2C-14	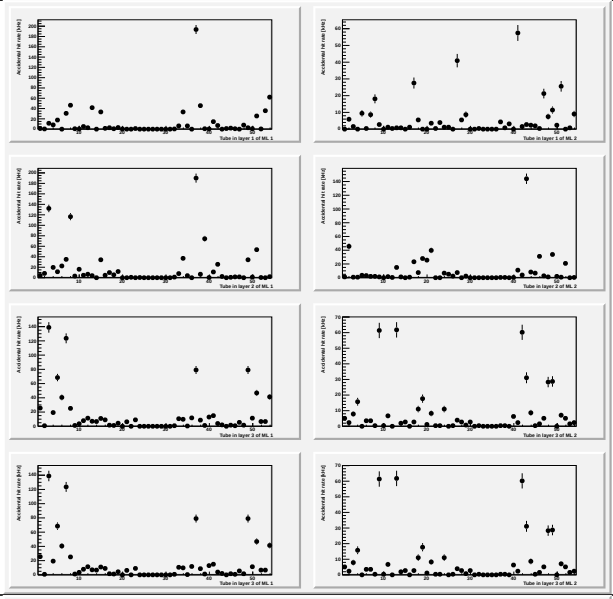
BMG-2A-12	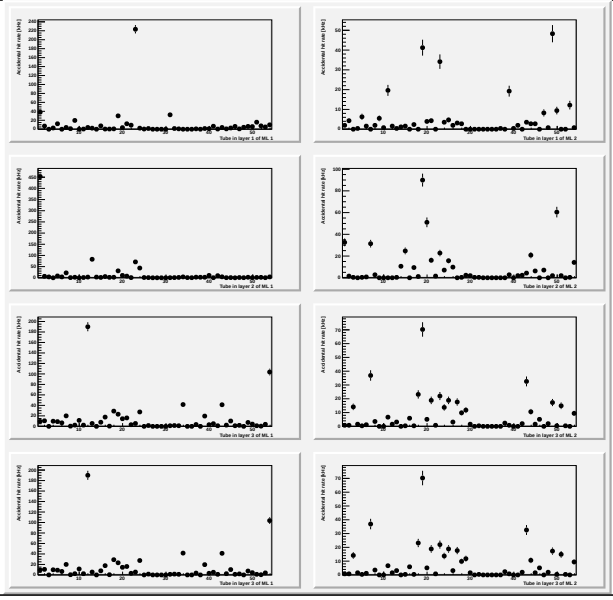

Not reviewed, for internal circulation only

Table 28: Measured noise rates for completed chambers at CERN with HV on and the ASD threshold of 112

Chamber	
BMG-6C-12	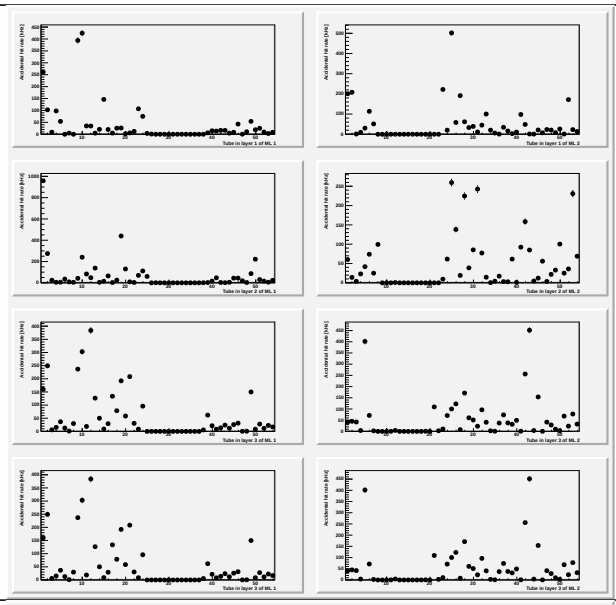
BMG-6A-12	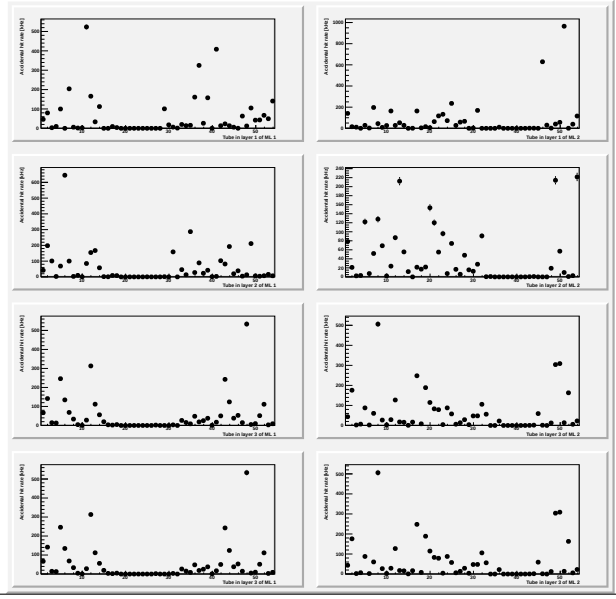

Not reviewed, for internal circulation only

Table 28: Measured noise rates for completed chambers at CERN with HV on and the ASD threshold of 112 (continued)

Chamber	
BMG-6A-14	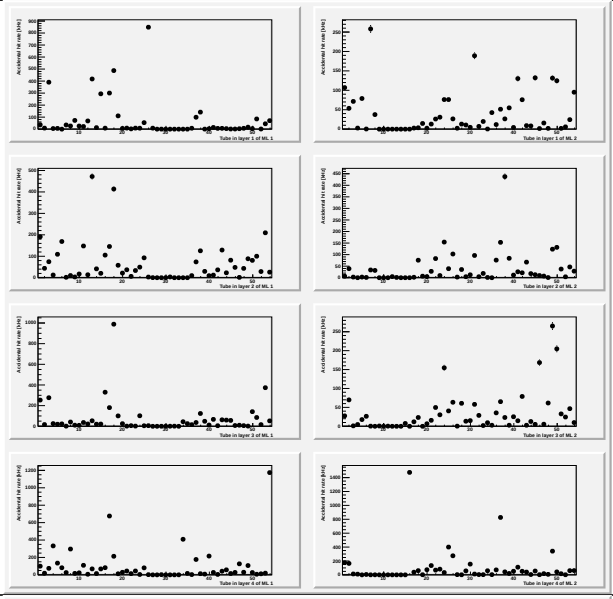
BMG-6C-14	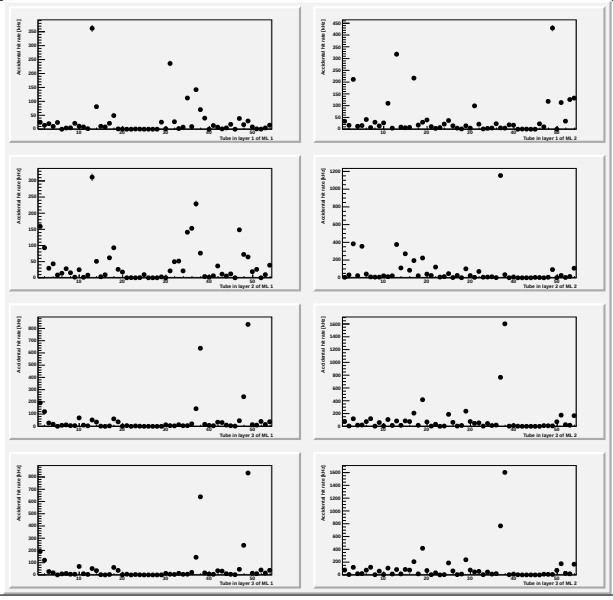

Not reviewed, for internal circulation only

Table 28: Measured noise rates for completed chambers at CERN with HV on and the ASD threshold of 112 (continued)

Chamber	
BMG-4C-12	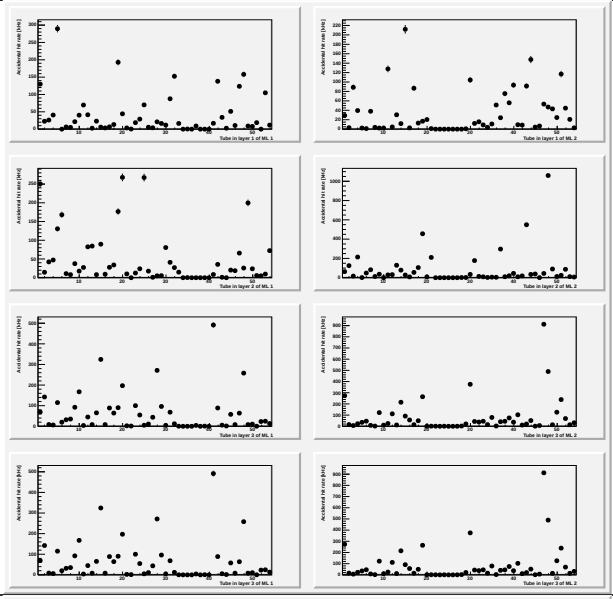
BMG-4C-14	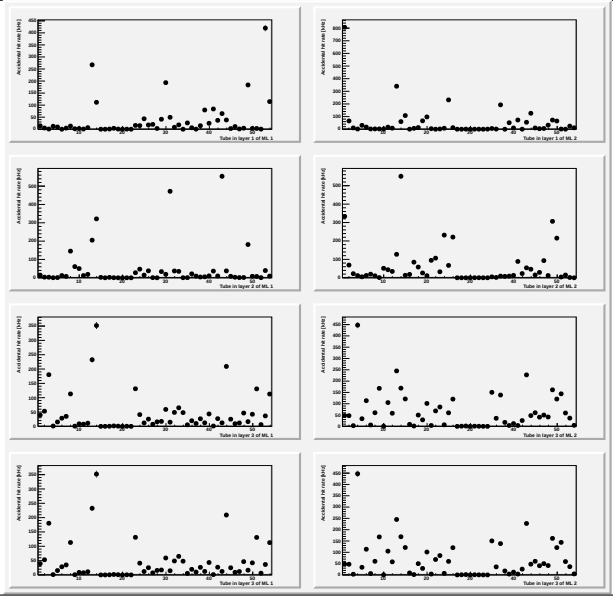

Not reviewed, for internal circulation only

Table 28: Measured noise rates for completed chambers at CERN with HV on and the ASD threshold of 112 (continued)

Chamber	
BMG-4A-14	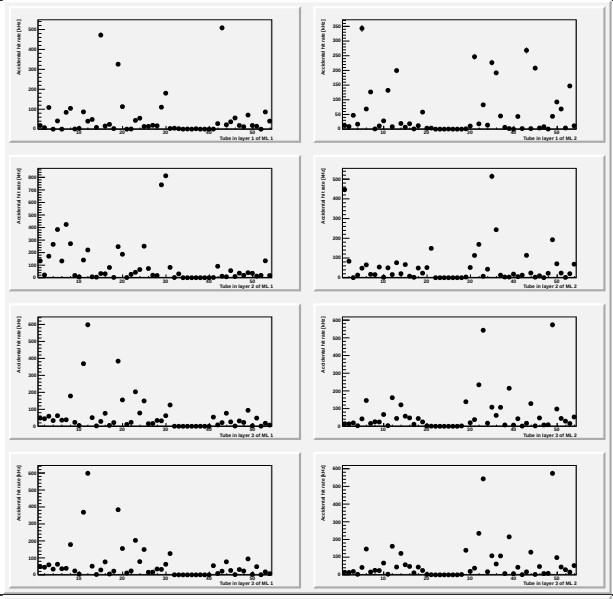
BMG-4A-12	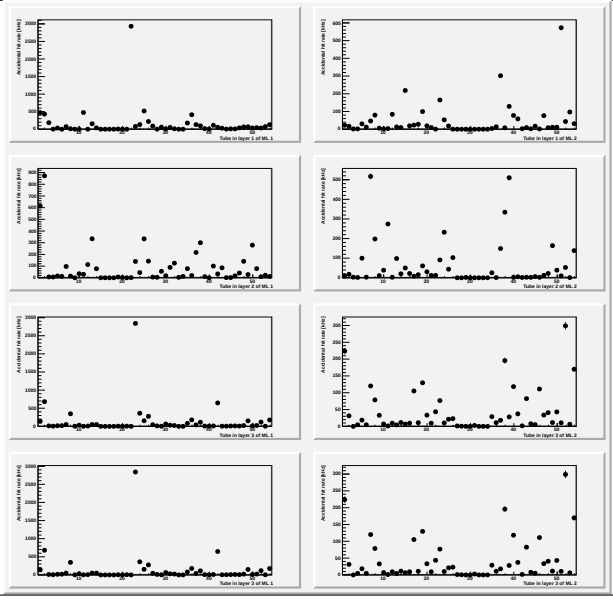

Not reviewed, for internal circulation only

Table 28: Measured noise rates for completed chambers at CERN with HV on and the ASD threshold of 112 (continued)

Chamber	
BMG-2C-12	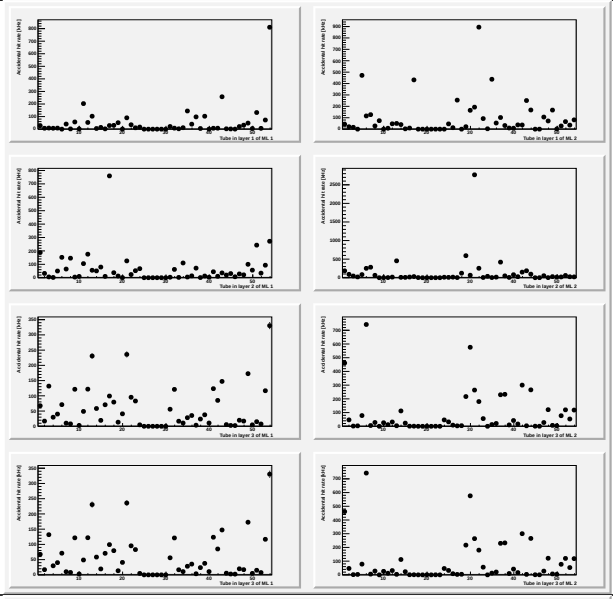
BMG-2A-14	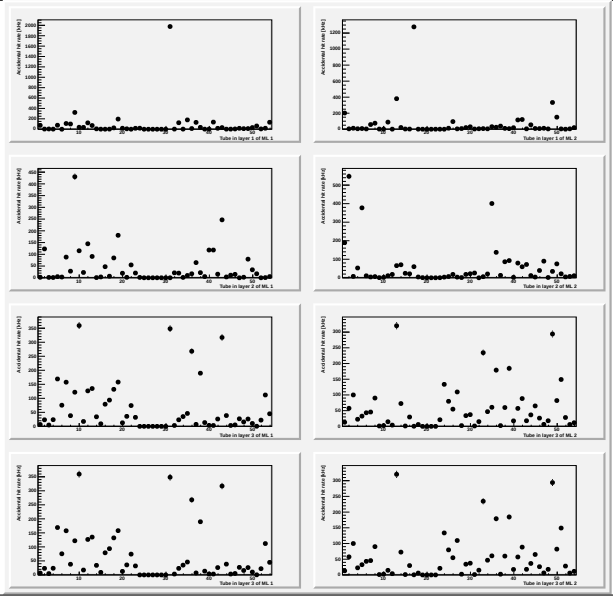

Not reviewed, for internal circulation only

Table 28: Measured noise rates for completed chambers at CERN with HV on and the ASD threshold of 112 (continued)

Chamber	
BMG-2C-14	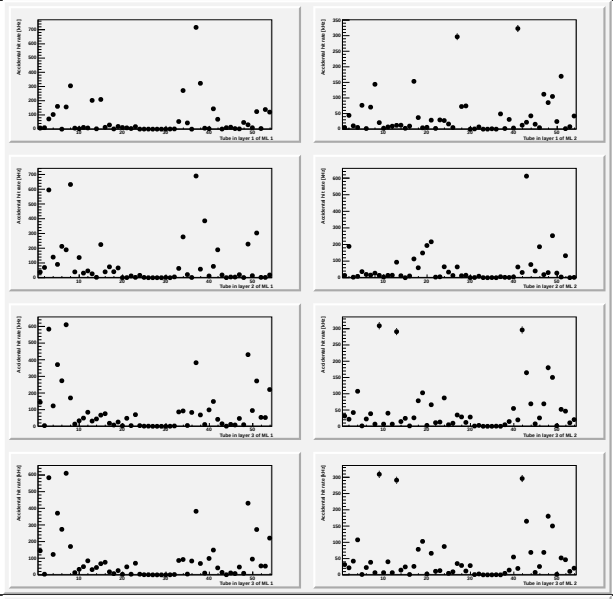
BMG-2A-12	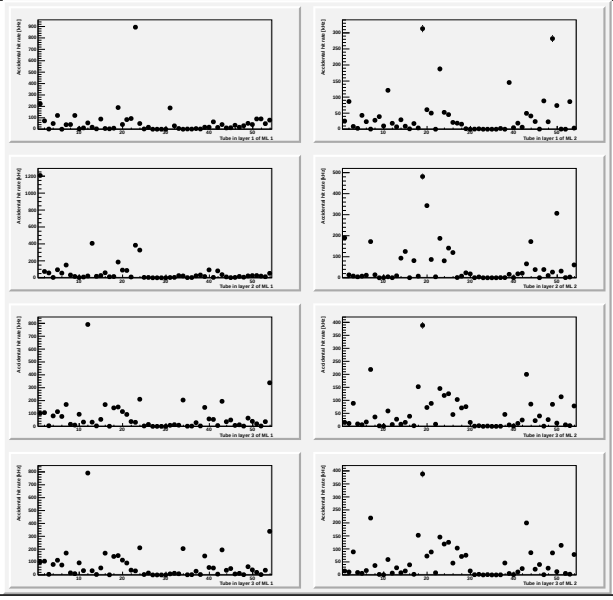

Not reviewed, for internal circulation only

Table 29: Measured noise rates for completed chambers at CERN with HV off and the ASD threshold of 103

Chamber	
BMG-6C-12	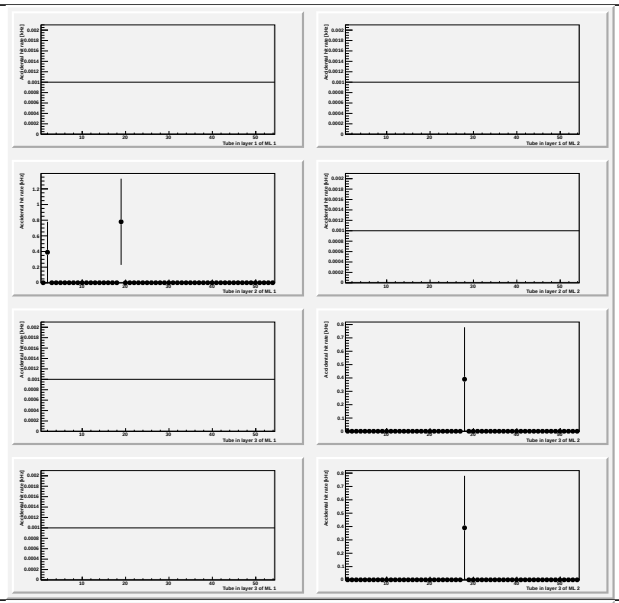
BMG-6A-12	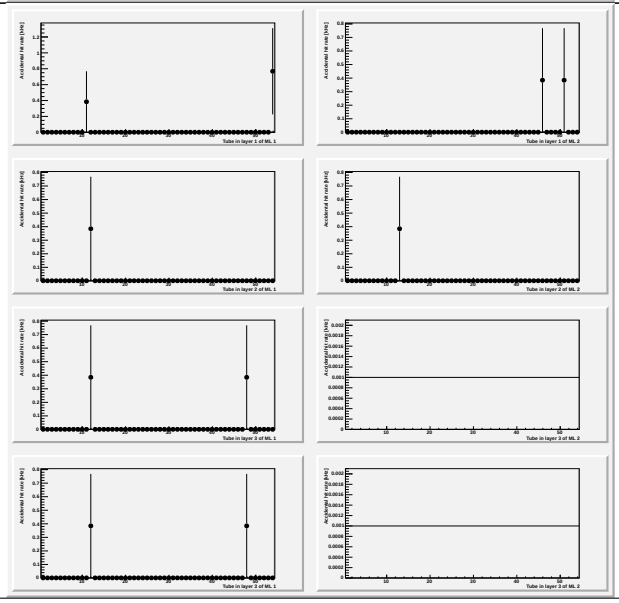

Not reviewed, for internal circulation only

Table 29: Measured noise rates for completed chambers at CERN with HV off and the ASD threshold of 103 (continued)

Chamber	
BMG-6A-14	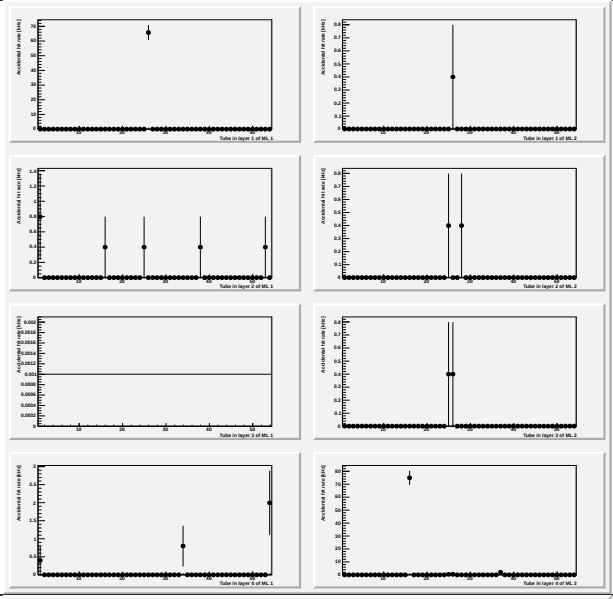
BMG-6C-14	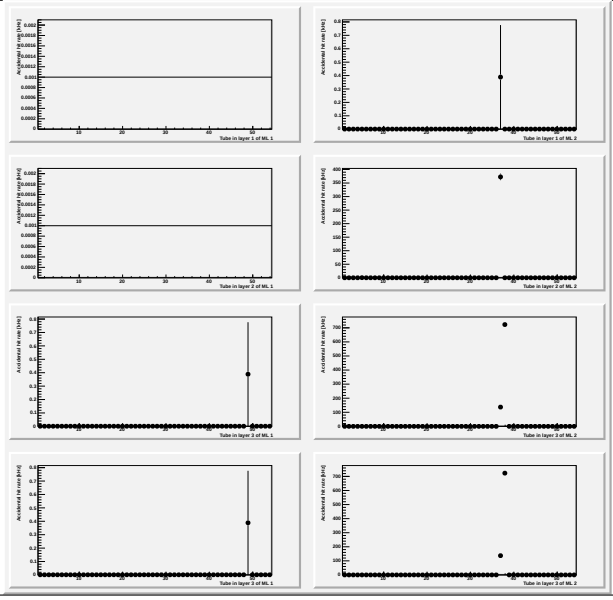

Not reviewed, for internal circulation only

Table 29: Measured noise rates for completed chambers at CERN with HV off and the ASD threshold of 103 (continued)

Chamber	
BMG-4C-12	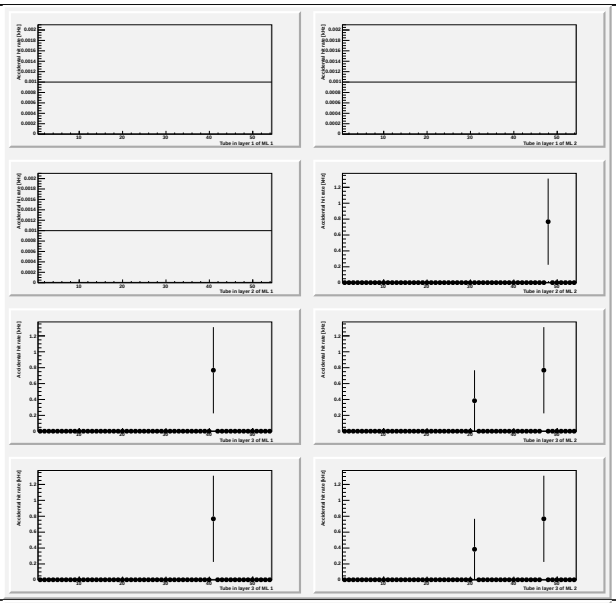
BMG-4C-14	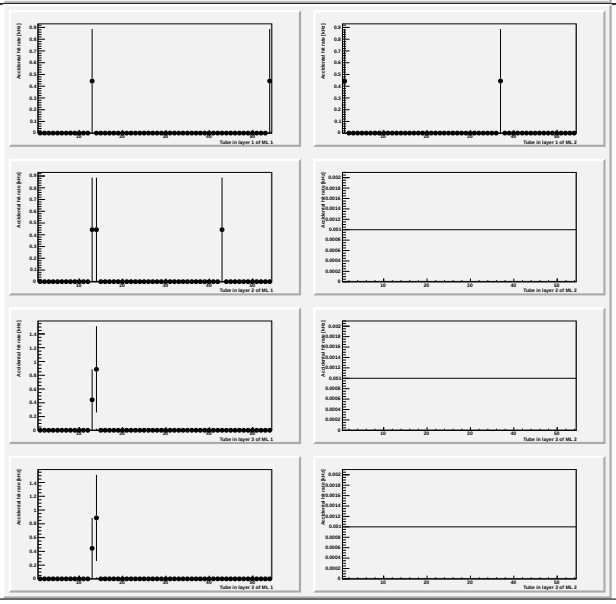

Not reviewed, for internal circulation only

Table 29: Measured noise rates for completed chambers at CERN with HV off and the ASD threshold of 103 (continued)

Chamber	
BMG-4A-14	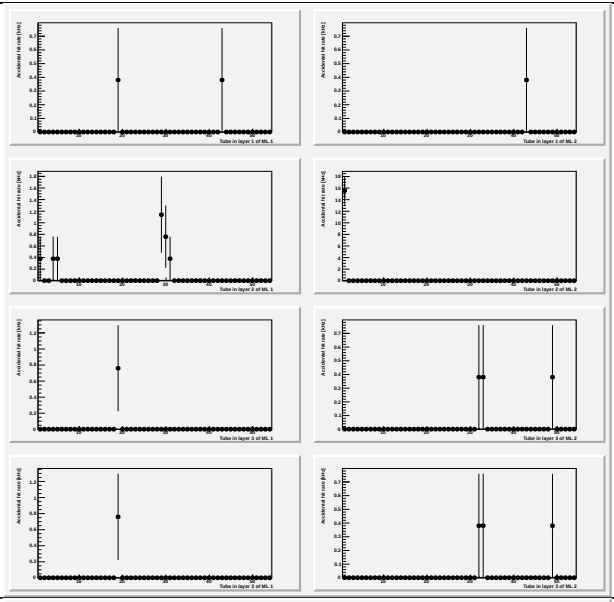
BMG-4A-12	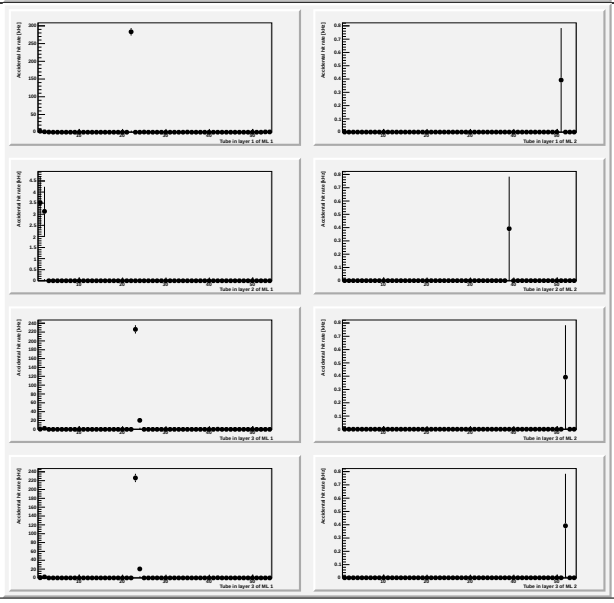

Not reviewed, for internal circulation only

Table 29: Measured noise rates for completed chambers at CERN with HV off and the ASD threshold of 103 (continued)

Chamber	
BMG-2C-12	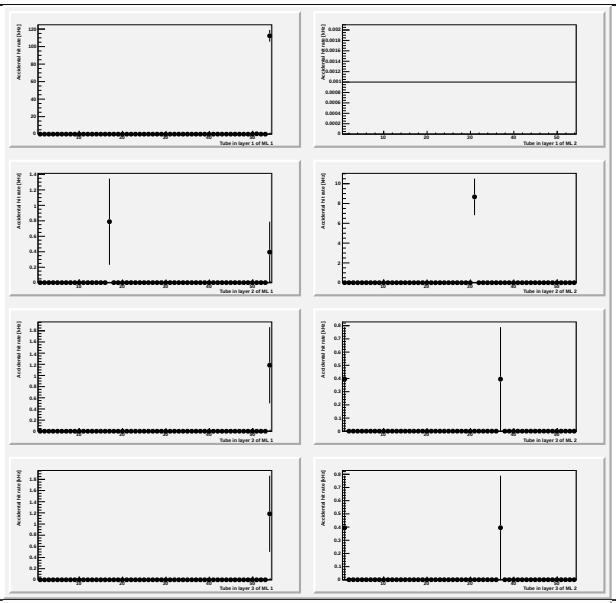
BMG-2A-14	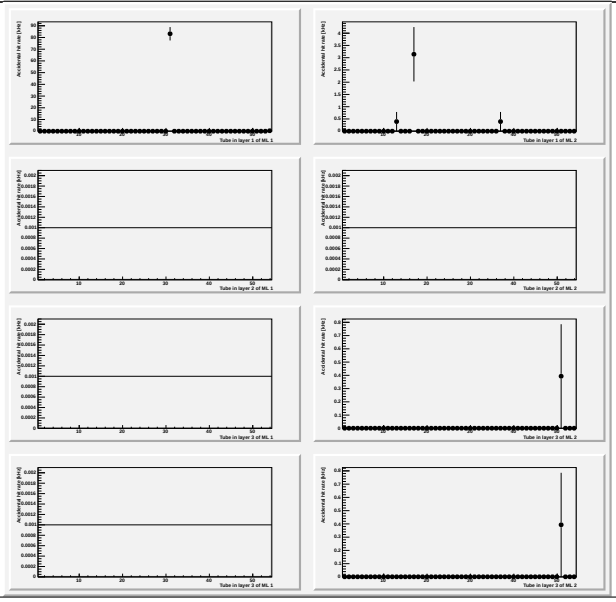

Not reviewed, for internal circulation only

Table 29: Measured noise rates for completed chambers at CERN with HV off and the ASD threshold of 103 (continued)

Chamber	
BMG-2C-14	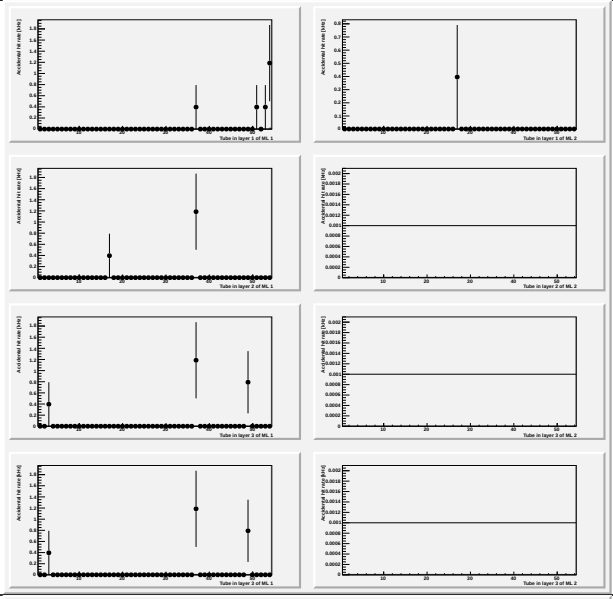
BMG-2A-12	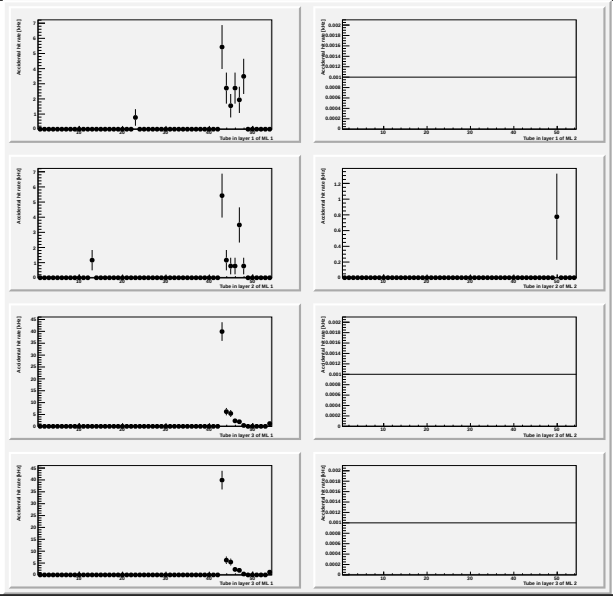

Not reviewed, for internal circulation only

Table 30: Measured noise rates for completed chambers at CERN with HV off and the ASD threshold of 106

Chamber	
BMG-6C-12	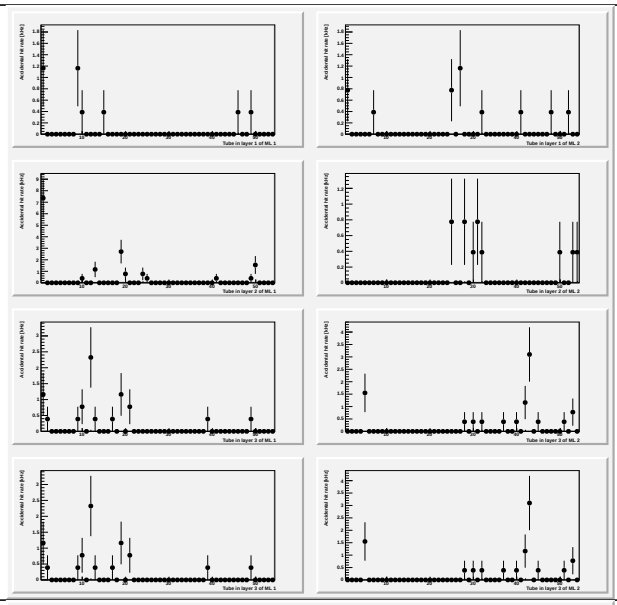
BMG-6A-12	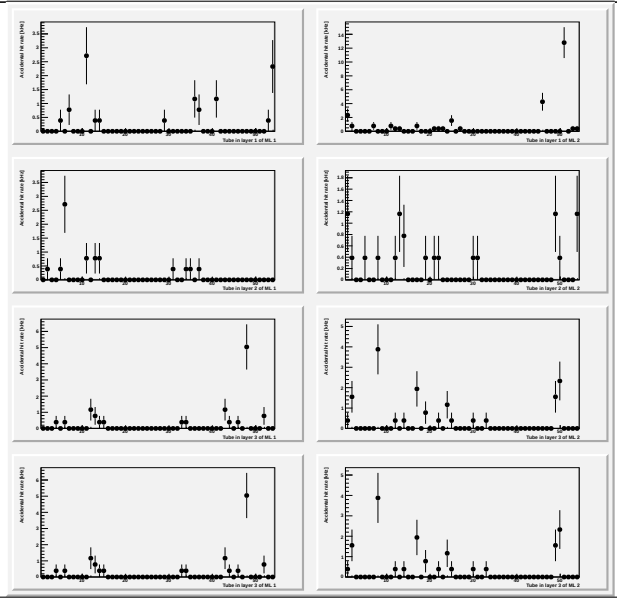

Not reviewed, for internal circulation only

Table 30: Measured noise rates for completed chambers at CERN with HV off and the ASD threshold of 106 (continued)

Chamber	
BMG-6A-14	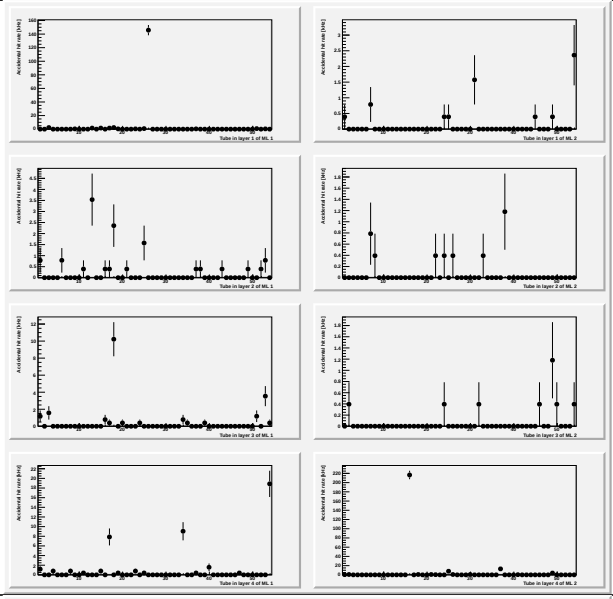
BMG-6C-14	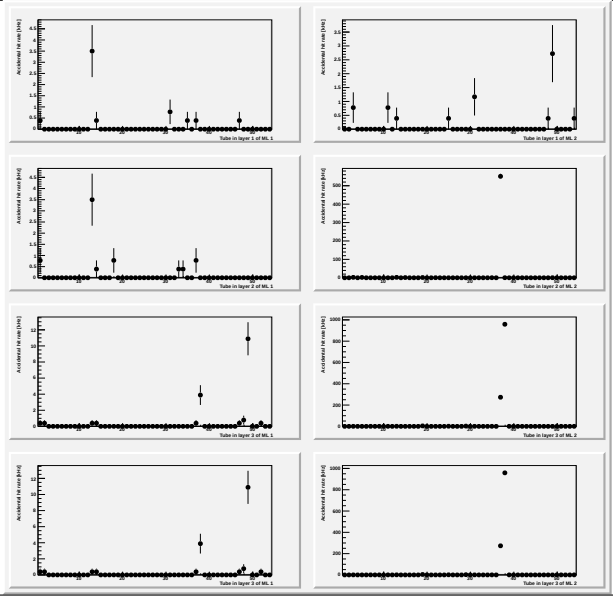

Not reviewed, for internal circulation only

Table 30: Measured noise rates for completed chambers at CERN with HV off and the ASD threshold of 106 (continued)

Chamber	
BMG-4C-12	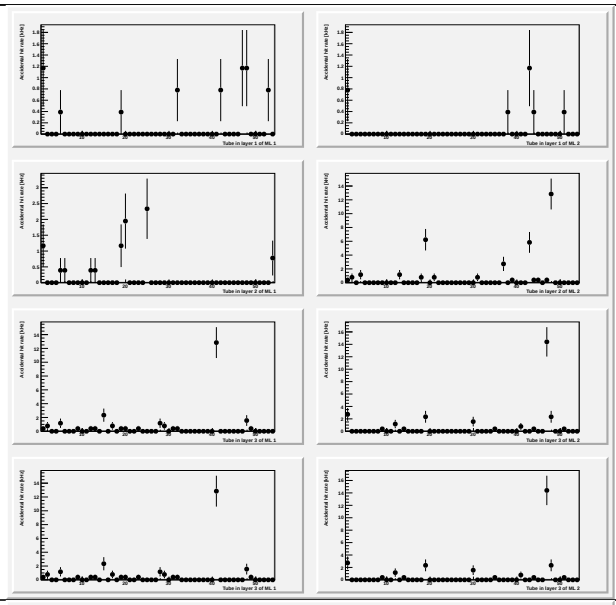
BMG-4C-14	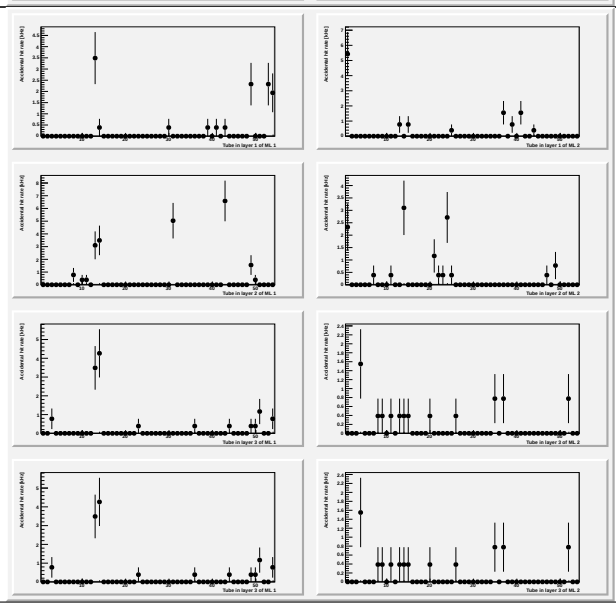

Not reviewed, for internal circulation only

Table 30: Measured noise rates for completed chambers at CERN with HV off and the ASD threshold of 106 (continued)

Chamber	
BMG-4A-14	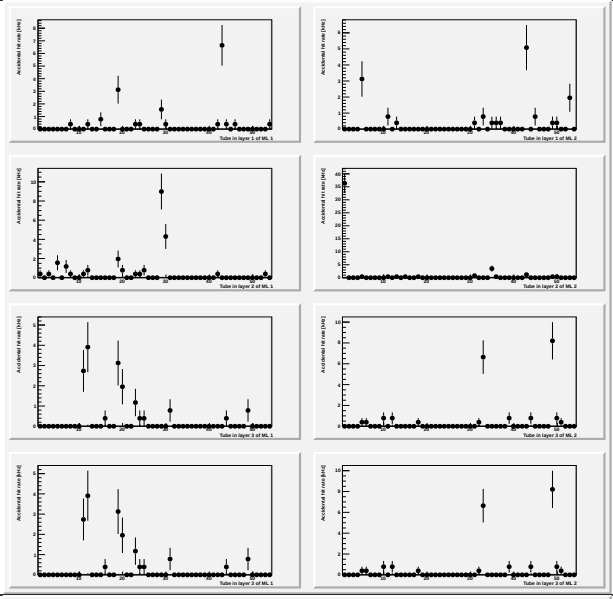
BMG-4A-12	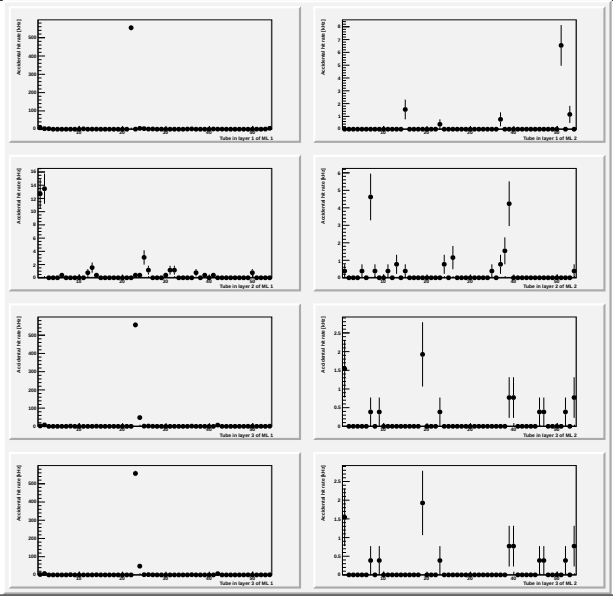

Not reviewed, for internal circulation only

Table 30: Measured noise rates for completed chambers at CERN with HV off and the ASD threshold of 106 (continued)

Chamber	
BMG-2C-12	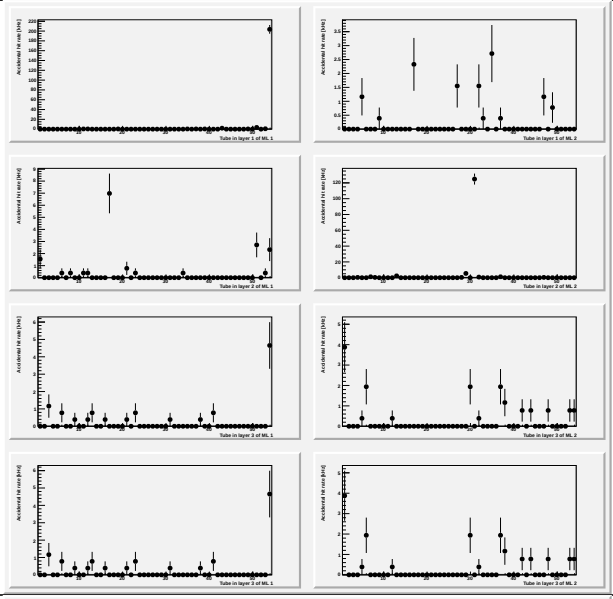
BMG-2A-14	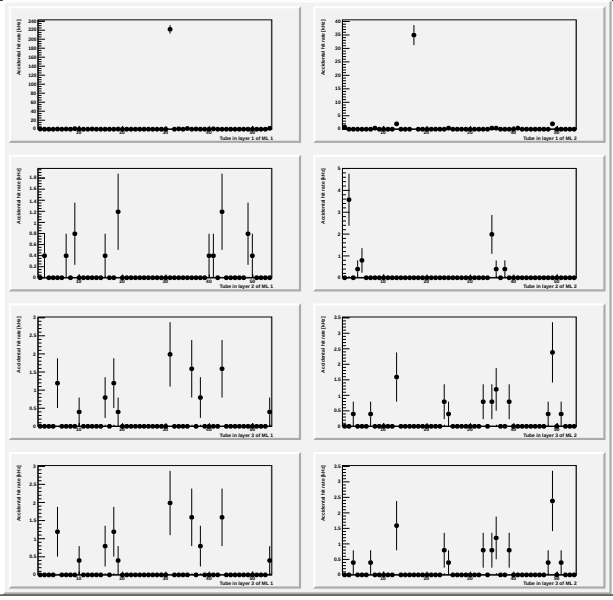

Not reviewed, for internal circulation only

Table 30: Measured noise rates for completed chambers at CERN with HV off and the ASD threshold of 106 (continued)

Chamber	
BMG-2C-14	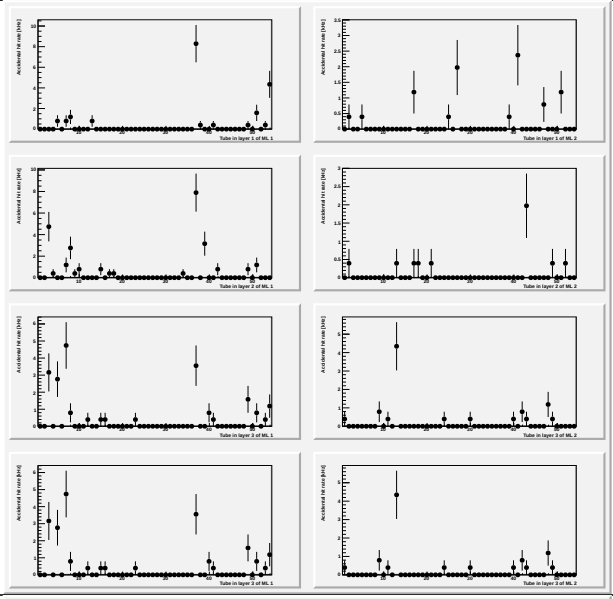
BMG-2A-12	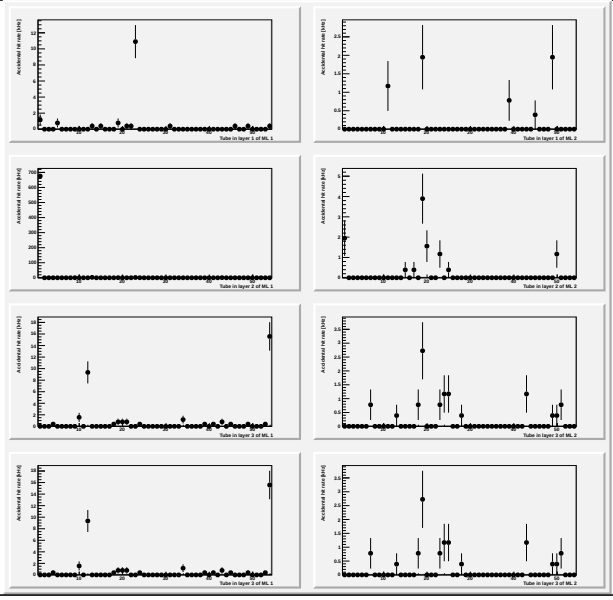

Not reviewed, for internal circulation only

Table 31: Measured noise rates for completed chambers at CERN with HV off and the ASD threshold of 108

Chamber	
BMG-6C-12	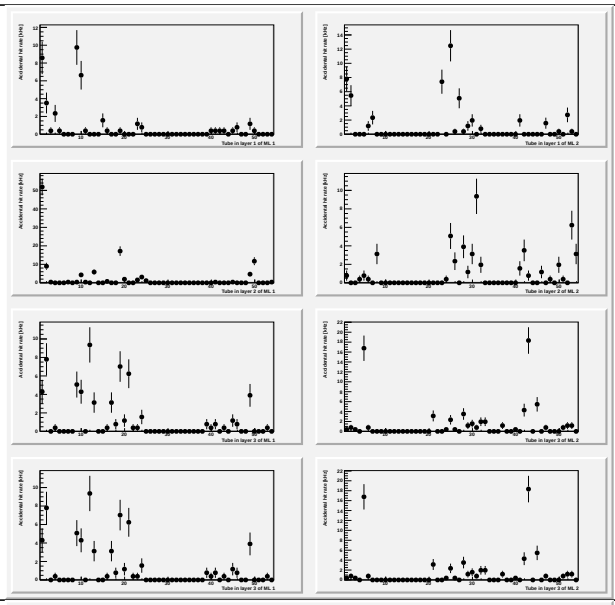
BMG-6A-12	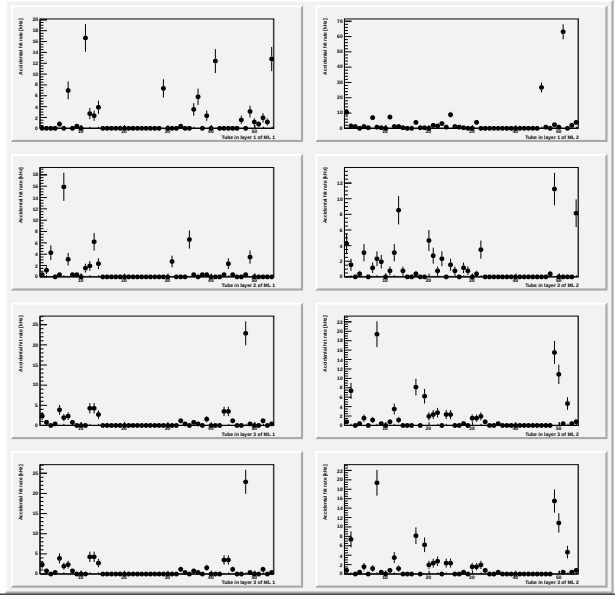

Not reviewed, for internal circulation only

Table 31: Measured noise rates for completed chambers at CERN with HV off and the ASD threshold of 108 (continued)

Chamber	
BMG-6A-14	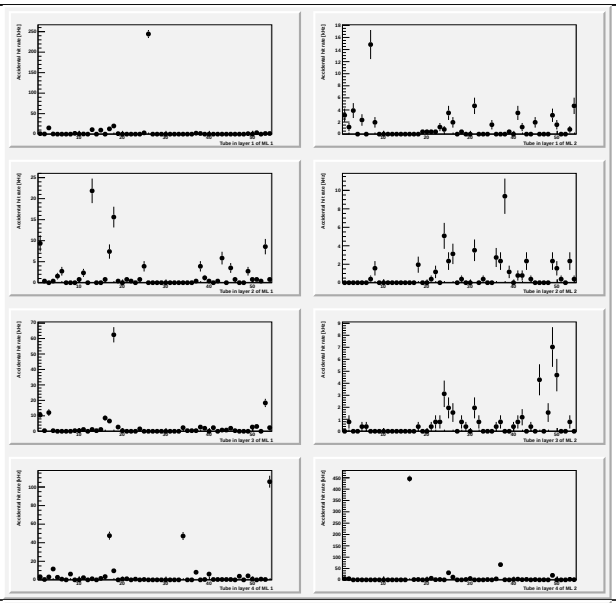
BMG-6C-14	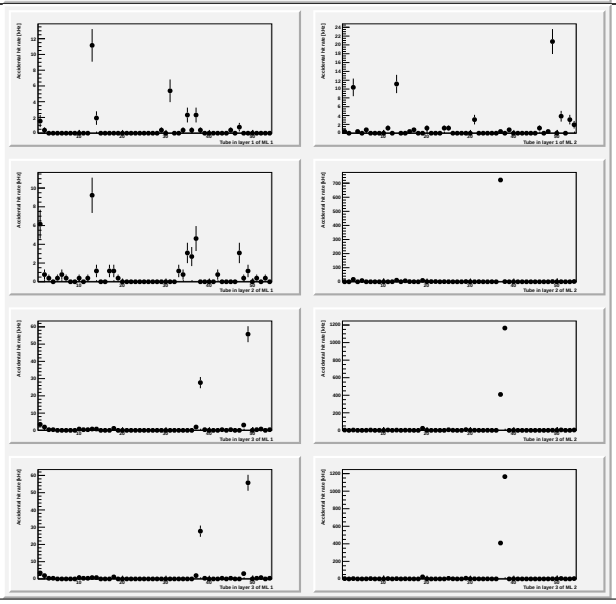

Not reviewed, for internal circulation only

Table 31: Measured noise rates for completed chambers at CERN with HV off and the ASD threshold of 108 (continued)

Chamber	
BMG-4C-12	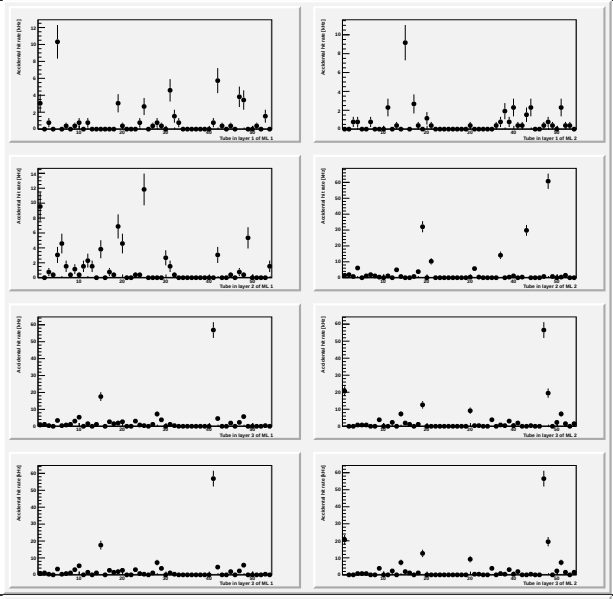
BMG-4C-14	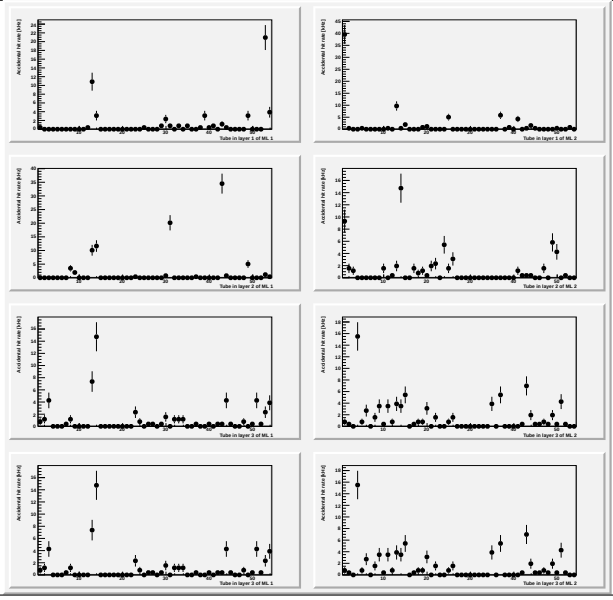

Not reviewed, for internal circulation only

Table 31: Measured noise rates for completed chambers at CERN with HV off and the ASD threshold of 108 (continued)

Chamber	
BMG-4A-14	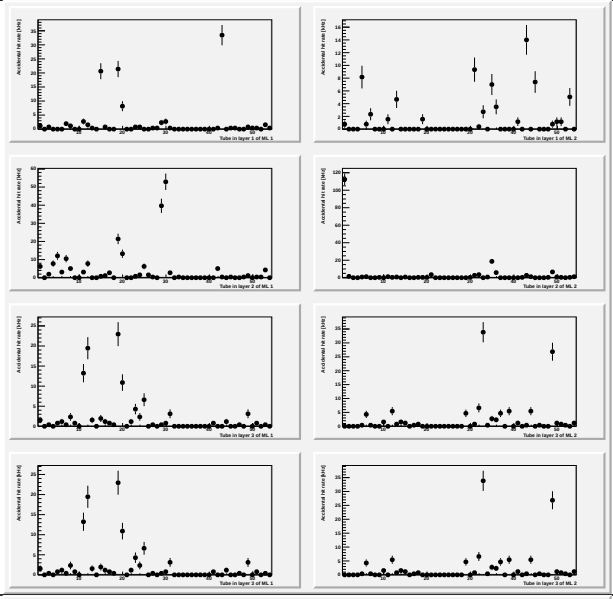
BMG-4A-12	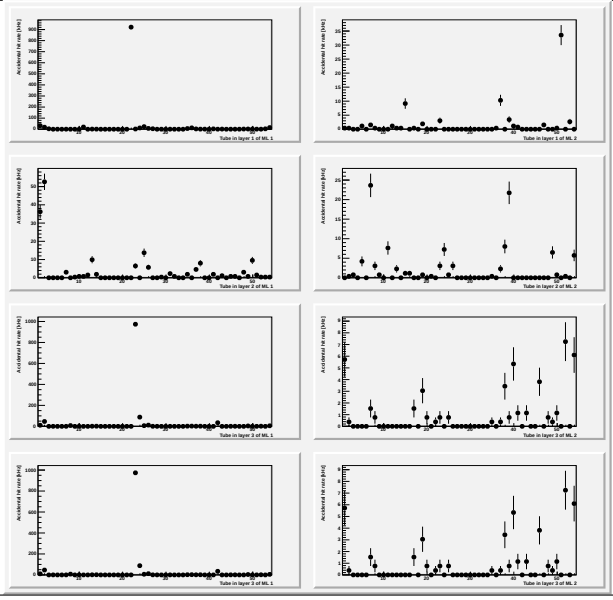

Not reviewed, for internal circulation only

Table 31: Measured noise rates for completed chambers at CERN with HV off and the ASD threshold of 108 (continued)

Chamber	
BMG-2C-12	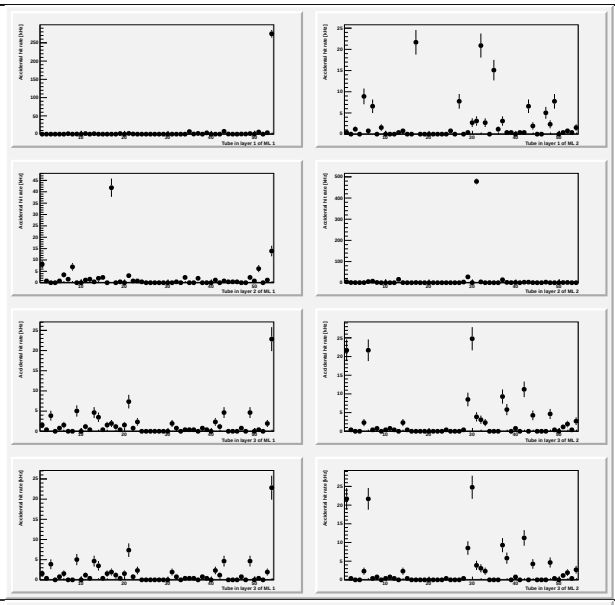
BMG-2A-14	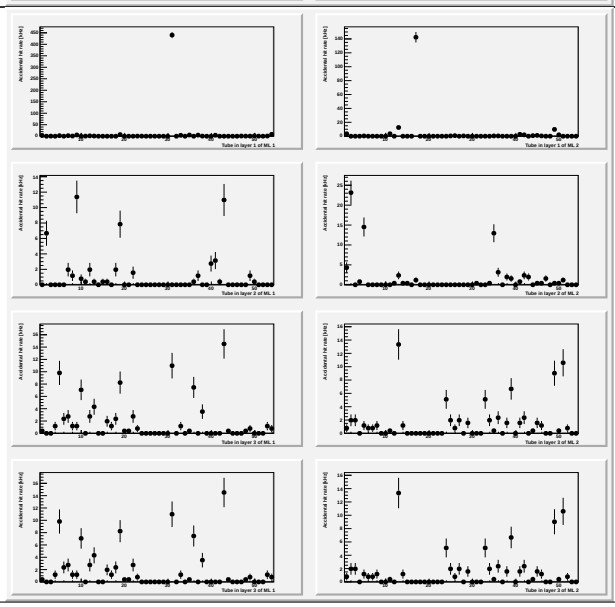

Not reviewed, for internal circulation only

Table 31: Measured noise rates for completed chambers at CERN with HV off and the ASD threshold of 108 (continued)

Chamber	
BMG-2C-14	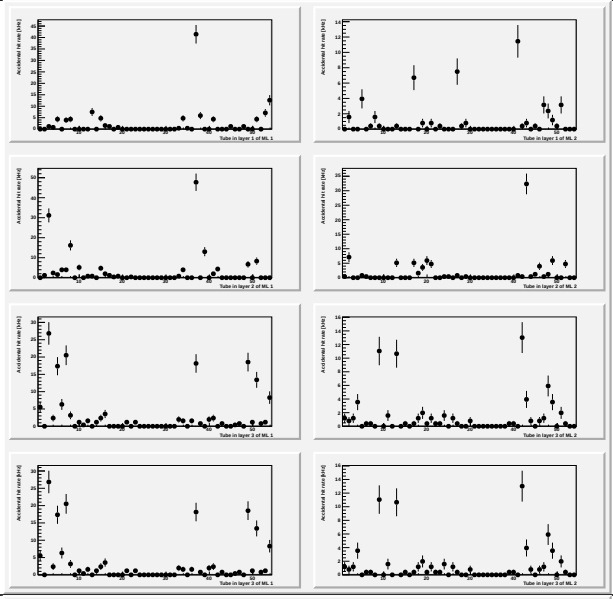
BMG-2A-12	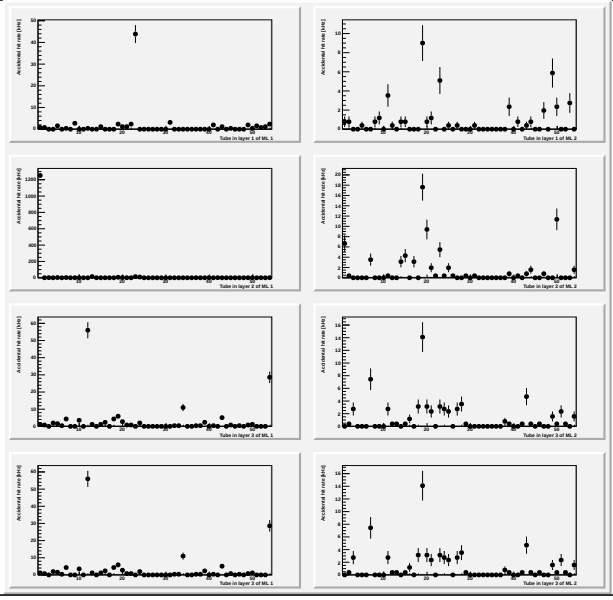

Not reviewed, for internal circulation only

Table 32: Measured noise rates for completed chambers at CERN with HV off and the ASD threshold of 110

Chamber	
BMG-6C-12	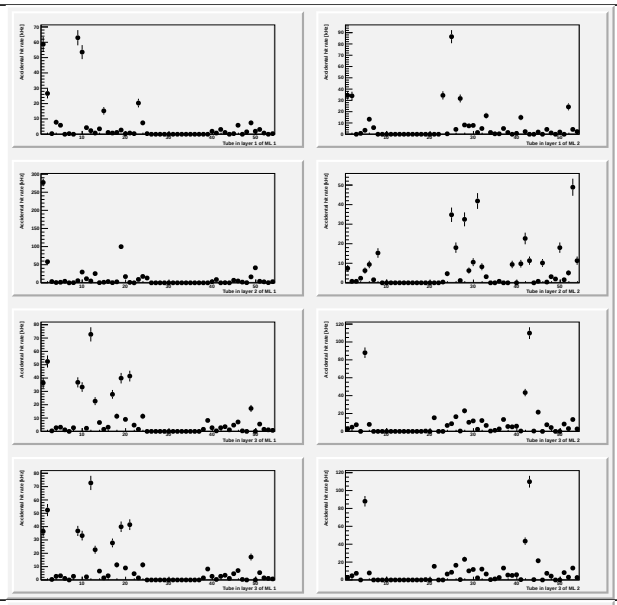
BMG-6A-12	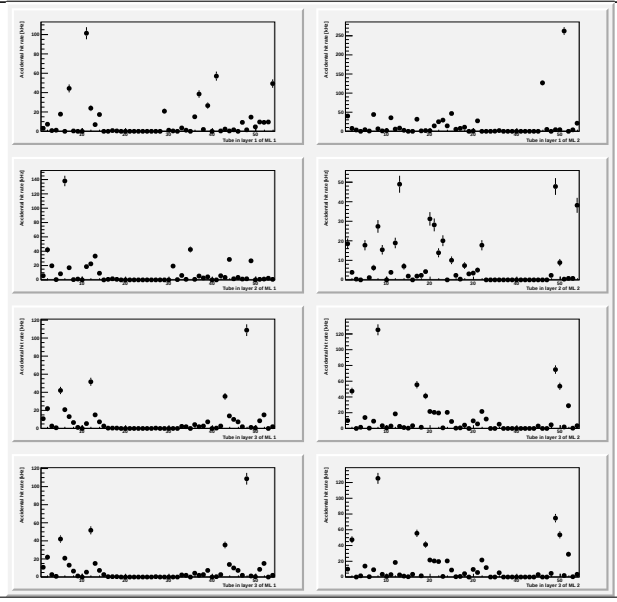

Not reviewed, for internal circulation only

Table 32: Measured noise rates for completed chambers at CERN with HV off and the ASD threshold of 110 (continued)

Chamber	
BMG-6A-14	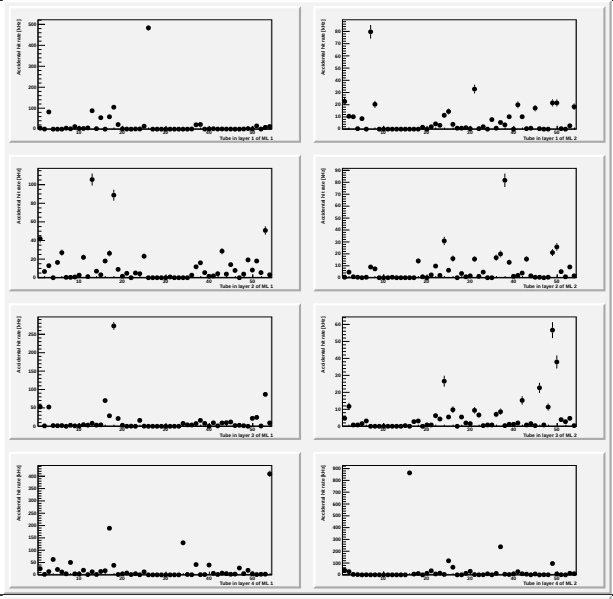
BMG-6C-14	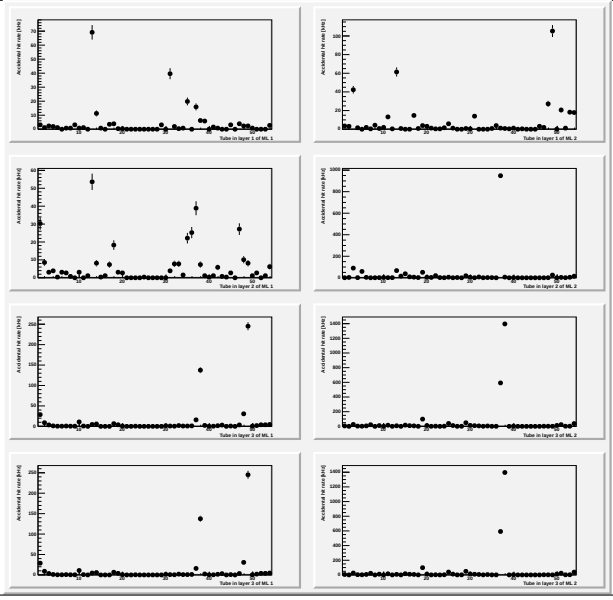

Not reviewed, for internal circulation only

Table 32: Measured noise rates for completed chambers at CERN with HV off and the ASD threshold of 110 (continued)

Chamber	
BMG-4C-12	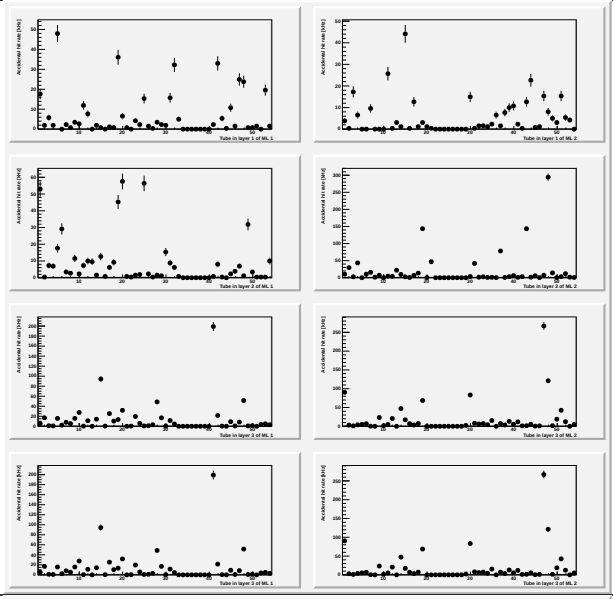
BMG-4C-14	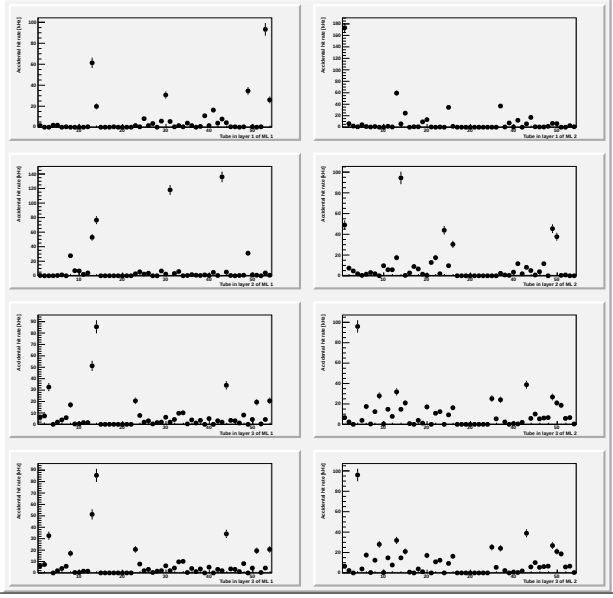

Not reviewed, for internal circulation only

Table 32: Measured noise rates for completed chambers at CERN with HV off and the ASD threshold of 110 (continued)

Chamber	
BMG-4A-14	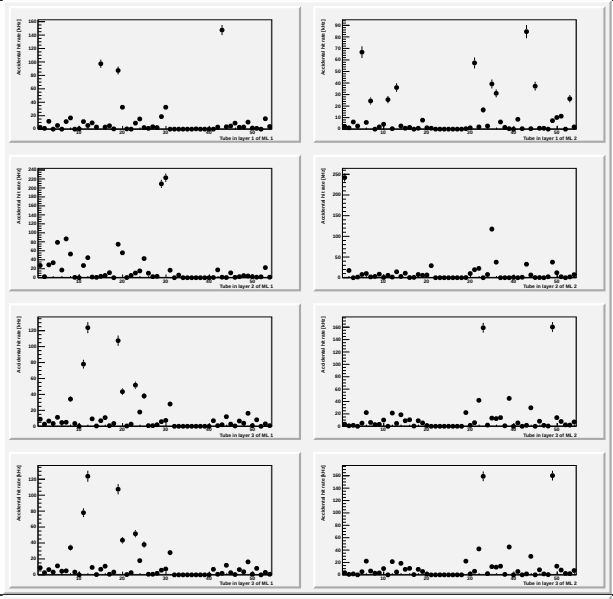
BMG-4A-12	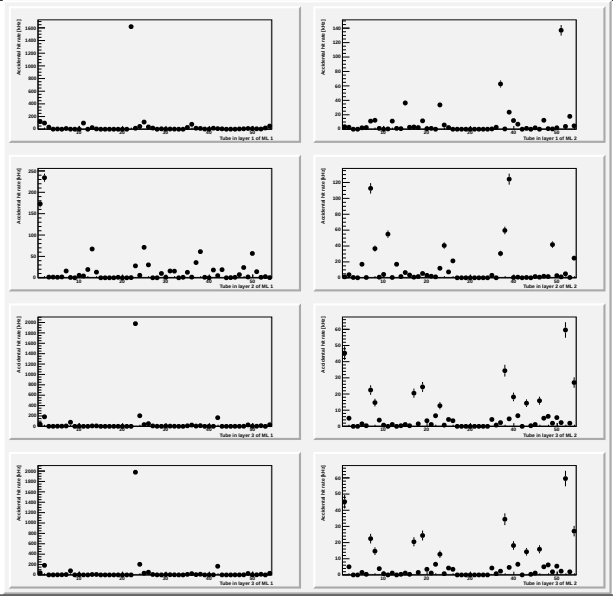

Not reviewed, for internal circulation only

Table 32: Measured noise rates for completed chambers at CERN with HV off and the ASD threshold of 110 (continued)

Chamber	
BMG-2C-12	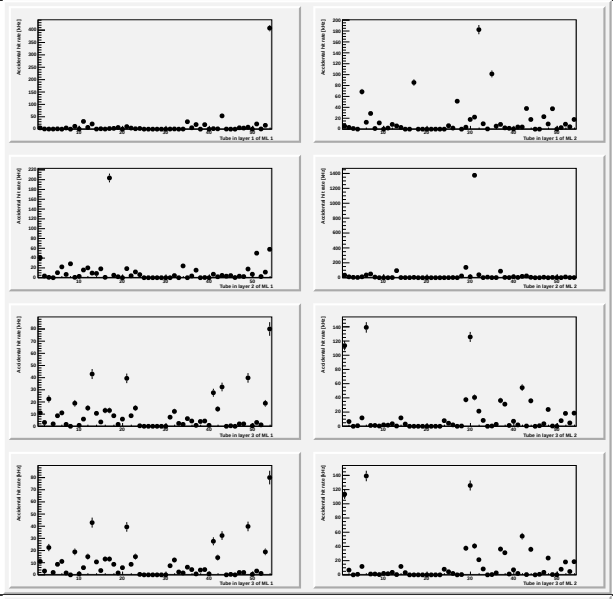
BMG-2A-14	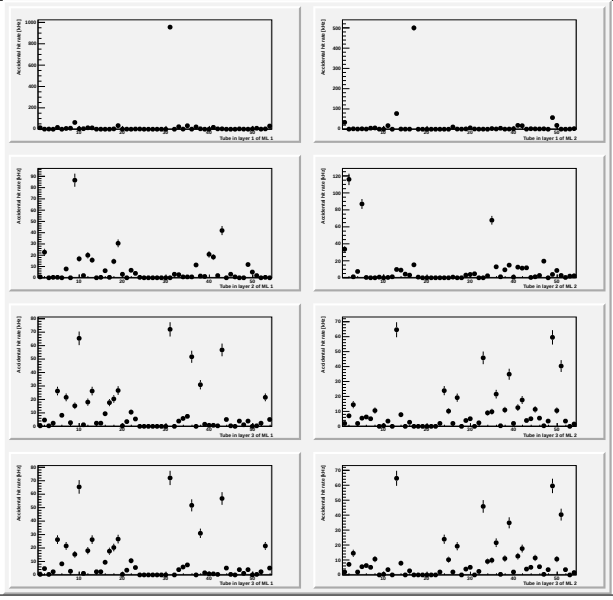

Not reviewed, for internal circulation only

Table 32: Measured noise rates for completed chambers at CERN with HV off and the ASD threshold of 110 (continued)

Chamber	
BMG-2C-14	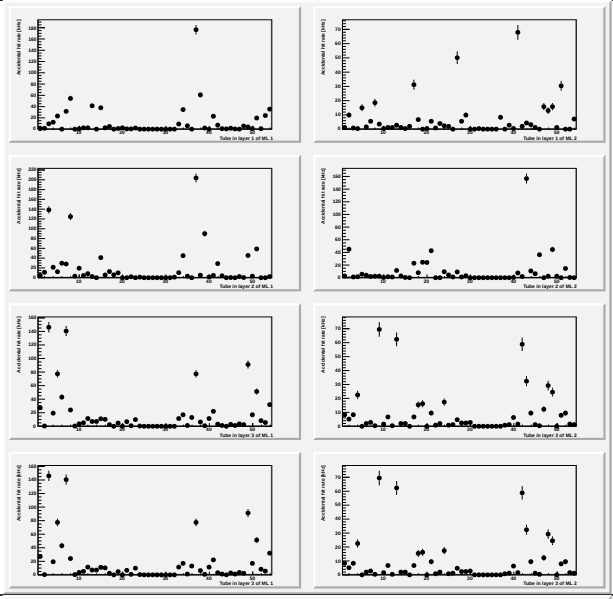
BMG-2A-12	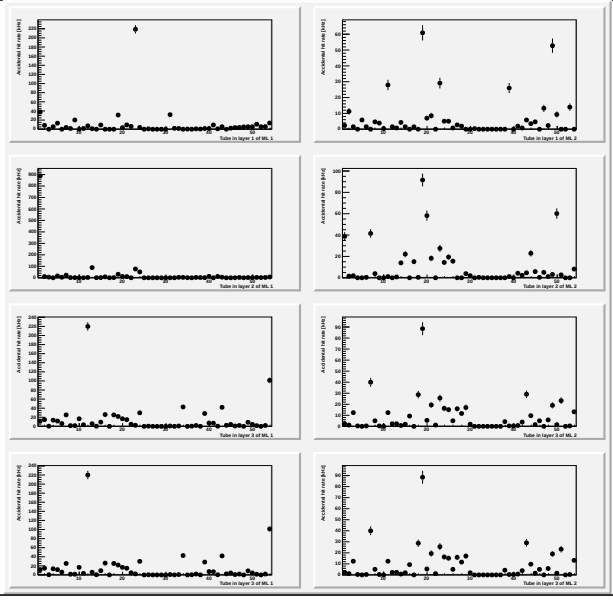

Not reviewed, for internal circulation only

Table 33: Measured noise rates for completed chambers at CERN with HV off and the ASD threshold of 112

Chamber	
BMG-6C-12	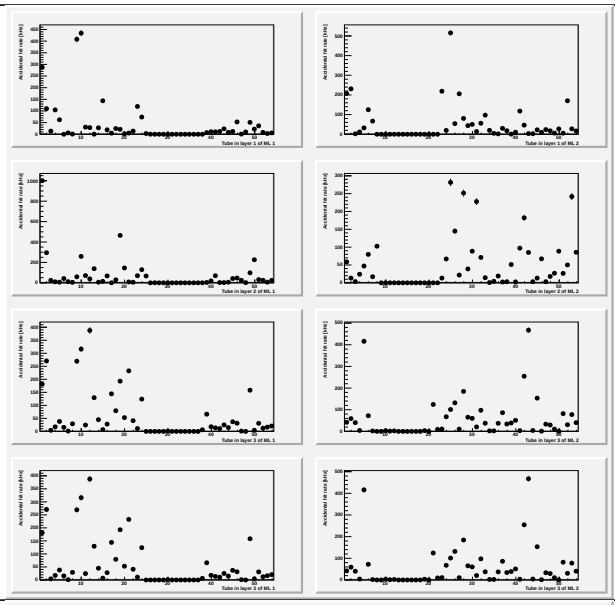
BMG-6A-12	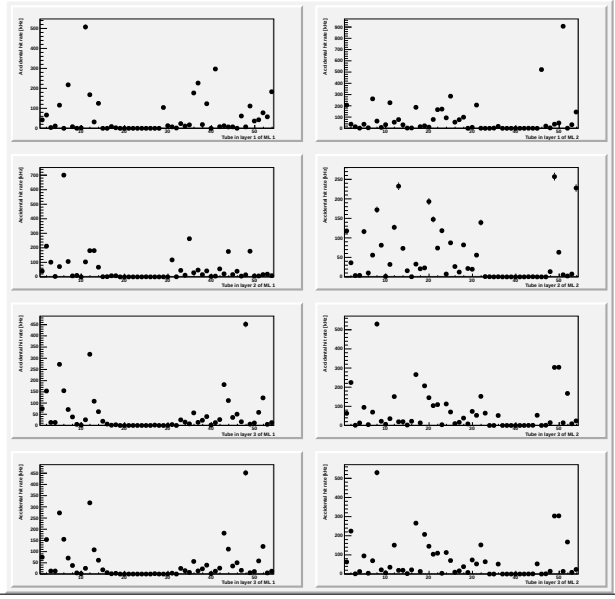

Not reviewed, for internal circulation only

Table 33: Measured noise rates for completed chambers at CERN with HV off and the ASD threshold of 112 (continued)

Chamber	
BMG-6A-14	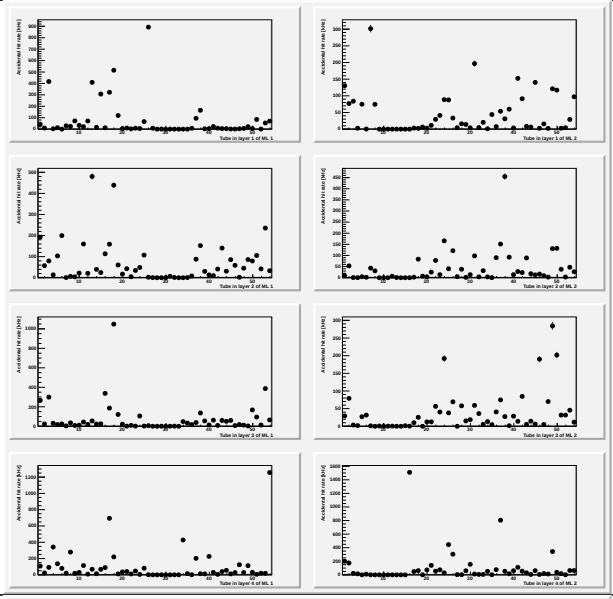
BMG-6C-14	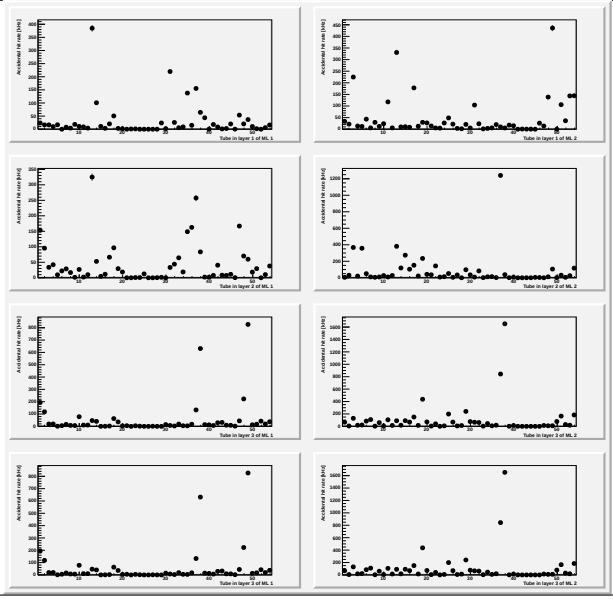

Not reviewed, for internal circulation only

Table 33: Measured noise rates for completed chambers at CERN with HV off and the ASD threshold of 112 (continued)

Chamber	
BMG-4C-12	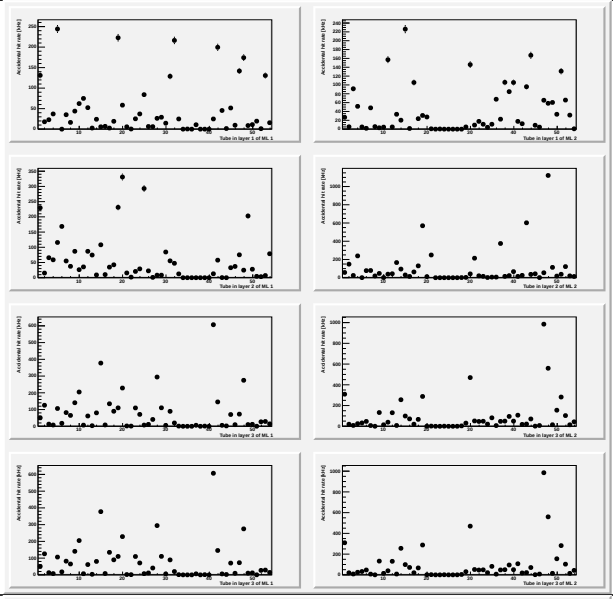
BMG-4C-14	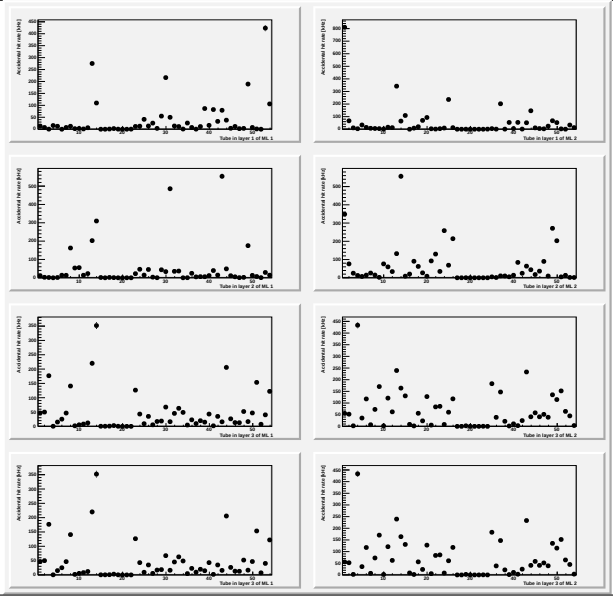

Not reviewed, for internal circulation only

Table 33: Measured noise rates for completed chambers at CERN with HV off and the ASD threshold of 112 (continued)

Chamber	
BMG-4A-14	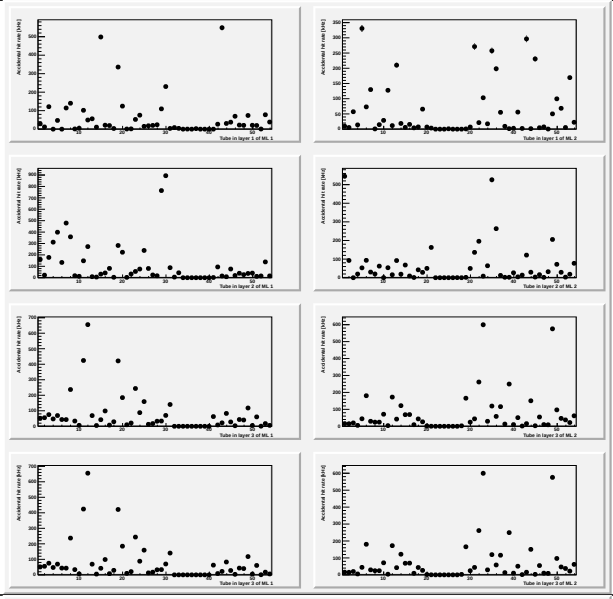
BMG-4A-12	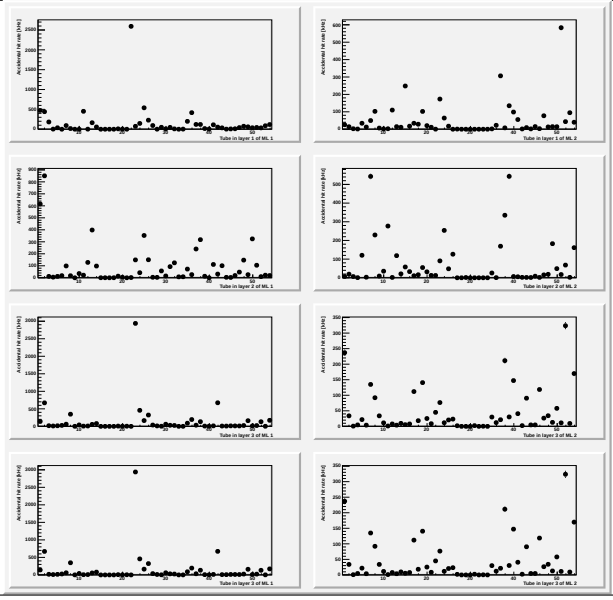

Not reviewed, for internal circulation only

Table 33: Measured noise rates for completed chambers at CERN with HV off and the ASD threshold of 112 (continued)

Chamber	
BMG-2C-12	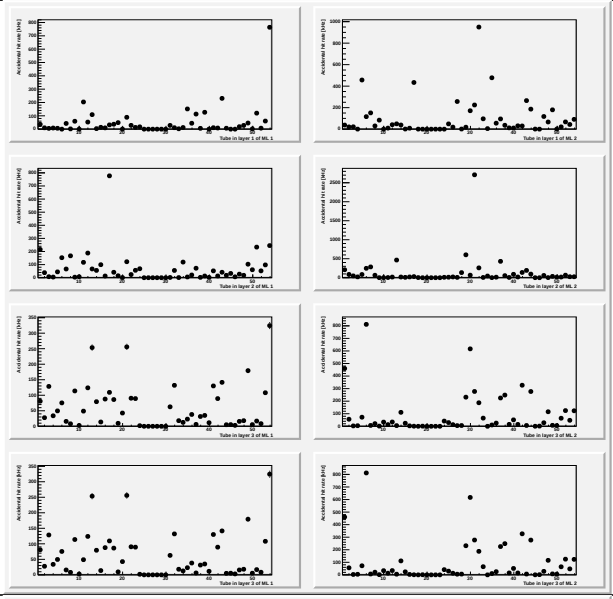
BMG-2A-14	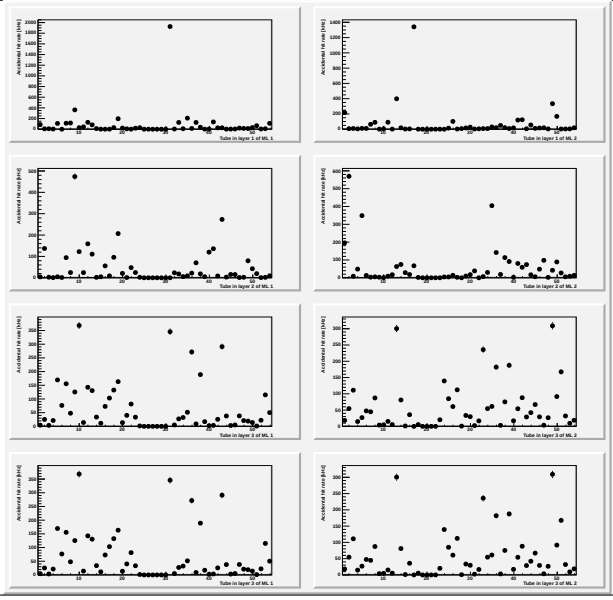

Not reviewed, for internal circulation only

Table 33: Measured noise rates for completed chambers at CERN with HV off and the ASD threshold of 112 (continued)

Chamber	
BMG-2C-14	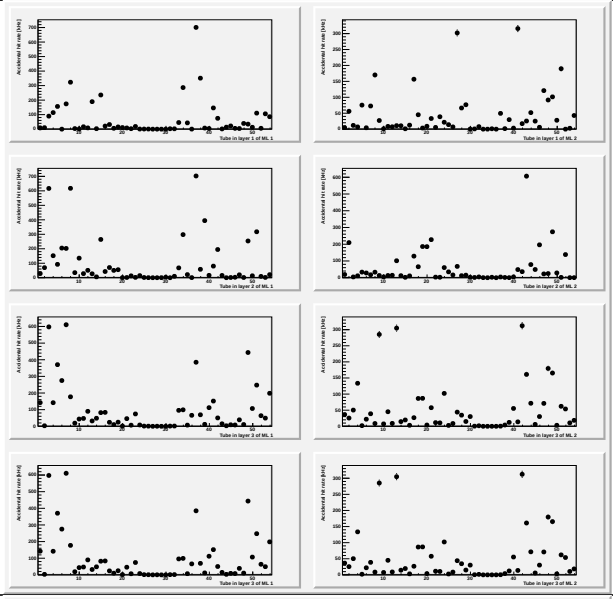
BMG-2A-12	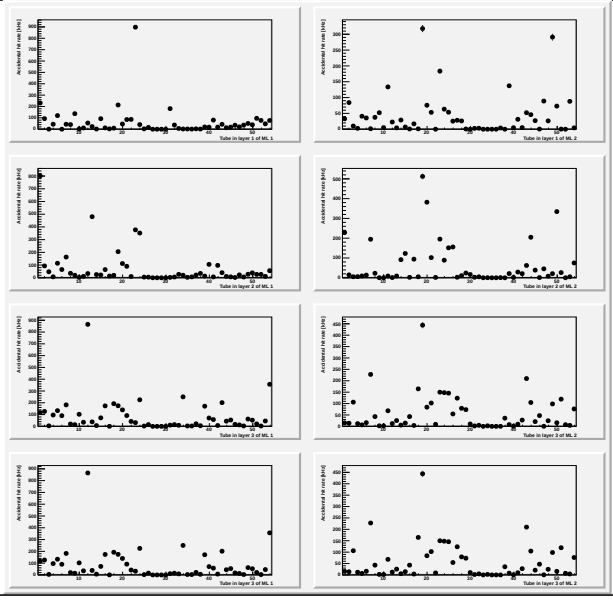

B.2 sMDT BMG Cosmic Ray Results

The measured cosmic ray hits for the chambers at CERN with the HV on and the ASD threshold at 108 are below.

Not reviewed, for internal circulation only

Table 34: Measured cosmic hit rates spectra for completed chambers at CERN. The total hits per tube is shown in black, and the hits associated with cosmic tracks are shown in red. As before, the left column corresponds to the upper multilayer, and the right column corresponds to the lower multilayer. The four plots in each column, from top to bottom, correspond to the four layers of tubes in each multilayer.

Chamber	
BMG-6C-12	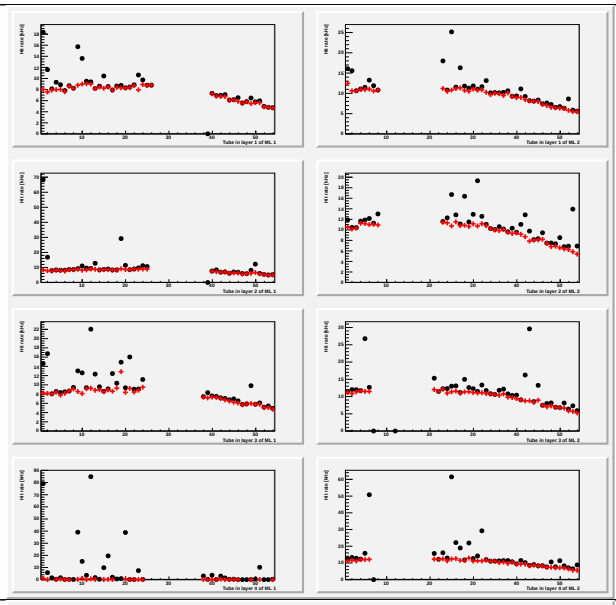
BMG-6A-12	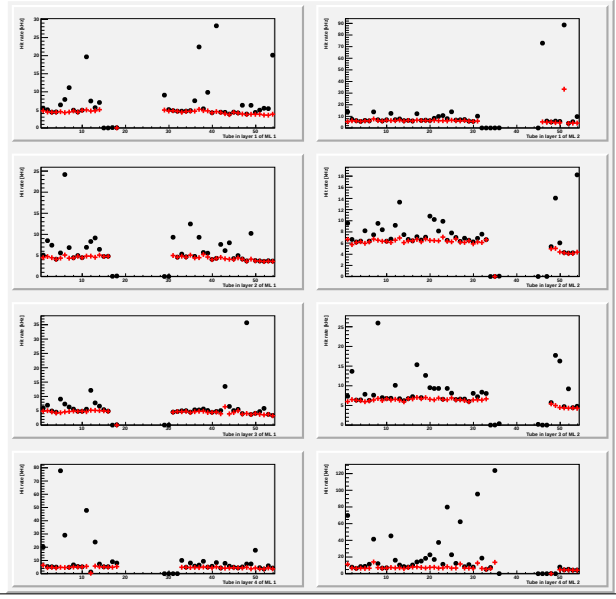

Not reviewed, for internal circulation only

Table 34: Measured cosmic hit rates spectra for completed chambers at CERN (continued).

Chamber	
BMG-6A-14	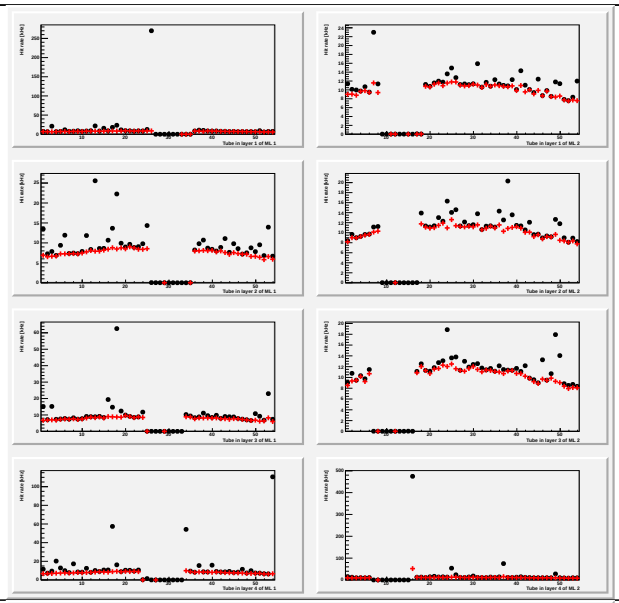
BMG-6C-14	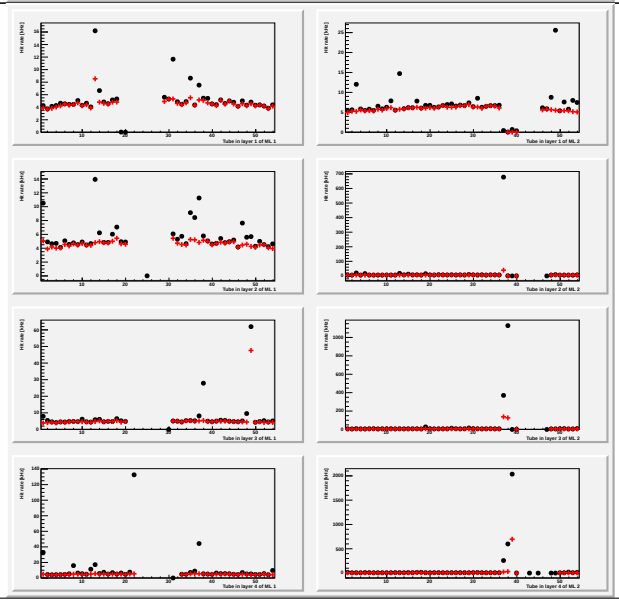

Not reviewed, for internal circulation only

Table 34: Measured cosmic hit rates spectra for completed chambers at CERN (continued).

Chamber	
BMG-4C-12	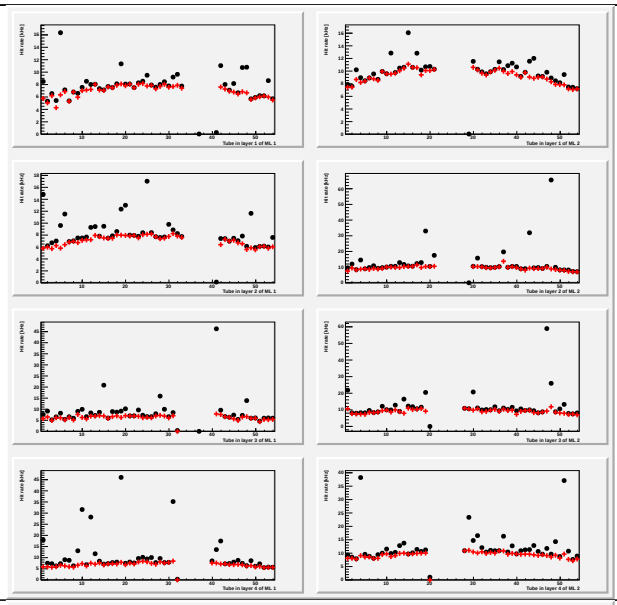
BMG-4C-14	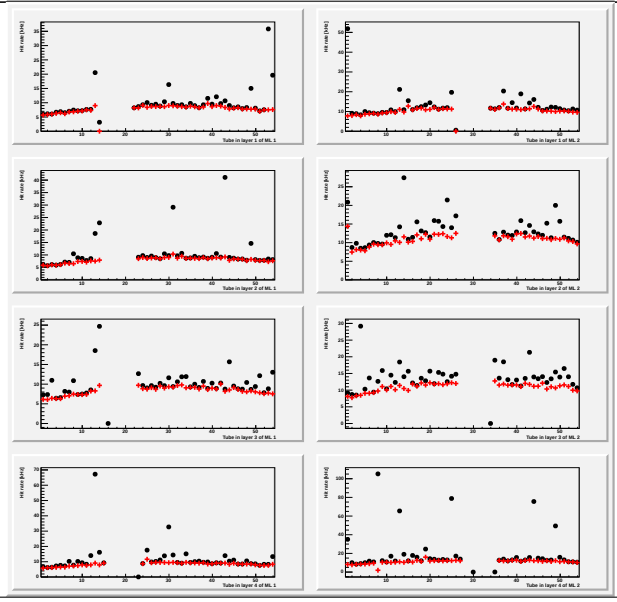

Not reviewed, for internal circulation only

Table 34: Measured cosmic hit rates spectra for completed chambers at CERN (continued).

Chamber	
BMG-4A-14	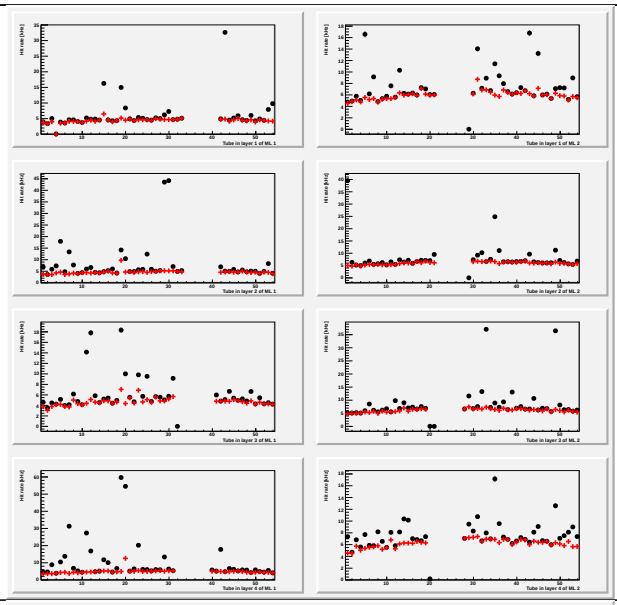
BMG-4A-12	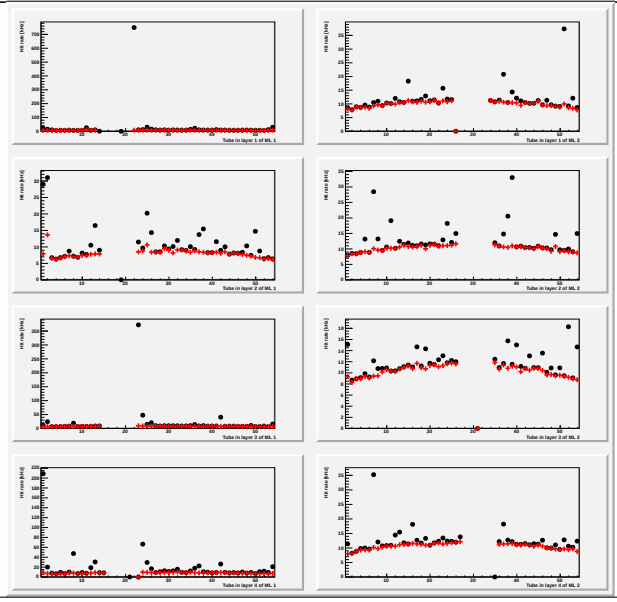

Not reviewed, for internal circulation only

Table 34: Measured cosmic hit rates spectra for completed chambers at CERN (continued).

Chamber	
BMG-2C-12	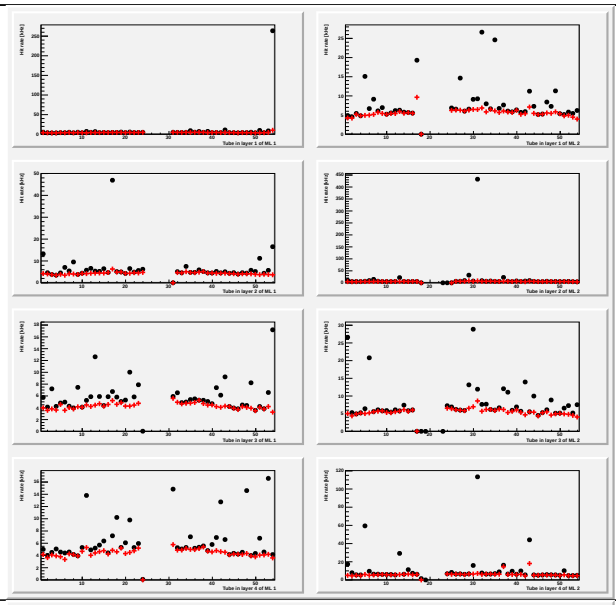
BMG-2A-14	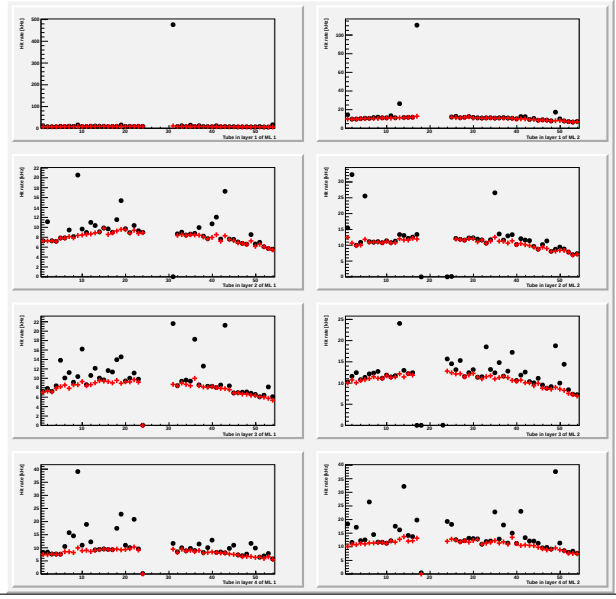

Not reviewed, for internal circulation only

Table 34: Measured cosmic hit rates spectra for completed chambers at CERN (continued).

Chamber	
BMG-2C-14	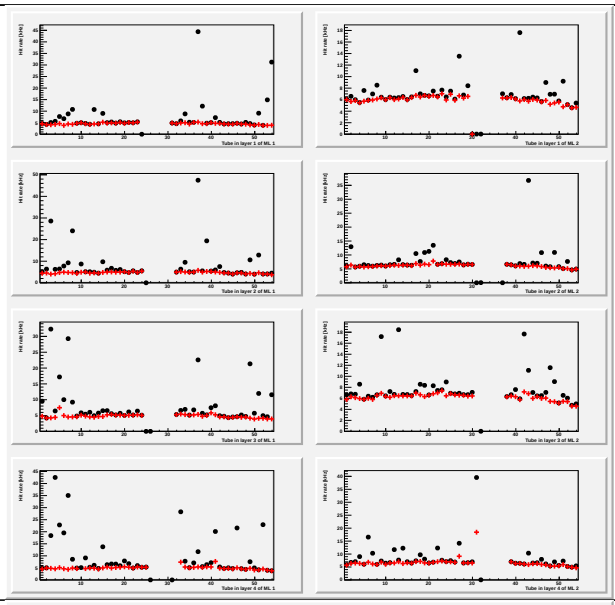
BMG-2A-12